THE SURFACE STRUCTURE OF SEMICONDUCTORS AND SOME OTHER MATERIALS, AND ITS DEPENDENCE ON ABRASION AND OTHER TREATMENTS.

BY

J. N. KING

A Thesis submitted for the Degree of Doctor of Philosophy of the University of London.

Applied Physical Chemistry of Surfaces Laboratory,
Imperial College of Science and Technology,
London, S.W.7.

May, 1963.

ABSTRACT.

The present work forms a detailed study of the nature of the abrasion process during unidirectional abrasion of silicon and calcite single crystals.

The surface orientations developed by unidirectional abrasion are investigated using electron diffraction. Beneath the abraded surface, composed of randomly oriented crystallites, is a transition region to the undeformed single crystal. In this transition region, lattice rotations are observed about a direction approximately normal to the abrasion direction and lying in the mean plane of the surface.

The friction coefficient μ does not vary with emery particle diameter D for $D > 30$ microns (silicon) or 50 microns (calcite), but the wear rate continues to increase with D, although less rapidly than at low D values. The value of μ falls rapidly on the finer emery grades, due to the clogging of the abrasive sheet by worn-off material, for calcite abraded dry and silicon abraded using a low-viscosity lubricant (propyl alcohol). However, μ increases on these emery grades for dry abrasion of silicon. This probably results from

rapid pick-up of emery particles by the silicon surface.

The compression and rolling textures of AgCl and AgBr are also considered. The compression texture depends on the conditions of compression; it is $\langle 100 \rangle$ with some oblique $\langle 110 \rangle$, for compression in a die, but $\langle 110 \rangle$ with additional $\{111\}$ twinning, for compression between parallel plates permitting extensive lateral flow. The rolling texture is $\{110\}\langle 1\bar{1}2 \rangle$ with pronounced twinning on the $\{111\}$ planes least steeply inclined to the rolling plane.

It is concluded that the "abrasion texture" is of the same type as, and closely related to, both the rolling texture and the compression texture observed when extensive lateral flow is permitted.

CONTENTS

		Page
1.	INTRODUCTION.	1
1.1.	General Introduction.	1
1.2.	The Deformation Processes of Crystals.	3
1.3.	A Brief Account of the Theory of Dislocations.	14.
1.4.	Preferred Orientations in Deformed Polycrystalline Materials.	18
1.5.	Previous Investigations into the Structure of Abraded Crystalline Surfaces.	22
1.6.	The Friction of Sliding Surfaces.	28
1.7.	The Processes and Theories of Wear.	40
1.8.	Methods of Measurement of the Hardness of Crystals and Polycrystalline Materials.	52
2.	EXPERIMENTAL.	54
2.1.	Materials.	54
2.2.	Etching Procedure.	56
2.3.	Determination of the Wear Rate.	58
2.4.	Determination of the Coefficient of Friction.	59
2.5.	Hardness Measurements.	59
2.6.	Examination by Optical Microscopy.	60
2.7.	Examination by Electron Diffraction.	61
2.8.	Examination by X-Ray Diffraction.	65

		Page
3.	RESULTS AND DISCUSSION.	66
3.1.	The Rolling and Compression Textures of AgCl and AgBr.	67
	3.1.1 The orientation of rolled AgCl.	67
	3.1.2. The orientation of AgCl and AgBr compressed between lubricated flats.	72
	3.1.3. The orientation of granular AgCl and AgBr compressed in a die.	73
3.2.	Discussion of the Rolling and Compression Textures of AgCl and AgBr.	76
3.3.	Unidirectional Abrasion of a Cleavage Face of a Calcite Single Crystal.	79
	3.3.1. Friction and wear of a calcite single crystal during unidirectional abrasion.	84
	3.3.2. Optical examination of abrasion grooves on a calcite single crystal.	88
	3.3.3. Electron diffraction examination of a unidirectionally abraded cleavage face of calcite.	92
3.4.	Discussion of Results for the Abrasion of Single-crystal Calcite.	98
3.5.	Unidirectional Abrasion of Silicon Single Crystals.	102
	3.5.1. Friction and wear of silicon single crystals during unidirectional abrasion.	102

Page

3.5.2. Optical examination of abrasion grooves on silicon single crystals. 109

3.5.3. Electron diffraction examination of a unidirectionally abraded single crystal of silicon. 110

3.6. Discussion of the Results for the Abrasion of Single-Crystal Silicon. 117

4. CONCLUSION. 123

ACKNOWLEDGMENTS. 125

APPENDICES. 126

REFERENCES. 135

INTRODUCTION

1. INTRODUCTION.

1.1. General Introduction.

In practice the wear of surfaces sliding on each other may occur by a number of different processes (e.g. abrasion, fretting corrosion, embedding, pitting and scuffing). However, in any fundamental investigation into the nature of the wear process it is necessary to isolate and study in detail one particular wear process at a time.

The present work is one of a series of investigations carried out in the Applied Physics and Chemistry of Surfaces Laboratory, Imperial College, to study the processes of abrasive wear.

When a hard material slides on a softer material, the friction is composed of adhesion and ploughing components, as Bowden and Tabor (1950) showed. Spurr's friction experiments (1956) also provided quantitative data on the magnitude of the ploughing component. Other workers have used optical and metallographic methods to study the groove form and the grain changes caused by abrasion.

For the study of the lattice re-orientation caused by abrasion or other surface deformation processes, however, electron diffraction is the most suitable technique, because the low penetration of the electron beam makes it possible to study the immediate surface structure and the variation with

depth. This technique has been used extensively in this laboratory, Scott and Wilman (1958) using it to show for the first time a correlation between the lattice orientation and the friction, for Be and Mg.

The results obtained from the friction and wear experiments of many metals sliding on various grades of emery paper (Avient, Goddard and Wilman, 1960) have been interpreted quantitatively in terms of the shape and orientation of the abrasive particles and the flow properties of the metal.

The author's own investigations,described in sections 2 and 3, are preceded here by a brief account of the mechanisms of crystal deformation, and a survey of the fundamental processes of friction and abrasive wear, with reference to previous work in this field.

1.2. The Deformation Processes of Crystals.

The following mechanisms have been proposed to describe the plastic deformation of crystals on a macroscopic scale:- translational slip, flexural translational slip, kinking, rotational slip, flexural rotational slip, twist slip and mechanical twinning. The movement of dislocations within the crystal may be used to describe on an atomic scale the deformation processes explained below.

(a) Translational slip.

When translational slip occurs, part of the crystal lattice moves relative to the remainder of the crystal, the plane of movement, or slip plane, being parallel to a definite crystallographic plane, usually the most heavily populated atomic plane; and the slip direction being along a definite lattice direction, usually the most heavily populated atomic row. For face-centred cubic metals the slip plane is usually $\{111\}$, the slip direction $\langle 110 \rangle$. In rocksalt-type ionic crystals, however, slip occurs on the $\{110\}$ plane and in the $\langle 110 \rangle$ direction. Close-packed hexagonal metals normally slip on (0001) planes in a $\langle 11\bar{2}0 \rangle$ direction. Different slip systems may become operative at extremely high or low temperatures (Barrett, 1952).

The extension of a single-crystal metal rod may be used to study slip (see Fig.1). In this case rotation of the

slip lamellae occurs about an axis parallel to their plane such that the slip direction rotates towards the axis of the torsion, i.e. the rod axis. The fact that slip bands can be seen in crystals indicates that the deformation is inhomogeneous and that slip occurs in lamellae whose thickness varies with the deformation conditions but may be of the order of microns. The displacement of each slip plane is usually hundreds of atomic spacings. The slip lamellae in the central region of the rod are almost undeformed. Sometimes these bands exhibit fine structure and consist of several thinner, submicroscopic slip layers combining to form the slip band. Heidenreich and Shockley (1947) observed this with aluminium and noted that the fine structure layers had a thickness of about 200 angstroms. Brown and Honeycombe (1951), however, have shown this effect to be typical of strained or worked surfaces of aluminium crystals. For strain-free surfaces isolated dislocations occur at first, later deformation on nearby planes producing this band effect. Slip will not occur until the shear stress resolved in the slip plane and slip direction exceeds a certain critical value (Schmid, 1924).

The high degree of symmetry of most crystals results in there being many crystallographically equivalent planes and directions, and slip will first occur in the slip plane and along the slip direction along which there is highest shear

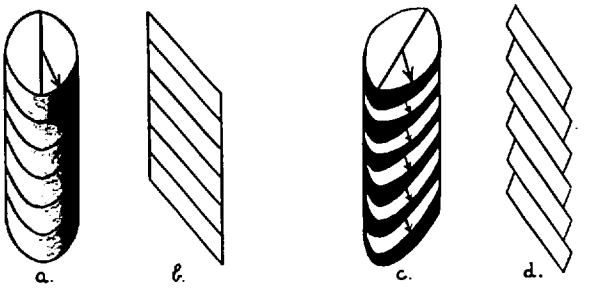


FIG. 1. DIAGRAM ILLUSTRATING TRANSLATIONAL SLIP IN THE EXTENSION OF A SINGLE CRYSTAL ROD ; (a) & (b) INITIAL STATE, (c) & (d) AFTER EXTENSION.

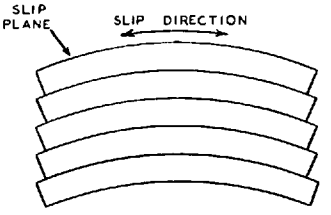


FIG. 2. FLEXURAL TRANSLATIONAL SLIP.

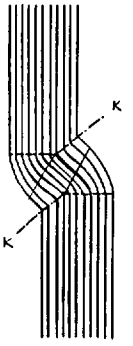


FIG. 3. STRUCTURE OF A KINKED CRYSTAL.

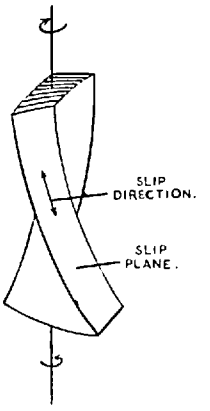


FIG. 4. TWIST SLIP.

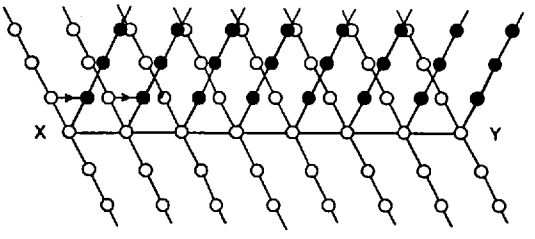


FIG. 5. DIAGRAM SHOWING THE MOVEMENT OF LATTICE POINTS IN MECHANICAL TWINNING.

O.....ORIGINAL LATTICE ; ●.....TWIN LATTICE

stress. If the deforming force continues, the rotation of the crystal lattice during slip will result in another slip system being equally favourably aligned for slip. Thus slip may continue to alternate on two or more similar slip systems. This is termed "multiple translational slip".

Irregular slip surfaces may be observed when slip takes place on different slip planes but along only one direction. This phenomenon is called pencil glide, an example being the ⟨110⟩ slip of AgCl (Nye, 1949).

(b) Flexural translational slip.

This results from the bending of a crystal about an axis in the slip plane, the bent slip lamellae remaining in coherent contact with each other with lattice dislocations at intervals, as in Fig. 2. Mark, Polanyi and Schmid (1922) observed this effect on stretching a zinc crystal wire, flexural translational slip occurring between the undeformed clamped regions of the crystal and the more extensively deformed central region. West (1954) and Gilman (1955) have found similar slip on bending single crystal rods of corundum and zinc respectively..

(c) Kinking.

If a crystal is compressed in a direction parallel to its translational slip planes it may collapse to form kinks (Fig. 3). In the region of these kinks the slip planes change

direction sharply where they cross a kink plane, k, which need not correspond to any definite crystallographic plane. In kinking, as in flexural rotational slip, the slip occurs in the normal translational slip direction, the kinking corresponding to a rotation of the lattice about an axis perpendicular to the slip direction in the slip plane. The most obvious example of this deformation is to be found in hexagonal crystals, which usually only slip on the basal plane, closely resembling ideal simple translational slip. Kinking was observed by Mügge in 1898 on compression of cyanite and graphite with the basal planes parallel to the compression axis and by Orowan (1942) for cadmium. For zinc, Hess and Barrett (1949) found that kink bands could be formed slowly under stress and might be regarded as a type of flexural translational slip.

Kinking may also result from tension, as found by Cahn (1951) for aluminium and Honeycombe (1951) for cadmium. Very narrow "micro-kink" bands have been observed in zinc single crystal cleavage surfaces (Jillson, 1950).

(d) Rotational slip.

Rotational slip is the name given by Wilman (1950, 1951) to the rotation of one part of a crystal, in contact with an adjacent part, about an axis normal to their common interface. In the study by electron diffraction of crystal growth in thin films and surface layers, Wilman observed that some lamellar

groups of crystals were often related to each other by a rotation about a normal to a heavily-populated plane, often the habit plane, the degree of rotation being such that a proportion of the atoms of one crystal face coincided with potential troughs on the neighbouring crystal face. Thus, in this slip process, part of the crystal on one side of the slip face rotates about an axis normal to the slip face to reach a new metastable position. Macroscopic rotational slip under torsion was demonstrated in potassium ferrocyanide trihydrate and gypsum crystals. Whapham (1956) and Whapham and Wilman (1956) observed rotational slip with zinc, lead and aluminium single crystals. Jillson (1950) obtained similar results for zinc, but offered no interpretation of his observations.

(e) Flexural rotational slip.

This is a more general case of rotational slip where the torsion axis is not normal to the slip plane, saddle-like flexure of the slip lamellae occurring together with rotational slip (Whapham and Wilman, 1956). This flexure results in a variation of the relative rotation of adjacent slip lamellae over the interface. The axis of flexure is also variable in direction.

(f) Twist slip.

Twist slip has been observed by Mügge (1898), Johnsen (1914) and Buerger (1930) on the torsion of parallel-

sided specimens of gypsum and other crystals, with the torsion axis along the slip direction of the crystal (Fig.4). Slip lines are visible at the ends of the crystal after twisting it and the process may be considered as either flexural rotational slip (see Wilman, 1951) or a combination of flexural and ordinary translational slip.

(g) Twinning.

Mechanical twinning is a different type of plastic deformation from slip. It is a process by which the deformed part of the crystal takes up a mirror-image structure with reference to the original crystal, about a certain crystal plane (twinning plane), or an orientation derived from the original crystal by a rotation about the twinning axis. In many cases the displacement of the atoms in the twinned region is proportional to their distance from the twinning plane, i.e. there is a homogeneous shear (Fig.5). However, the atoms usually move less than one atomic spacing, whereas in slip the movement is many spacings. Also the orientation of the twinned region is different from that of the original crystal and the deformation occurs in every plane, whereas in slip it occurs only in widely separated lattice planes. Finally, twinning may occur on planes which are not slip planes. Barrett (1952) and Hall (1954) have summarized the observations of many workers on twinning in metals.

(h) Fracture by cleavage.

Under certain conditions crystals may fracture by

cleavage on crystallographic planes of low indices, with or without the occurrence of slip or twinning. This may be readily observed in hexagonal and rhombohedral crystals by choosing orientations such that the resolved stress tending to cause slip is only a small component of the applied stress. The applied stress required for cleavage varies with the crystal orientation, being least when the angle between the tension axis and the cleavage plane is a maximum. This variation may be accounted for by assuming that cleavage occurs at a critical value of the stress that is resolved normal to the cleavage plane (Barrett, 1952).

Wooster (1938) indicated a few general rules about cleavage in non-metallic lattices. It is always found that non-metals with layer lattices (i.e. graphite, mica, MoS_2 and CdI_2) cleave parallel to these layers, as do hexagonal metals. Cleavage does not occur so as to break up radicals in ionic crystals or molecular complexes in homopolar crystals, but within the limits imposed by these two restrictions the cleavage planes are those most widely spaced. In ionic crystals which have no radicals, cleavage occurs so as to expose planes of anions, where such planes exist;where they do not, large cations may also be exposed on the cleavage surface. Thus in fluorspar, CaF_2, the cleavage plane is $\{111\}$ and the cleavage exposes net planes of anions (fluorine ions). Cubic crystals of NaCl and CsCl types cleave on $\{100\}$ planes.

Diamond, silicon and germanium, all having the diamond-type structure, have an octahedral cleavage plane. In the similar structure of zinc-blende, ZnS, the cleavage plane is $\{110\}$. It should be noted that a plane parallel to $\{111\}$ in zinc-blende has only zinc ions on one side and sulphur ions on the other and hence is not favourable for easy cleavage because of the strong electrostatic attraction, whereas a plane parallel to $\{110\}$ has an equal number of zinc and sulphur ions on either side.

The theoretical strength of a perfect crystal has been calculated from the energy required to form two new surfaces at the break, with results usually 100 to 1,000 times greater than the cleavage strengths experimentally observed (see, for example Polanyi, 1921; Zwicky, 1923).

Griffith (1924) postulated that this discrepancy might be accounted for by assuming that the material contained imperfections, principally cracks, which might concentrate the stress. The theoretical stress might then be locally attained with a comparatively low mean stress. He also considered that fracture was immediate if the spreading of the crack decreased the free energy of the system. In later modifications to Griffith's equations the only significant differences lay in the numerical factors.

The Griffith crack in metals may be identified with slip planes in which the dislocations accumulate at the

grain boundary, giving rise to very high localised stresses. Stroh (1954) showed that a crack should be formed near a piled-up group of about 1,000 dislocations. The stress system due to the crack was obtained and it was shown that, while the crack would have a stable equilibrium length, this would probably be determined by the amount of plastic flow which takes place around the tip of the crack. However, experimental work suggests that this number of dislocations would not be expected to pile up in one slip line in a ductile material, and if they did they would probably produce slip first. Stroh (1955) later suggested that cracks might be produced by general accumulations of different slip planes acting in co-operation, even though each alone is not able to produce a crack. Thus the number of dislocations per slip plane required is reduced to a few hundred.

Cottrell (1958) suggested an alternative mechanism. A wedge, in the form of an extra half plane, can be produced in the cleavage plane by the coalescence of two slip dislocations, and the addition of further dislocations increases the size of the wedge until it becomes, effectively, a crack lying in the cleavage plane. Whether such a crack can spread depends on the amount of plastic flow which occurs. If flow is inhibited the crack may grow until it reaches a critical size (of the order of a grain diameter) beyond which unstable fracturing may occur if this critical size is large enough.

This mechanism does not require the existence of grain boundaries for initiation, and is therefore applicable to single crystals, but the slip-fracture transition is determined by the grain size. Thus cracks form at the yield point in both coarse-and fine-grained materials; in the former case the crack is unstable by the time it has extended across one grain and brittle fracture results, and in the latter case plastic flow around the tip of the crack inhibits further growth and stable micro-cracks are formed.

If the build-up of the stress at the tip of a crack is slow enough the upper yield stress will be reached in an adjacent grain and plastic flow will release the local stresses (Biggs, 1960). The transition from ductile to brittle fracture in a given specimen is caused by the speed of crack propagation (Irwin, 1948). Once the stress builds up too quickly then the fracture stress is reached within the stress decay time of the material, and cleavage occurs.

Secondary cleavage may occur (Zapffe, 1947) by fracture on suitably oriented planes separating the various primary elements of the fracture. Forty (1957) observed a sharp swing of some 45^{o} away from the direction of crack propagation, after the crack velocity had slowed down (probably by a momentary change in the stress distribution), before the crack settled down in the original direction of propagation.

Biggs (1960) pointed out that mechanical twins, present in the crystal prior to the propagation of the fracture or induced by the stresses ahead of the crack, give rise to a marked increase of cleavage steps on the exit side of the twin due to the slowing down of the crack by the volume of twinned material. A screw dislocation may offer a similar barrier to the progressing crack.

Tipper (1957) studied crack propagation in a mild steel plate and confirmed that the "V" shaped crack observed was caused by discontinuous regions of cleavage fracture and shear. A similar series of fractures by cleavage and shear alternately in a mild steel plate was observed by Robertson (1953). For recent detailed discussions of the mechanisms of fracture, reference should be made to the report of the Conference on Fracture, 1959 (see Averbach, Felbeck, Hahn and Thomas, 1959).

Since there is a critical shear stress for slip, a definite normal stress required to cleave crystals and a critical stress seems to exist for twinning, it can be assumed that when a stress is applied to a crystal it may cause slip, twinning or cleavage, depending on which resolved stress is the first to exceed the critical value for that process.

1.3. A Brief Account of the Theory of Dislocations.

The classical interpretation of slip, which suggested the gliding of one portion of the crystal over another, involves the initial separation of these two parts in a direction normal to their interface (Frenkel, 1926). This requires a shear stress of the order of a thousand times that observed in the deformation of real crystals. Becker (1925) suggested that thermal motion in the crystal lattice might contribute to the formation of slip, but later calculations by Becker and Boas (1929) using this theory showed that the discrepancy between the measured and calculated values of the shear stress necessary to induce slip could not be fully explained by thermal vibrations within the lattice. Smekal (1933) proposed that imperfections within the crystals, with resultant weakness at these points, enabled deformation to occur at a much lower shear stress value than for a perfect crystal.

Orowan (1934), Polanyi (1934) and Taylor (1934) proposed that the movement of these crystal imperfections and dislocations within the crystal lattice might explain the process of slip occurring at such low shear stress values. If the dislocations are already present in the crystal then the yield strength is the stress required to move them. Alternatively the dislocations may start from these cracks and imperfections, in which case the yield strength is the stress

necessary to start slip from them. In either case slip starts in some places before others and occurs by movement of these dislocations.

If slip occurs in part of a crystal above the remainder of the undeformed crystal then the slip, except in regions very near the dislocation, may be described by a vector B, the Burgers vector (J.M.Burgers, 1939), which indicates the distance and direction of the displacement of the deformed crystal region above the slip plane in relation to the lower, undeformed region. This vector is characteristic of the nature of the dislocation. The simplest case is that of a unit dislocation, when the Burgers vector is a lattice vector of magnitude one lattice spacing, since the atoms must always slip from one position of equilibrium to another. It may be that there are positions of equilibrium between the actual lattice positions, in which case the Burgers vector may not be an integral number of lattice spacings. For a dislocation of more than one lattice spacing it might be expected to find intermediate unit dislocations. The sign of B is ambiguous unless the slipped region is identified. When the crystal is subjected to a force the dislocations in it will try to move in a direction so as to reduce this force.

Dislocations generally may be resolved into a combination of two types, the edge dislocation and the screw dislocation.

The edge dislocation.

In edge dislocations the Burgers vector is perpendicular to the dislocation line, the line which marks the boundary of the slipped region. The movement of an edge dislocation is shown in Fig. 6 (from Taylor, 1934). The slipping is not considered to occur instantaneously throughout the slip plane but rather over a very limited region, this region moving from one side of the crystal to the other during a finite time. This was observed with a single crystal of rocksalt by Joffé (1928), when breakdown under stress occurred in a certain region and then traversed the crystal.

In Fig. 6 it is assumed that, following the passage of a unit dislocation, a perfect crystal arrangement is reformed. In diagrams (a) to (d) the region of slip moves from left to right across the crystal and in (e) to (h) from right to left. A positive unit dislocation from left to right means a shift of the upper part of the crystal by one atomic spacing to the right, relative to the lower part, and is identical to a negative unit dislocation from right to left, when the lower part of the crystal moves one atomic spacing to the left. Edge dislocations are now accepted as being responsible for translational slip.

The screw dislocation.

J.M. Burgers (1939, 1940) introduced dislocations of the screw type which are characterized by a dislocation line

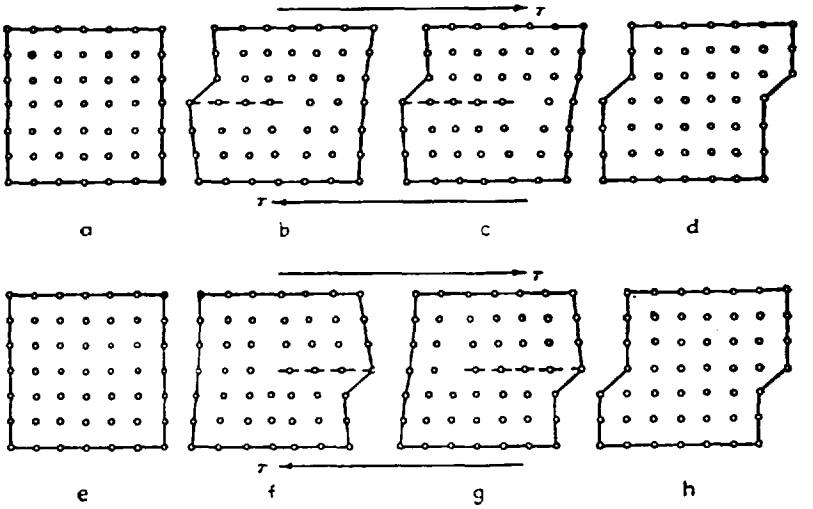


FIG. 6. THE GENERATION AND MOVEMENT OF AN EDGE DISLOCATION.

a, b, c, d..... +ve. dislocation moving to the right,

e, f, g, h.... −ve. dislocation moving to the left.

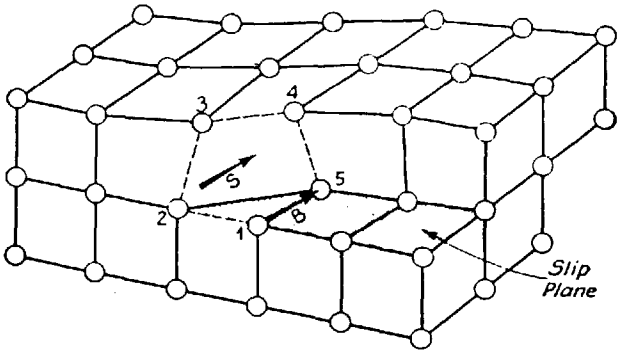


FIG. 7. A SCREW DISLOCATION IN A SIMPLE CUBIC STRUCTURE.

parallel to the displacement direction of the discontinuity. Fig. 7 (from Barrett, 1952) illustrates such a dislocation with a displacement of one atomic spacing as indicated by the Burgers vector, B. The misfitting caused by this displacement is concentrated at the screw dislocation S. Following a circuit round S through atoms 1, 2, 3, 4 and 5 leads to a forward movement parallel to the screw dislocation by an amount B. The line of the screw is always straight and parallel to the slip direction.

Although both edge and screw dislocations are linear discontinuities, combinations of these two types of dislocation can give dislocations of non-linear form and it is probable that the dislocations in actual crystals are of this combined form. Most deformation processes in crystals have been explained by various dislocation theories and these are reviewed by Cottrell (1949, 1953a, 1953b) and Read (1953).

1.4. Preferred Orientations in Deformed Polycrystalline Materials.

When a polycrystalline metal or non-metal is plastically deformed there is generally a change in the orientation of the individual grains towards a preferred orientation in which certain lattice directions are aligned with the principle directions of flow in the material. The ideal textures characteristic of various crystal structures have been reviewed by Hibbard and Yen (1948) and Barrett (1952) and are summarized in Table 1. However, there is often a wide spread of orientation superimposed upon this texture, or a combination of two such textures, as well as irregularities in the surface region.

Textures of drawn polycrystalline wires.

In face-centred cubic metals the wire texture is usually a double fibre texture, the crystallites having either a ⟨111⟩ or a ⟨100⟩ direction parallel to the wire axis, with a random azimuthal orientation about this axis.

The body-centred cubic metals, Fe, W and Mo, have a ⟨110⟩ texture, whilst close-packed hexagonal metals develop various textures, depending on the metal (Barrett, 1952).

Table 1. Preferred orientations in cold-worked metals.

Structure Type	Drawing Textures (// wire axis.)	Compression Textures	Rolling Textures
Face-centred cubic	$\langle 111 \rangle^{I}$ $\langle 100 \rangle$	$\langle 110 \rangle^{I}$ $\langle 100 \rangle$	$\{110\}\ \langle 112 \rangle^{I}$ $\{112\}\ \langle 111 \rangle$ $\{100\}\ \langle 001 \rangle$ $\{110\}\ \langle 001 \rangle$
Body-centred cubic	$\langle 110 \rangle$	$\langle 111 \rangle^{I}$ $\langle 100 \rangle$	$\{100\}\ \langle 011 \rangle^{I}$ $\{111\}\ \langle 112 \rangle$ $\{112\}\ \langle 110 \rangle$
Close-packed hexagonal	$\langle 210 \rangle$ (Zn:- hexagonal axis 70° from the wire axis.)	$\langle 001 \rangle$	$\{0001\}$

I indicates the principal textures.

Compression textures.

Face-centred cubic metals tend to develop a ⟨110⟩ fibre texture on compression, i.e. with a ⟨110⟩ direction along the compression axis. In practice there is a deviation from this ideal texture and for aluminium half the crystallites are more than 10 degrees from this orientation, independent of the amount of compression. There is an absence of orientations about the ⟨111⟩ and ⟨100⟩ directions (Barrett, 1952). Similar compression textures are found for nickel and copper. Body-centred cubic metals have predominently a ⟨111⟩ compression texture with a weaker ⟨100⟩ texture as well, and the hexagonal metal magnesium has a [001] texture with the hexagonal axis parallel to the compression axis (Ono, 1925; Barrett, 1939).

A brief review of the theories proposed to explain these compression textures is given by Barrett (1952). Several sets of slip planes are operative in each grain because the grains of a polycrystalline material must fit together again without voids after the deformation. Boas and Schmid (1931) proposed three active slip systems, the deformation texture being composed of orientations which werestable under the action of these slip systems, and were able to account for the ⟨100⟩ and ⟨111⟩ tension and compression textures for f.c. cubic metals. Their theory also predicts the major

textures for b.c. cubic metals but not some of the minor textures. Taylor (1938) proposed a much more rigorous theory involving the operation of at least five slip systems for the grains to fit together after deformation, and for the change in shape of the grains to be the same as that of the aggregate. The systems operating are those which make the total work of deformation a minimum. However, his mathematical solution of the deformation structures is too complex for practical application.

The compression textures of many polycrystalline non-metals have been investigated in this laboratory by compacting the materials in powder form in a steel die. Salts of the NaCl structure type develop a ⟨100⟩ texture, except for MgO which has a ⟨111⟩ texture, and CsCl type salts develop a ⟨111⟩ texture (Dobson and Wilman, 1961, 1962a; King and Wilman, 1962a).

Rolling textures.

Preferred orientations developed by cold-rolling must be specified in terms not only of the crystallographic directions parallel to the direction of rolling but also of the crystallographic planes parallel to the plane of the rolled sheet. The details of the scatter about these ideal orientations are often described in terms of pole figures. Hibbard and Ming-Kao Yen (1949) and Barrett (1952) have fully reviewed a considerable amount of experimental data, see Table 1.

The principal orientation for all cold-rolled face centred cubic metals is $\{110\}\langle 112\rangle$, that is with a $\{110\}$ plane parallel to the rolling plane and a $\langle 112\rangle$ type of crystallographic direction parallel to the rolling direction. The indices $\{112\}\langle 111\rangle$ are generally used to describe the other orientations also present in many of the metals. For sheets of Al, Cu and 70-30 brass rolled in one direction only without reversal, Hu, Sperry and Beck (1952) observed that the pole figure for the surface texture is not symmetrical about the transverse direction. Wever (1931) stated that a degree of correlation exists between rolling textures and the simple elongation and compression textures, as if the rolling process could be considered as a superposition of elongation in the rolling direction and compression normal to the rolling plane.

For body-centred cubic metals the principal rolling texture is $\{100\}\langle 110\rangle$. For metals with a close-packed hexagonal structure, rolling tends to rotate the slip plane (0001) into the rolling plane. This simple structure is observed in magnesium, zirconium and hexagonal cobalt, but zinc and cadmium have rolling textures in which the hexagonal axis is frequently inclined between 20° and 25° towards the rolling direction.

1.5. Previous Investigations into the Structure of Abraded Crystalline Surfaces.

The existence of a disorientated surface region on some abraded non-metallic crystals, (i.e. calcite, lithium fluoride, quartz and rocksalt), which may extend to a depth of up to 10 microns, has been demonstrated by X-ray diffraction (Gay and Hirsch, 1953). Electron diffraction is a much more precise tool, however, for examining the variation of structure with depth, because of the low depth of penetration of the electron beam.

Although there have been many electron diffraction studies of worked surfaces, particularly by polishing, it is only in recent years that the structure of these surfaces, and the immediate regions beneath them, have been fully investigated. The surface region of the crystalline specimen is deformed, whether it be a metal or a non-metal, and the results obtained for metals are of direct importance to the study of abraded non-metallic surfaces.

Lees (1935) observed a normal $\langle 110 \rangle$ fibre orientation on the surface of polished copper and gold, and pointed out that this is the same as the compression texture for face-centred cubic metals. Finch, Quarrell and Wilman (1935) showed that on polished polycrystalline graphite, and on abraded cast iron, the graphite at the surface becomes strongly orientated with (0001) planes parallel to the surface. On

abrading cleavage faces of galena (PbS) parallel to a cube edge, Germer (1936) reported the rotation of parts of the crystal about the perpendicular cube edge in the surface. Similar results were observed by Raether (1947) with rocksalt. Bénard and Lacombe (1946) examined abraded iron and aluminium crystals with X-rays. They reported the observation of preferred orientations a few microns below the random polycrystalline surface region, the orientation varying with the direction of abrasion and the initial orientation of the crystal, but the orientations were not identified.

Using electron diffraction, Evans and Wilman (1950) found rotations about a $[1\bar{1}0]$ axis, possibly indicating rotational slip, on the abrasion of a (110) cleavage face of zinc blende (ZnS) in the $[001]$ direction. Evans, Layton and Wilman (1951) studied the surface deformation of (110) faces of b.c. cubic iron and f.c. cubic copper single crystals, abraded in various directions. They observed large rotations of parts of the crystal lattice about an axis which was usually but not always parallel to the surface and normal to the abrasion direction. They interpreted their results as possibly due to the rotational slip of lamellae parallel to densely populated planes which were normal to the rotation axis (Wilman 1950, 1951). Similar rotation axes for the abrasion of brass, nickel and silicon iron crystals have

been observed by Nagata, Tomoda and Ide (1954).

In this laboratory Agarwala and Wilman (1953, 1954, 1955) investigated the variation of structure with depth, of a unidirectionally abraded (110) face of an iron crystal. Removal of the topmost layer of disorientated α- iron by etching revealed first a region of randomly orientated γ - iron, then a region of α- iron in a range of orientations corresponding in the mean to the rotation of parts of the original crystal about an axis which was usually in the surface and normal to the abrasion direction. However, in one case two rotations about symmetrically related axes were observed. Further etching revealed, below this layer, some strongly orientated γ- iron, the set of geometrically equivalent orientations being independent of the abrasion direction and corresponding to a $\{100\}$ plane of the γ - iron being parallel to a $\{110\}$ plane of the α- iron (this evidently being the contact face), with a $\langle 110 \rangle$ γ direction parallel to a $\langle 111 \rangle$ α row. The formation of γ - iron suggests the occurrence of high temperatures at localised hot-spots during abrasion, since the α-γ transformation normally occurs only above 900°C; but in this case the deformation processes may have assisted the transformation.

Courtel and his co-workers (Courtel, 1949a, 1950a, 1950b; Courtel and Loriers, 1950) investigated various

f.c. cubic metals and concluded that ⟨111⟩ fibre orientations were developed with the axis tilted away from the surface normal. However, the relation between the direction of this tilt and the abrasion direction is not clear. For abraded magnesium (c.p. hexagonal) he concluded that (0001) planes became orientated parallel to the surface and for iron a ⟨110⟩ fibre texture was developed (Courtel and Leger, 1948; Courtel, 1949b, 1950b). Takahashi (1951), in electron diffraction studies of abraded and polished f.c. cubic copper and silver, reported a combination of ⟨100⟩ and ⟨111⟩ fibre textures with a tilt away from the outward surface normal towards the direction of motion of the abrasive particles.

Experiments by Scott and Wilman (1958) showed that unidirectionally abraded polycrystalline beryllium and magnesium and single-crystal beryllium (c.p.hexagonal metals) developed a tilted [001] fibre orientation. The tilt was away from the outwardly directed normal to the surface back towards the direction from which the abrasive particles came, and the tangent of the angle of tilt, δ, agreed closely with the measured coefficient of friction, μ (i.e. $\tan.\delta \simeq \mu$).

The structure of various single crystal and polycrystalline metal surfaces after unidirectional abrasion has been extensively investigated in this laboratory (Harker, 1958; Goddard, 1959; Avient, 1961; Wilman, 1957, 1960). For

face-centred cubic metals Goddard, Harker and Wilman (1962) observed a backwardly inclined $\langle 110 \rangle$ orientation with $\{111\}$ twinning, above the transition region to the underlying undisturbed initial structure, which is several microns below the surface. The angle of tilt of the $\langle 110 \rangle$ orientation axis increases with depth below the surface. Abraded body-centred cubic metals exhibited a mixture of $\langle 211 \rangle$ and $\langle 100 \rangle$ fibre orientations; again the axis of the orientation was tilted backwards from the specimen normal towards the direction from which the abrasive particles came. Below about 500 Å depth the $\langle 100 \rangle$ orientation was strongly developed, followed by a region of transition to the undeformed metal. On the abrasion of tetragonal indium and tin a $\langle 110 \rangle$ oblique texture relative to the face-centred pseudo-cubic axes was developed.

Porgess and Wilman (1960) have reported a backward tilt of the $[00\bar{1}]$ fibre orientation developed in graphite on unidirectional abrasion. Similar results have been obtained with various compressed graphite-powder compacts, commercially graphitized carbons and pyrolytic graphites (King, 1960).

Recent work in this laboratory (Dobson and Wilman 1962b, 1962c; King and Wilman, 1961) has shown that compressed non-metallic powders also develop inclined textures

on abrasion. NaCl, KCl, KBr, AgCl and AgBr have an azimuthally-limited inclined ⟨110⟩ fibre texture, NiO an inclined ⟨100⟩ texture, and NaF and LiF a normal ⟨100⟩ texture and MgO an inclined ⟨111⟩ texture. All these materials are of the NaCl structure type. CsCl, TlCl, NH_4Cl and NH_4Br (materials of CsCl structure type) develop an inclined ⟨110⟩ orientation which is azimuthally limited.

1.6. The Friction of Sliding Surfaces.

(a) The basic laws of friction.

The two basic laws of friction have been known for centuries, namely that the frictional force between two materials is directly proportional to the load upon their interface and is independent of their apparent area of contact (Amontons, 1699). Thus for any particular pair of surfaces the ratio of friction to load is constant, this constant being called the coefficient of friction. These laws, Amontons's laws, are obeyed for a wide range of materials for a large variety of apparent contact areas and applied loads, although deviations have been observed at very low loads.

As Bowden pointed out, for smooth sliding surfaces the frictional force is chiefly the force required to overcome adhesion between the surfaces, a force equal to the product of the shear stress of the softer material and the real contact area between the surfaces. In the case of metals the adhesion may be strong enough for the contacting regions to be joined by welding, and shearing often takes place in one of the metals and not at the weld. If the shearing surfaces are of the same material a continuous region may be developed at these points of contact, followed by shearing in other less-work-hardened regions near the weld.

Unless the contacting surfaces are cleavage faces they are not microscopically flat and contact between them

only occurs at widely separated points, this actual contact area being of the order of a thousandth of the apparent contact area with resultant exceedingly high loading at these contact points, usually far in excess of the elastic limit of the materials.

If it is assumed that plastic flow takes place at these regions of contact then their total area, A_r, will increase by plastic flow until the pressure on these contact points is reduced to the maximum flow pressure of the softer surface, p_m. For a load W the following relationship is then true:-

$$A_r = W/p_m$$

The frictional force, F, required to shear these contact points, having a shear strength s, will be

$$F = A_r s$$

Thus the coefficient of friction, μ, is given by

$$\mu = F/W = A_r S/A_r p_m = s/p_m,$$ a constant for any given pair of substances. Spurr and Newcomb (1957a) showed that the static friction between a bituminous material and a cast iron disc is due to adhesion between the surfaces, the friction being reduced on removal of the load because of the elastic recovery of the surfaces.

If the surfaces deform elastically according to Hertz's classical equations (Hertz, 1886; see Bowden and Tabor, 1950) then the contact area is no longer proportional

to W but to $W^{2/3}$. Thus

$$A_r = c\, W^{2/3},$$

$$F = ks\, W^{2/3},$$ c and k being constants.

Then μ varies with the applied load. This has been observed for diamond sliding on diamond, which is so hard that the pressure at the contact points is below diamond's elastic limit and entirely elastic deformation occurs at light loads, the frictional force being found to be roughly proportional to $W^{2/3}$ (Bowden and Young, 1951b).

In general one may say that $F = ks\, W^n$, where $2/3 \leq n \leq 1$, and values of n between these two extremes might be expected to result from a combination of plastic and elastic deformation. Archard (1953, 1957a, 1957b, 1961) suggested that intermediate values of n would be expected according to the shape and size of the contact points.

Moore and Tegart (1952) observed a linear decrease of μ with increasing hardness for a Cu - Be alloy bar heat-treated to give a longitudinal temperature gradient. Avient, Goddard and Wilman (1960) found for various metals abraded at 1 kg load on dry emery papers, that μ of the emery/metal contacts decreased linearly with increase in hardness H_D; whereas the total μ at the equilibrium stage of pick-up of abrasive particles decreased rapidly as H_D increased from 10 to 100 kg/mm^2 (Pb to Cu), but then decreased approximately linearly with H_D to a hardness of 460 kg/mm^2 (tungsten). A

similar linear relationship between μ and H_D was observed by the author for various ball-milled graphite compacts for which H_D ranged from 2 to 15 kg/mm^2 (King and Wilman, 1962b).

(b) Previous studies of the real contact regions.

Greenwood and Tabor (1955, 1957) studied the friction of large-scale model junctions in annealed aluminium, lead, indium and plasticine and concluded that the force required to separate the junctions formed by sliding metals adhering strongly at their contact points was in good agreement with the theoretical values. However, the values of the shear strength and flow pressure in the junction regions are not those of the bulk materials. Also, plastic deformation occurs as a result of many stresses, and the force necessary to shear an adhered junction under such stresses is not the same as that required when the stresses are absent.

Observations and measurements of the real contact area between two surfaces (Courtney-Pratt and Eisner, 1957; Tabor, 1959) have shown that this area increases on application of a tangential force, growing steadily as this force is increased until sliding occurs, For clean, film-free metal surfaces the contact regions grow until practically all the surface is in real contact before sliding occurs. In this case there is gross seizure and μ may be as high as 100. However, such seizure may be prevented by the formation of surface films. Bowden and Young (1951a) observed that these

films might be removed by outgassing in a vacuum, but were readily reformed on admission of a small amount of gas or water vapour. Such films reduced the shear strength of the contact interface and only a small increase in contact area was observed, on the application of a tangential force, before sliding commenced (Tabor, 1959), whilst the value of μ dropped to about 1. Under these conditions Tabor found that the area of contact when sliding occurred was directly proportional to the load.

(c) The ploughing component of friction.

There is an additional resistance to motion resulting from the ploughing of asperities on one surface through asperities on the other surface (Bowden, Moore and Tabor, 1943). The ploughing component of friction, μ_p, is small for surfaces of similar hardness and may usually be neglected in such cases. For surfaces of different hardness the previous equations have to be modified, so that

$$F = A_r s + A_t p'_m$$

and $\mu = \mu_a + \mu_p$, where the adhesion components $\mu_a = \frac{s}{p_m}$ and $\mu_p = A_t\, p'_m/W$, A_t being the transverse section of the ploughed out grooves and p'_m the mean flow pressure required to displace metal by ploughing.

For indium, Bowden and Tabor (1950) suggested that $p'_m \simeq 1.5\, p_m$. Spurr (1956) calculated μ_p for balls and

wedges of hard steel sliding on soft metals and found that these values agreed well with the experimental results.

In this laboratory expressions for μ_p, μ_a and μ have been derived for spheres, cones and square- and triangular pyramids (with axis normal to the metal surface) ploughing along the surface of a metal (Goddard, Harker and Wilman, 1959; Goddard and Wilman, 1962). The effects of clogging of bonded abrasives such as emery paper by worn-off metal, and the pick-up of abrasive particles by the metal surface, were also considered quantitatively. Experimental study of the abrasive wear and friction of metals sliding on various emery papers, of mean particle diameter D ranging from 5 to 150 microns, showed that for emery particles with D greater than about 70 microns μ is constant. For smaller particles μ decreases with D to a value approaching that for the metal sliding on metal. This is because, with these smaller particle emery papers, there is rapid clogging of the emery by the worn-off metal and the sliding conditions for the rear portion of the metal specimen approximate to metal sliding on metal. Although Spurr and Newcomb (1957b) had reported a linear dependence of μ on D for metals and other materials sliding on emery papers, this seems to be due to their use of a smaller range of D and shorter specimens, thereby reducing the clogging effect, so that the μ/D locus approximates to a straight line over the range considered.

(d) The elastic deformation of the contact region.

Tabor (1955) studied the friction of hard steel cylinders and spheres rolling over a rubber surface and found it could be attributed almost entirely to hysteresis losses during the elastic deformation of the rubber. If spheres were rolled along preformed grooves in the rubber there was interfacial slip, but this contributed little to the value of the friction. Similar results were obtained using soft metal sheets instead of rubber, and elastic hysteresis losses again accounted for the greater part of the friction. Further analysis of these hysteresis losses was made by Greenwood, Minshall and Tabor (1961).

From determinations of the friction coefficient of steel spheres and cones sliding on a well-lubricated rubber surface Miss Sabey (1958) and Greenwood and Tabor(1958)concluded that, under these conditions, the friction arose primarily from hysteresis losses in the rubber.

The deformation component of friction arises from the plastic and elastic deformation of high-spots on the two surfaces as they come into contact on sliding. The energy consumed in the plastic deformation is almost entirely unrecoverable and there is some hysteresis loss in the elastic deformation and recovery of the regions in the vicinity of the contacting points. Most energy is lost in the former process but both contribute to the total friction of sliding.

(e) The sliding friction of non-metals.

Savage (1948, 1956) and Bowden and his co-workers (Bowden and Young, 1951b; Bowden, Young and Rowe, 1952) have investigated the dependence of the friction of carbon, graphite and diamond on adsorbed surface films. In all cases the friction increases to a high value on the removal of these films by outgassing the materials in a vacuum. With carbon and graphite the readmission of a small amount of oxygen or water vapour changes the coefficient of friction back to its original value, indicating that this low value is chiefly the result of physical adsorption of the surface films. At the pressure required to bring about this change, it is likely that only a monolayer film is formed on the surface (Harkins, Jura and Loeser, 1946).

From experiments in various atmospheres Savage concluded that the more readily compressible vapours (high boiling point) were more efficient in lubricating the sliding surfaces by the formation of films which present a surface of low cohesive energy. For water, a vapour pressure of only 3 mm of mercury is necessary to eliminate the wear of graphite sliding on a copper disc. Measurements for similar experiments by Bowden on diamond were complicated by the formation of a film, probably of graphite, on heating to the high temperatures necessary for outgassing. However a large increase in the friction was observed on outgassing. Brushes made from graphitic carbons and also from natural graphite

flakes were used by Savage (1948) in his wear experiments conducted under vacuum, but the wear debris was a fine carbon dust not graphite flakes as might be expected, at least from the natural graphite flakes specimen, if the sliding process was simply slip of the graphite basal-plane layers over each other.

Although graphite sliding on graphite and diamond on diamond have high coefficients of friction when their surfaces are clean and film-free, they do not seize completely under these conditions, as metals do (Bowden and Young, 1951a). The lamellar structure of graphite enables it to shear easily, whilst these lamellae are not easily penetrated. Thus, on sliding there may be strong adhesion at the interface, with slip and shear on lamellae below it.

Savage (1959a, 1959b) observed the deformation of graphite cleavage faces by indenting metal probes, under a microscope. Shadow lines, many times the radius of the indenter, were developed in the graphite, many of these lines [illegible] disappearing on the withdrawal of the probe. If the applied load was sufficient for the probe to penetrate the basal plane, then a graphite fragment was removed and a wear track usually resulted if the probe was then slid across the graphite face.

Studies by Wilman and his co-workers (Porgess and Wilman, 1960; King and Wilman, 1962b) have shown that there is

cracking and some breakaway of graphite particles near the grooves formed by abrasion on emery papers, as well as plastic flow by slip on (0001) planes. Evidence of low adhesion between the graphite and ploughing particles is given by the absence of any forward curvature of the surfacing striae across rounded grooves caused by sliding graphite on "Scotchlite" reflective sheeting, composed of a close-packed array of glass spheres of about 120 microns diameter. Grooves formed under similar conditions on silver halide surfaces showed considerable forward curvature of these striae, indicating appreciable adhesion between the abraded surface and the ploughing particles (King and Wilman, 1961).

Kenyon (1954), studying the anisotropy of friction with crystal orientation on a (110) diamond surface, showed that the direction of low friction, the $\langle 110 \rangle$ direction, was also the direction of least abrasion and the direction of highest friction was the direction of greatest abrasive wear, i.e. the $\langle 100 \rangle$ direction. In 1957 Seal investigated the frictional anisotropy of various diamond surfaces and diamond sliders, both diamonds being capable of rotation with respect to each other. He observed fourfold anisotropy on a (001) face, the maxima occurring when the sliding direction was approximately parallel to a crystallographic axis in this face. The magnitude of the anisotropy depended on the relative orientation of the slider and sliding direction. Seal concluded that a maximum anisotropy

occurred when the [001] axis of the slider was parallel to the sliding direction, i.e. when the sliding direction was a direction of easy abrasion of both crystals. No frictional anisotropy was observed for a natural (111) diamond surface. Duwell (1962) reported that the coefficient of friction of spherical single crystals of sapphire (α- Al_2O_3) sliding on a wet steel surface varied by a factor of three with azimuth.

Shooter (1952), investigating the friction of a group of linear polymer plastics at loads from 0.04 to 10,000 gm, found that the friction was proportional to the real contact area, except at very light loads where results deviated from Amontons's Laws. The real contact area was determined from groove-width measurements and found to be proportional to the load, the coefficient of friction being constant for loads above 100 gm. The force required to shear unit contact area was calculated and found to equal the specific shear strength of the bulk plastic, indicating that there is strong adhesion at the contact points and that shear occurs within the bulk of the material, rather than at the interface. This was substantiated by the observation of material transfer between the surfaces. Polytetrafluorethylene had a much lower friction than the other plastics investigated and the shear strength value calculated from the friction was only a fraction of the bulk shear strength, indicating that there was weak interfacial adhesion and shear occurred at the interface, not in the bulk

of the plastic.

From these results it would appear that the friction mechanism for non-metals is similar to the Bowden-Tabor theory for metals with shear at, or near, the contact regions and the coefficient of friction theoretically equal to the ratio of the shear strength to the flow pressure of the softer material. Adsorbed gas films, which are normally present on the surface, affect the friction of non-metals as well as metals. Whilst plastic flow occurs in the regions of immediate contact, further elastic deformation occurs within the neighbouring bulk material. These elastic stresses are released on removal of the load and the resultant displacement may break the contact regions formed under compression. However, with soft metals, such as indium, strong normal adhesion may be observed (McFarlane and Tabor, 1948; Parker and Hatch, 1950).

1.7. The Processes and Theories of Wear.

The progressive removal of material from the surface of a body by mechanical action has only been studied as a subject over recent years. Much work has been done in the field of lubrication in efforts to prevent wear and also reduce friction at the same time. However, to use lubrication to its best advantage it is necessary to understand fully the wear processes operating and the means by which material is removed from a surface.

(a) Mechanisms of wear between two metallic sliding surfaces.

Because of the relatively small area of real contact, even between two carefully polished surfaces, the load supported on each contacting asperity is exceedingly large and in general beyond the elastic limit of the material. Thus plastic deformation occurs in these regions, increasing the total area of contact until it is large enough to support the total applied load, the pressure at the contact regions then being reduced to the yield pressure of the softer material. Under these high pressures strong adhesion occurs and an effectively continuous region is formed between the surfaces over the contact points. In metals this is referred to as cold welding or pressure welding (Bowden and Tabor, 1950). These junctions must be sheared for the surfaces to slide over each other. Work hardening occurs in these regions of plastic deformation as a

result of the strains imposed. In general the shear strength of the contact region is greater than that of the bulk materials so that shear takes place in the softer material rather than at the interface, with resultant metal transfer from the softer to the harder metal. Transfer of copper to steel, for example, is recorded by Bowden and Tabor (1950).

Ming-Feng (1952) considered the wear and material transfer of crystalline materials to result from the interlocking of the contact regions. The regions of actual contact are roughened by plastic deformation under the applied load, this deformation resulting in abrupt movements along several sets of crystallographic planes interlocking the two contacting interfaces. There is strain hardening in this region so that, on application of a tangential force, shear will occur in one of the materials away from the interface. When shear occurs there is a temperature flash (Bowden and Tabor, 1939; c.f. also Archard, 1959) and, if the heating is sufficient and the diffusion rate rapid enough, adhesion will occur at the interlocked interface. If adhesion does not occur the sheared off fragment may leave the contact region as a loose wear particle. In this theory the welding of the fragment and material transfer occur as a consequence of the friction, as opposed to the welding theory of Bowden and his co-workers, in which the friction occurs as a result of the welding.

Some recent experiments (see Clark, Connolly and Hirst,1963) have indicated that, provided the real regions of contact between the sliding surfaces are on asperities whose slopes relative to the general surface are less than an angle ϕ, the deformation at these regions of contact may be elastic. The maximum slope of an irregularity which can be elastically deformed flat into the general plane of the surface may be calculated from criteria given by Halliday (1955) and is inversely proportional to the elastic modulus. Clark, Connolly and Hirst (1963) calculated a value for ϕ of up to 15^{o} for their electrographite specimens compared with values of less than 1^{o} for metals. Hirst and Lancaster (1960) concluded that the removal of a fragment from one of the surfaces is the result of a succession of localized encounters, during which the metal beneath the surface gradually weakens, and that it is this weakening, rather than strong adhesion at the surface, which ultimately enables a fragment to be detached.

(b) The basic wear equations for metals sliding on metals.

Holm (1946) derived a theoretical expression for volume wear in terms of a welding theory and assuming the removal of material on an atomic scale. Burwell and Strang (1952) showed that wear particles may be hundreds of angstroms in diameter and, substituting surface asperities for atoms in Holm's theory, obtained the expression for volume wear given

below:-

$$v = kWd,$$

where v is the volume wear, W the applied load, d the distance slid and k a constant. Their results for the wear of a soft metal pin on a hard steel disc were in agreement with the theory. To obtain this formula they assumed plastic flow to occur at the contact regions, the total contact area A, for a given load W, being given by:-

$$A = W/p_m,$$

where p_m is the flow pressure of the softer material.

They assumed a statistical probability of a wear particle being removed from an interfacial contact. At higher loads, when the average contact pressure is greater than one third of the hardness of the pin, a large increase in the wear rate was observed. They suggested that, at these loads, the actual contact area increases so much by plastic flow that the wear particles are imprisoned on the surface, where they produce further wear particles in a self-accelerating process.

In 1953 Archard derived a similar relationship, assuming that contact occurs only at widely separated asperities. During sliding, when these asperities come into contact, there is a definite probability, K, that a wear particle will result (cf. also Archard, 1961). He assumed these wear particles to be hemispherical and of the same cross-section

as the assumed circular region of contact. With these assumptions he derived a relation for the mass loss m, as given below:-

$$m = KWd/p_m,$$

where K is dependent on the nature of the bearing surfaces. This equation agrees with the equation of Burwell and Strang, the wear rate being independent of the apparent contact area and proportional to the load. Hirst (1957) pointed out that the magnitude of K is very small and that this constant wear rate is characteristic of run-in materials indicating that either:-

(1) the opposing surface is not wearing at all, i.e. it is far harder than the other bearing surface;

or (2) the surface wears in such a way as to neither decrease or increase the severity of its attack on the mating surface;

or (3) the wear is unaffected by the surface topography.

When the damage resulting from wear is such that it further increases the wear rate, then an exponential increase of the wear with distance travelled might be expected with originally a small wear rate building up to large scale failure or seizure (Barwell, 1957a, 1957b).

The wear may then be expressed thus,

$$m = ke^{cd},$$

c and k being constants.

A different relation may hold for the state when wear decreased with distance, as in the case of running-in when the wear process removes imperfections in the surface, the wear being reduced as these irregularities are removed. Barwell (1957a) derived the relation given below for the wear rate under these conditions.

$$m = (c/a)(1 - e^{-ad}),$$

c and a being constants.

Piggott and Wilman (1957), studying wear during the running-in of mild steel on mild steel at 100 kg/cm^2 and at low speed in lubricated conditions, obtained a logarithmic relation for the mass loss,

$$m = c \log kd,$$

c and k being constants. This relation was obeyed over the whole of the running-in period, beyond which the wear rate became practically constant. This equation was shown to be compatible with the wear being of an abrasive nature, caused by the hard pearlite grains in the steel. Piggott and Wilman concluded that the wear was due mainly to the ploughing action of these grains in the softer ferrite matrix (as the observed grooves showed) and not from local welding and subsequent shearing of these junctions.

(c) The wear of materials on abrasive surfaces.

A theory of friction and wear during the abrasion of metals has been developed recently by Wilman and his co-workers (Goddard, Harker and Wilman, 1959; Avient, Goddard and Wilman, 1960; Goddard and Wilman, 1962) for various shapes of asperities ploughing along the metal surface. The theory shows good agreement with the experimental results for metals abraded on various emery papers. A linear relation was observed between M, the mass loss per unit sliding distance, and μ, at the equilibrium state of abrasion under a load W. Thus,

$$M = kW(\mu - \mu_o),$$

where k is a constant and μ_o is the intercept on the μ axis, of the M/μ linear locus.

To allow for the effects of partial clogging of the finer emery papers and of the pick-up of abrasive particles by the metal surface, it is assumed that μ_{em}, μ_{ee} and $\mu_{mo.mo}$ and f_{em}, f_{ee} and $f_{mo.mo}$ are the coefficients of friction and the fractions of the total load W supported on emery /metal, emery/emery and metal/metal contacts respectively. Then,

$$\mu = f_{em}\,\mu_{em} + f_{ee}\,\mu_{ee} + f_{mo.mo}\,\mu_{mo.mo}$$

and

$$f_{em} + f_{ee} + f_{mo.mo} = 1$$

and the wear rate M is given by

$$M = (W\rho/p'_m)\overline{(1 - a_o/a_v)}\left\{\mu_p/(\mu_{em} - \mu_{mo.mo})\right\}(\mu - \mu_o),$$

where ρ is the density of the metal, p'_m the dynamic flow

pressure of the metal, a_v the cross-sectional groove area and a_o is the equivalent part of this area that corresponds to metal displaced from the groove but remaining on the specimen, and μ_p is the ploughing component of μ. And, since p'_m is related to the hardness H_D of the metal,

$$H_D = k/(M/\rho),$$

k being a constant. The reciprocal of the volume wear rate was in fact found to be proportional to H_D. Khruschov (1957) reported a similar relation for many commercially pure metals in the annealed state abraded on corundum particles. Previous work hardening failed to increase their resistance to wear. Experimental results also agreeing with this theory have been obtained for various non-metals by Porgess and Wilman (1959), King and Wilman (1961, 1962b) and Dobson (1961).

(d) Further particular cases of the continuous wear process.

The wear of unlubricated metals against each other may be of mild or severe form. Widespread intermetallic welding occurs in severe wear and metal is removed in large fragments by the rupture of these contact junctions (Hirst 1957). In mild wear the wear detritus may be only 100 Å in diameter. These small wear particles result from oxide or other films being formed on the surfaces and preventing intermetallic contact and welding. These films are self perpetuating and the conditions for easy oxide film formation are those for

sustaining mild wear.

Lancaster (1957), considering the wear rate of 60/40 brass on tool steel, observed an increase of wear rate with temperature, resulting from the reduction of hardness of the brass with temperature rise. Low sliding speeds were used to keep the frictional heating small and the temperature was varied by external heating.

Radioactive tracer wear experiments by Kerridge (1955), for a soft metal sliding on a much harder one, showed that a dynamic equilibrium of metal transfer was reached, the soft metal transferred subsequently being oxidized and removed as wear particles. Thus the wear rate was determined by the rate of oxidation and not by the initial transfer rate. For brass on steel the transferred brass fragments grew to many times their original size before becoming detached as wear particles (Kerridge and Lancaster, 1956).

When hard tool steel was slid on hard tool steel, junctions were formed initially, with small metal transfer and general smoothing of the surface asperities until the surfaces were separated by aggregates of wear particles. The wear was then defined by the abrasion of the surfaces by the wear particles (Archard and Hirst, 1957).

The experiments of Hirst (1957), on the wear rate and hardness of pins of various metals sliding in severe wear

conditions on a hardened tool-steel annulus, showed that the wear increased more rapidly than the hardness decreased.

Hughes and Spurr (1955) investigated the relation between wear rate and hardness for a low melting-point wax sliding against a cast-iron disc. The wear rate and the temperature of the wax sliding surface were measured at various loads and speeds of sliding and the hardness of the wax at various temperatures was then determined. They reported that the wear increased linearly with distance of sliding and that it was inversely proportional to the hardness of the wax.

Many workers (e.g. Slawson and Kohn, 1950; Wilks, 1952; Hukao, 1955) have studied the anisotropy of the wear-rate of diamond on diamond with crystal orientation and abrasion direction. For example, Kenyon (1954) showed that the wear-rate in the $\langle 100 \rangle$ direction is greater than in the $\langle 110 \rangle$ direction on a $\{110\}$ surface. Also the direction of easy abrasion is the direction of highest friction whilst that of least abrasion is the direction of lowest friction. $\{110\}$ surfaces are abraded more readily than $\{100\}$ surfaces (Wilkes, 1952).

Anisotropic wear of diamond on glass was observed by Scott (1957), the wear being greatest for sliding in a "soft" direction of the crystal face. There was a rapid

increase of wear with increase of speed of sliding. In general, sliding in dry atmospheres led to a higher wear rate with the production of amorphous carbon on the surface, indicating very high temperature flashes. A high wear rate at high speeds was obtained in a nitrogen atmosphere also, so the wear process was unlikely to be thermal oxidation. No fragmentation was observed and it was deduced that carbonisation was the most likely wear process.

Steijn (1961, 1962) determined the wear resistance of single crystals of synthetic sapphire (α- Al_2O_3) abraded on a sintered tungsten carbide plate as a function of crystallographic orientation with respect to the plane of wear and to the rubbing direction. Distinct anisotropy was found, the wear being highest when the rubbing face was parallel to the basal plane. For abrasion on other faces low wear resulted on abrasion perpendicular to the c axis, whilst chipping and conchoidal fracture resulted on abrasion parallel to the c axis. Plastic deformation occurs at room temperature, both basal and prismatic slip systems being operative, although in conventional deformation tests, these slip systems do not operate until very high temperatures (1000°C for basal slip, 1800°C for prismatic slip) are reached.

Duwell (1962) also studied the friction and wear of spherical single crystals of sapphire, sliding on a wet surface and observed a variation of the wear rate with azimuth by more than three orders of magnitude, and the friction coefficient by a factor of three. The wear rate was greatest when the crystal structure offered least resistance to shear parallel to the sliding surface and in the direction of slide. He concluded that wear of sapphire on steel proceeds by shear through the sapphire.

1.8. Methods of Measurement of the Hardness of Crystals and Polycrystalline Materials.

Hardness may be defined generally as the resistance to penetration. This resistance depends on the crystal face examined and the direction of motion across the face for single crystals. Tertsch (1949) reviewed many such hardness determinations. The numerical values of hardness depend on the method of determination, the chief methods being the determination of scratch hardness, indentation hardness and rebound or dynamic hardness. The theory and experimental techniques of these methods are discussed lucidly by Tabor (1951) and Mott (1956).

Scratch hardness was the earliest form of hardness determination and depends on the ability of one solid to scratch another or to be scratched by it. Mohs (1822) developed the first practical hardness scale. Later Seebeck (1833) measured hardness in terms of the load on a crystal required to produce a just-visible scratch when moved across the specimen. Hardness may also be determined in terms of the reciprocal of the volume wear rate under a given load. Tertsch (1949) described such measurements on calcite cleavage faces, illustrating the variation of hardness with direction.

The dynamic hardness may be measured directly by dropping the indenter onto the specimen, the hardness being described in terms of the energy of impact and size of the

remaining indentation (Martel, 1895) or the height of the rebound (Shore, 1918).

The hardness of metals is determined chiefly by indentation methods. In the Brinell hardness test (Brinell, 1900) a hard, spherical indenter is pressed under known normal load against a smooth surface of the specimen under examination. After about 30 seconds the load and indenter are removed and the diameter of the permanent indentation of the specimen is measured. The Brinell hardness number (B.H.N. or H_B) is defined as the ratio of the load to the curved area of indentation:-

$$\text{B.H.N.} = H_B = 2W/\pi D\left\{D - \sqrt{(D^2 - d^2)}\right\} \text{ kg/mm}^2,$$

W being the load in kg, d the mean chordal diameter and D the diameter of the spherical indenter, both in mm. In fact it is more satisfactory to use the projected area of the indentation in this ratio, as this is the area over which the load is applied (Meyer, 1908). The hardness then is M.H.N. = $4W/\pi d^2$ kg/mm^2. Nowadays a diamond pyramid indenter of standard apex angle is generally used (dihedral angle between two opposite pyramidal faces = $2\theta = 136^\circ$). In this case the hardness is referred to as the Vickers diamond hardness (V.D.H. or H_D) and is the ratio of the load to the pyramidal area of indentation:-

$$H_D = 2W \sin\theta/d^2 \quad \text{kg/mm}^2.$$

EXPERIMENTAL.

2. Experimental.

2.1. Materials.

Single crystal specimens of silicon and calcite have been examined in the present electron diffraction and optical microscope study of the surface deformation resulting from unidirectional abrasion. The silicon crystals were kindly provided by Standard Telecommunication Laboratories Ltd., Harlow.

The wear and friction experiments were performed by sliding the specimens on emery papers of various grades manufactured by Messrs. J. Oakey & Sons Ltd., London, and Messrs. Hubert, France. Table 2 lists the typical chemical analysis of the emery and the mean particle size of each grade of abrasive. The emery particles are of rather obtuse angular shape and reasonably uniform diameter for any particular grade, corresponding well with the values given in Table 2. Figs. 8(a) to 8(f) show typical micrographs of particles from various grades of emery papers, from which the glue and paper backing was dissolved in water and then the emery particles were examined by transmission in the Vickers projection microscope.

The AgCl and AgBr, used for the compression and rolling texture determinations, were obtained from Messrs. Hopkin & Williams Ltd., and the purity was stated to be 99.8%. The granular material (0.1 to 2 mm diameter granules) was

Table 2. Emery Paper Data.

The data given below was supplied by Messrs.J.Oakey and Sons Ltd., and applies to their "emery polishing papers".

(a) Typical chemical analysis of emery.

Al_2O_3 .. 62.18%, SiO_2 .. 12.30%, α-Fe_2O_3 .. 18.33%

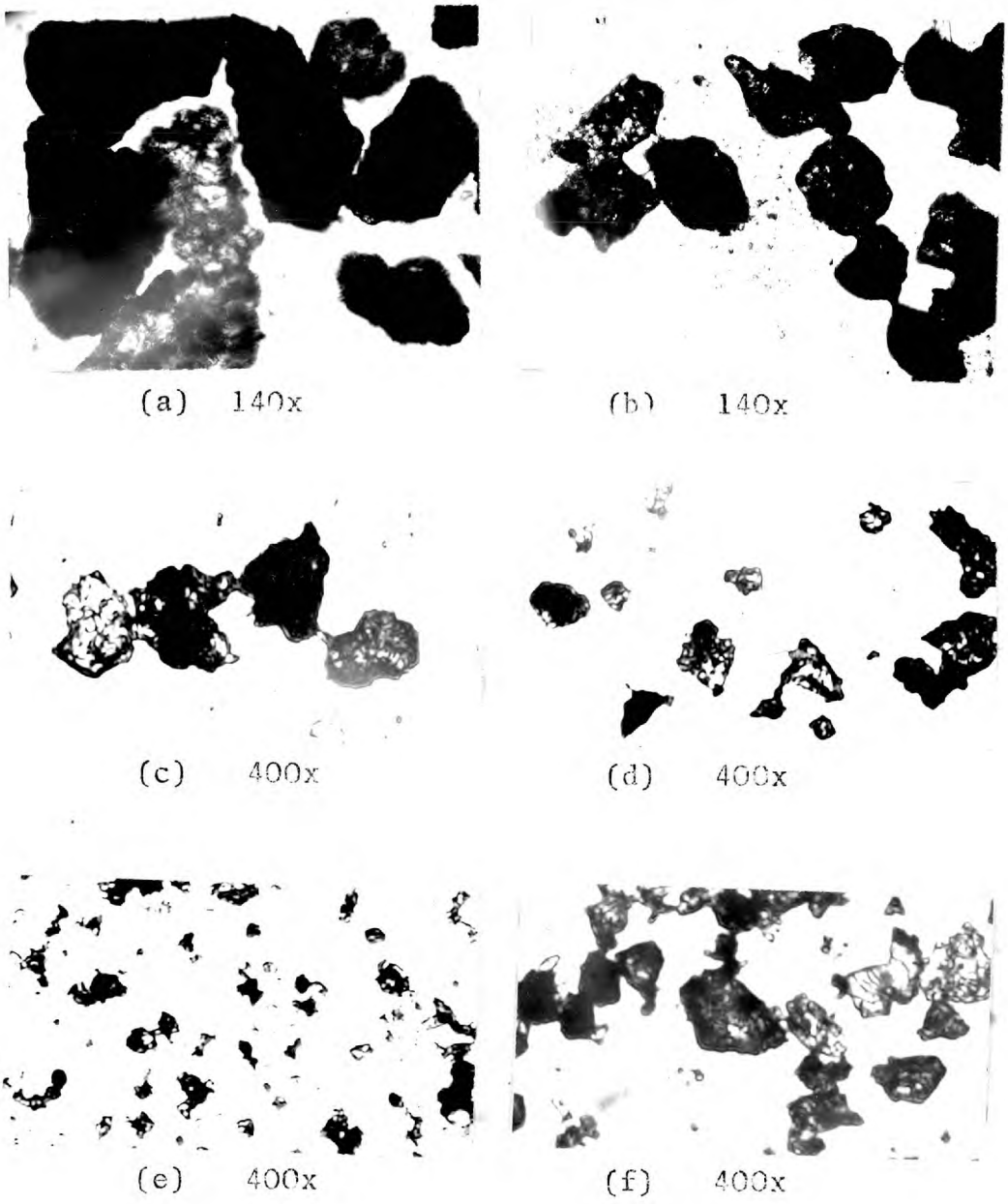
CaO, MgO .. 4.87%

(b) Mean particle size of emery on various grades of emery paper.

Emery paper grade	Mean particle size (microns)
4/O	5
3/O	10
2/O	15
O	35
1F	40
1	45
1M	50
1G	70
2	100
3	150

Grade O_H, $2/O_H$ and $3/O_H$ emery papers, manufactured by Messrs. Hubert, have mean emery particle sizes within the range 15 to 35 microns.

Fig. 8. Typical abrasive emery particles.



(a) 140x (b) 140x

(c) 400x (d) 400x

(e) 400x (f) 400x

(a) Grade 3 emery (mean particle size 150 microns);
(b) 1G emery (70 microns); (c) 0 emery (35 microns);
(d) 2/0 emery (15 microns); (e) 4/0 emery (5 microns);
(f) $2/0_H$ emery ($\simeq$ 20 microns).

All Oakey's emery papers except (f) which is a Hubert paper.

compressed at 32 tons/sq.in, in a die of stainless steel of internal diameter 0.5 inches (1.3 cm). The specimens obtained were 0.2 to 0.5 cm thick.

Specimens of about 1 cm diameter and 0.3 cm height were also prepared by melting and resolidifying the halide on a glass slide, and were used as starting material for rolling, and also for compression between oil-lubricated polished steel flats in a vice. In these cases the specimens were reduced to less than 20% of the initial thickness. The rolling was done in about 20 stages in the same direction, without reversal, and without lubrication between the highly polished steel rollers, which were $2\frac{1}{2}$ inches in diameter.

2.2. Etching Procedure.

Different etchants were required in the present work for two different purposes. Firstly, a fast etch was required to remove the worked surface regions containing the embedded emery particles picked up by the specimen surface during abrasion on a particular grade of emery paper. These particles must be removed before satisfactory wear and friction measurements can be taken for abrasion on another grade of emery paper, hence a depth of a few microns must be removed by etching.

Secondly, a much slower etch was required for the electron diffraction examination of the underlying regions of the abraded surfaces. Under these circumstances it may be required to etch the surface only a few hundred angstroms. Silicon. As only the abraded surface was to be etched the remainder of the crystal was masked with a protective rubber paint (Red Grade "A", supplied by Detel Products Ltd.). The etchants were mixtures of concentrated HNO_3 (Analar, specific gravity 1.42 g/cc) and HF (Analar, 40%). Polythene containers were used throughout and the crystal was placed in a perforated holder used to stir the etchant at an approximately constant speed, since speed of stirring is known to affect considerably the etch rates of silicon (Klein and D'Stefan, 1962). The etchant was then quickly diluted with

distilled water and the specimen was removed, thoroughly washed in distilled water and then in propyl alcohol, and then desiccated.

For etching the specimen during the abrasion experiments a 1 : 5, HF : HNO_3 etch was used, having an etch rate of approximately 20 microns/minute. For the electron diffraction experiments two etches were used, 1 : 50 and 1 : 200, HF : HNO_3 having etch rates of approximately 2 and 0.5 microns/minute respectively, on an abraded $\{111\}$ face.

Calcite. For the abrasion experiments a solution of N/5 HCl was used, having an etch rate of approximately 20 microns/minute, whilst for the electron diffraction examination a solution of N/100 HCl was used, etching away approximately 2 microns/minute. The washing and drying procedure was the same as for the silicon crystals.

Silver Halides. A 0.1% aqueous solution of KCN was used to etch the silver halides for electron diffraction examination, this etchant removing the surface of both halides at about 2,400 Å/minute when freshly prepared.

2.3. Determination of the Wear Rate.

Wear determinations were made for silicon and calcite sliding on various emery papers. The emery paper was placed on a clean sheet of plate glass, the cleanliness of this glass and the sheet of emery paper being extremely important, particularly for the finer emery grades. The specimens were run-in on the grade of emery paper being investigated, the paper being flooded with propyl alcohol to virtually eliminate any pick up of emery, until the specimen surface had attained a roughness characteristic of that grade of emery paper. The specimen was then desiccated and weighed.

Wear rates on the dry emery papers were then determined directly by mass loss using an Oertling semi-micro balance. The specimens were always slid on fresh emery paper under 1 kg load and at about 5 cm/sec.

2.4. Determination of the Coefficient of Friction.

The frictional force exerted on the specimens sliding on various grades of dry emery paper was determined as simply as possible by the weight required, at the end of a thread passing over a low-friction pulley, to produce non-accelerated motion of the loaded specimen at approximately 5 cm/sec. The friction was normally determined at the same time as the wear and on the same abrasive sheet, so that the sliding conditions for both the wear and the friction experiments were identical.

2.5. Hardness Measurements.

The Vickers indentation hardness (see section 1.8.) of the specimens was determined using a Vickers micro-indentation hardness tester with pyramidal diamond indenter fitted to the Vickers projection microscope used for the optical examination of the specimens.

The specimens were surfaced on the fine grade emery papers, so that it was the hardness of the abraded surfaces which was measured for comparison with data from the abrasion experiments. The value of the applied load was chosen so that the resulting indentation was much greater than the width of the surface abrasion grooves.

2.6. Examination by Optical Microscopy.

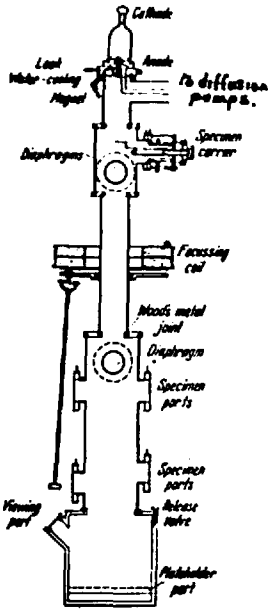
The physical nature of the specimen surfaces and changes to these surfaces on unidirectional abrasion were examined on a microscopic scale, by means of a Vickers projection microscope, using both reflection and transmission methods. The reflection method was used to study silicon and the transmission method for calcite. The size and shape of the abrasive particles were also studied.

2.7. Examination by Electron Diffraction.

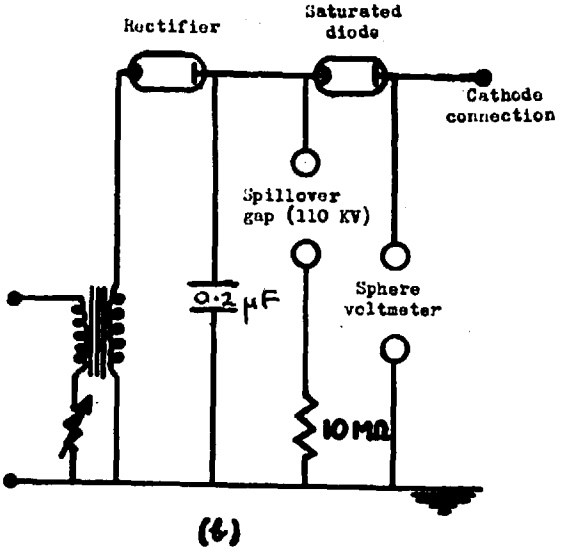
Electron diffraction techniques have been used since 1927 to study the composition and orientation of crystals and deposits. For full details of the diffraction of electrons by crystalline materials and the interpretation of the resultant electron diffraction patterns, reference should be made to the standards texts, e.g. Thomson (1930); Finch, Quarrell and Wilman (1935); Beeching (1936); Finch and Wilman (1937); Thomson and Cochrane (1939); Pinsker (1949, 1953); Wilman (1948a,1948b, 1950, 1951, 1952).

The Finch type of electron diffraction camera, described by Finch and Wilman (1937), was used in these present experiments (see Fig.9), but with oil diffusion pumps and "O" ring rubber seals. An electron-accelerating potential of 50 - 75 kV was used and a camera length (distance between the specimen and the photographic plate) of approximately 50 cm.

The electron beam will only penetrate a few thousand angstroms of the material in the beam direction and, when it is used at grazing incidence of about 1^{o} to the mean surface plane (i.e. the "reflection" method), the penetration normal to the surface is only about 50 - 100 Å, even when the material is made up of light, weakly-scattering atoms, or less for highly polished surfaces. For roughened surfaces, as obtained in abrasion experiments, the pattern is formed



(a)



(b)

Fig. 9. Diagrams of (a) the electron diffraction camera, (b) the high tension supply.

mainly by transmission (at nearly normal incidence) of the electrons through the surface projections.

(a) Patterns from randomly-orientated and one-degree orientated polycrystalline specimens.

The patterns obtained from randomly orientated polycrystalline surfaces may be interpreted in terms of Bragg reflections of the primary beam by net planes in the crystal such that $n\lambda = 2d \sin\theta$, λ being the wavelength of the electrons, d the net plane spacing and θ the angle between both the incident and the reflected beams and the net plane. Thus the reflected beams lie on cones of semi-apical angle 2θ which intercept the plane normal to the electron beam (e.g. the plane of the photographic plate) in a series of circles (Debye-Scherrer rings) whose radii are given by :-

$$R = \lambda L/d,$$

where L is the camera length.

Suppose the surface examined has a one-degree orientation, i.e. the crystallites are orientated with a certain axis $[UVW]$ in common and normal to the electron beam, with random azimuthal distribution about this axis. Then the resultant diffraction pattern consists of short arcs at the intersection of the appropriate "layer lines", which are normal to the projection of the $[UVW]$ direction, with the

Debye-Scherrer rings. The separation of these layer lines is $\lambda L/T_{UVW}$, where T_{UVW} is the lattice translation along the [UVW] direction. Diffraction arcs will occur at the intersection of these layer lines with the rings, subject to the condition that for the layer line of order h' and the h k l ring the relation $h' = hU + kV + lW$ is satisfied.

The orientation may be described by stating either the indices (HKL) of the net plane which is normal to the rotation axis, this plane being usually but not always parallel to the surface; or those of the rotation axis [UVW]. Wilman (1952) has derived the general relationship between this normal and the plane. For cubic lattices this relation reduces to:-

$$U : V : W = H : K : L,$$

and for hexagonal lattices to:-

$$U : V : W = 2H + K : H + 2K : 3La^2/2c^2.$$

If the orientation is very strong then the pattern consists of very short arcs or spots; if it is only weakly developed then the arcs are spread out along the rings. Thus the angular spread of these arcs is a measure of the spread of orientation of the crystallites from the mean orientation. In some cases there may be a combination of two such orientations present in the specimen. In unidirectionally-abraded surfaces an orientation may be developed with its

axis tilted away from the surface normal. However, the above theory still applies.

(b) Examination of surfaces.

The surfaces of the single crystals were examined in the electron diffraction camera both in the unabraded state, to determine the azimuthal orientation of the single crystals, and after unidirectional abrasion on a particular grade of emery paper. Loose wear debris was removed from the abraded surface by gentle brushing before the specimen was examined in either the electron diffraction camera or the microscope. The specimens were always abraded under a load of about 1 kg at about 15 cm/sec.

The abraded surface was examined with the electron beam perpendicular to the abrasion direction, parallel to the abrasion direction and at an angle of 30° or 45° to the abrasion direction. Similar examinations were made at various stages of etching of the abraded surface.

The polycrystalline silver halide specimens were likewise examined before compression or rolling to determine whether the specimens had any initial texture, and then after the deformation. Similar examinations were made after etching the surface. These specimens were also examined using X-ray diffraction (see section 2.8.).

2.8. Examination by X-Ray Diffraction.

The compression and rolling textures of AgCl and AgBr were studied by X-ray diffraction because the X-ray beam has a depth of penetration many orders of magnitude greater than the electron beam, and therefore bulk textures, rather than surface textures, of the specimens may be investigated. Use of the X-ray apparatus was by kind permission of Dr. G.S. Parry of this department. The wavelength of the molybdenum Kα radiation (with Zr filter) was 0.7107 Å, the applied voltage 50 kV and the current 10 mA. The X-ray beam was at about 10° grazing incidence, and photographic recording was on a flat film 4 cm from the specimen. Patterns were also obtained at normal transmission from a thin rolled sheet of AgCl ($\simeq$ 0.07 mm thick).

RESULTS AND DISCUSSION.

3. Results and Discussion.

The experimental results are considered in three groups (silver halides, calcite and silicon) and, for convenience, the discussion of the results for each material directly follows the results concerned.

The results for the silver halides are described first (sections 3.1. and 3.2.), since these non-metals are readily plastically deformable and deform during abrasion, compression and rolling in a similar manner to most metals. These results show that the previously observed abrasion texture for AgCl and AgBr (King, 1960; King and Wilman, 1961) is closely related to both the rolling texture and the compression texture that is observed when extensive lateral flow is permitted.

Secondly, the abrasion of single-crystal calcite is studied (sections 3.3. and 3.4.), calcite being a good example of a readily-cleavable material of medium hardness (H_D = 140 kg/mm^2). The abrasive wear of calcite is seen to involve considerable brittle fracture, which extends beyond the regions of contact between the abrading particles and the calcite surface. Finally, in sections 3.5. and 3.6., the results of the abrasion of single crystals of silicon are considered, silicon being very brittle at room temperature like calcite, but being considerably harder (H_D = 1050 kg/mm^2).

3.1. The Rolling and Compression Textures of AgCl and AgBr.

The rolling and compression textures of AgCl and AgBr were determined using specimens as described in section 2.1. in order to understand more fully the nature of the surface re-orientation caused by unidirectional abrasion. These materials are particularly plastically deformable and the deformation textures have been determined by X-ray and electron diffraction methods as described in section 2.8. and section 2.7.

3.1.1. The orientation of rolled AgCl.

Five different specimens, prepared by melting and resolidifying the halide on a glass slide, were rolled without lubrication between highly polished steel rollers ($2\frac{1}{2}$ inch diameter). They were then examined by X-ray diffraction with the beam normal to the rolling direction, and at about 10^{o} grazing angle to the rolling plane of the specimen for examination by reflection. Figs.10 to 13 were obtained by such examination, whilst Fig.14 is a transmission pattern with the X-ray beam normal to the rolling plane.

The direction of motion of the halide strip during rolling was from left to right in Figs. 10 to 13. Fig.10,

Figs.10 to 14. X-ray diffraction patterns from rolled AgCl. (Mo K α radiation; flat plate at 4 cm from specimen.)

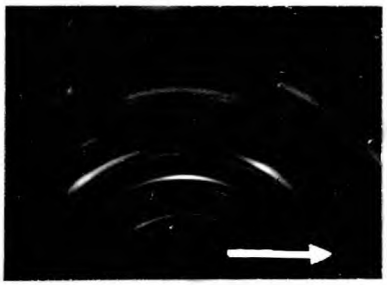


Fig.10.

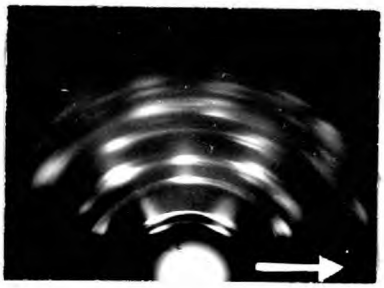


Fig.11.

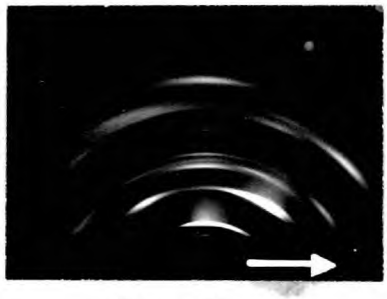


Fig.12.

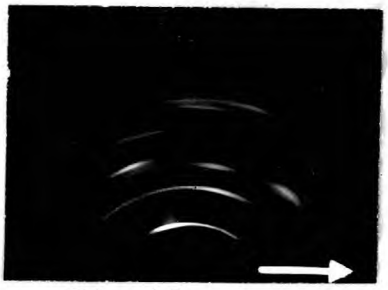


Fig.13.

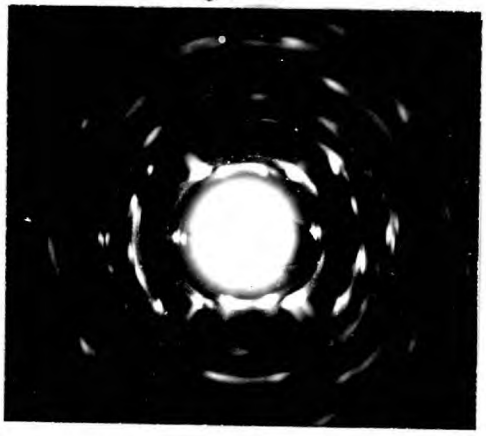


Fig.14.
Rolling direction vertical (bottom to top).

Direction of motion of the AgCl strip during rolling was from left to right in Figs.10 to 13.
Fig.10. 60% reduction; Fig.11. 90% reduction;
Figs.12 and 13. 80% reduction;
Fig.14. 97% reduction.

from a specimen rolled to 60% reduction, shows the basic orientation to be such that a {110} plane is parallel to the rolled surface or nearly so. This plane gives rise, by Bragg reflection of the primary beam, to the 220 arc centred on the plane of incidence. The other strong arcs in the pattern lie on layer lines (horizontal in Fig.10) corresponding to a range of lattice rotation azimuthally round this {110} plane normal, i.e. round the common ⟨110⟩ axis of orientation of the crystal grains of the rolled sheet, as may be seen by comparing Fig.10 with Fig.14 (neglecting the triangular symbols there). Some less strong arcs are also present which correspond to twinning of the above main orientation on {111} planes (cf. Fig.10 and the triangular symbols of Fig.14). Fig.11, from a specimen rolled to 90% reduction, shows the same basic {110} orientation still more strongly developed, and with very strong {111} twinning.

The positions of the short diffraction arcs in Fig.11 are displaced appreciably round the ring positions as compared with those of the corresponding reciprocal-lattice points shown in Fig.15; and the horizontal layer lines become slightly curved instead of being straight. This is due to the relatively large Bragg angle at which reflection of the primary X-ray beam occurs (as compared with the Bragg angle for electrons), together with the fact that the beam is incident on

the specimen at about 10^{o} grazing angle. For example, the radii to the two 111 diffractions in Fig.11 enclose an angle of approximately 65^{o} (as compared with 70^{o} 32' between the corresponding points in Fig.15) and this agrees with the angle estimated for this diffraction in the present case. These 111 diffractions would only occur at an azimuth approximately 35^{o} from the main lattice orientation, which has a $\langle 1\bar{1}2 \rangle$ direction along the rolling direction (see below).

The 200 diffraction arcs lying above these 111 arcs (and the 400 arcs also) are clearly due to $\{111\}$ twinning. They correspond in their positions and their relatively strong intensity, to a cube face of the twins concerned being very close to the position required for Bragg reflection, already at an azimuthal orientation of the initial lattice near the main $\{110\}\langle 1\bar{1}2 \rangle$ orientation of the rolled strip, especially in view of the observed $\pm$ 10 - 15^{o} spread of orientation round the rolling direction (see below relative to the transmission pattern, Fig.14). The combination of this rotation round the rolling direction, and the $\simeq 35^{o}$ azimuthal rotation round the normal to the $\{110\}$ rolling plane, is also seen to be responsible for the drawing out of these 200 diffractions towards the plane of incidence, and their coalescence there. The 111 arcs, however, are

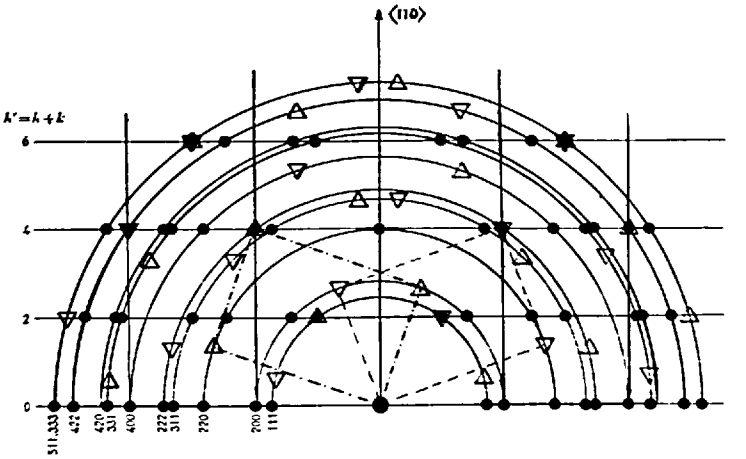


Fig.15. Diagram showing the reciprocal-lattice points corresponding to the diffractions observed in the reflection patterns Figs.10 and 11. The filled-in circles represent the lattice-points in the main reciprocal-lattice planes passing through the vertical ⟨110⟩ rotation axis which is normal to the rolling plane. The full-line centred-√2-rectangle array corresponds to a vertical {110}* type of plane. The triangles indicate the centred-√2-rectangular arrangement of the lattice points (shown by broken lines) in the corresponding {110}* planes of two octahedral twins relative to the initial lattice; these rectangles have one diagonal coinciding with a diagonal of the full-line rectangles.

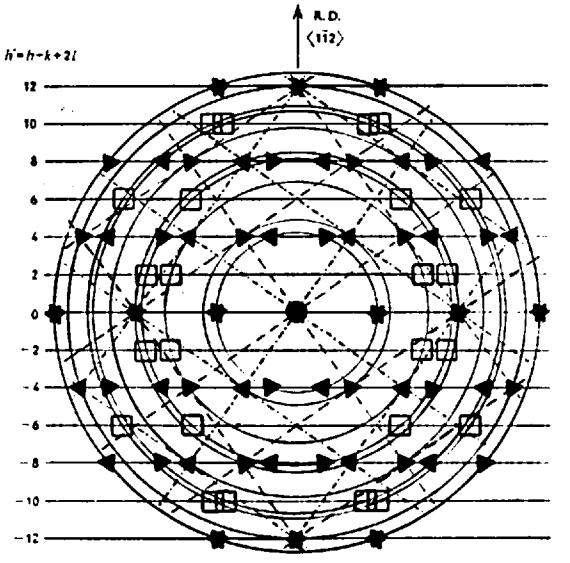


Fig.16. Reciprocal lattice points corresponding to the diffractions in the transmission pattern of Fig.14. The triangles correspond to the two centred-√2-rectangle arrangements (shown by the broken lines) of the points in the {110}* reciprocal-lattice planes parallel to the rolling plane, in the two symmetrically disposed {110}⟨1$\bar{1}$2⟩ lattice orientations. The positions denoted by □ show where other recirrocal-lattice points cross this plane as a result of rotation of these lattices by ±10-15° round the rolling direction, which is vertical. Laue indices for ring position as in Fig.15.

not elongated in this way because the corresponding $\{111\}$ planes are much more inclined (at 35° 16') to the rolling plane, and the rotational spread round the rolling direction is small compared with this angle. Similar considerations account for the relatively strong 311 arc which is centred on the plane of incidence in Fig.11, and is also due to the $\{111\}$ twins.

Some photographs show the above type of orientation except that the $\langle 110 \rangle$ axis is inclined away from the specimen surface normal towards the leading edge of the rolled strip. For example, in Fig.12 this tilt is about 10°, and in Fig.13 it is about 30°, although otherwise these patterns are closely analogous to Fig.11.

In order to determine the preferred lattice direction aligned along the rolling direction, transmission photographs such as Fig.14 were obtained with the beam normal to the rolled strip. These showed extremely strong azimuthal orientation of the crystal grains, with a $\{110\}$ plane parallel to the rolled strip and a $\langle 1\bar{1}2 \rangle$ lattice row along the rolling direction. The two equivalent lattice orientations of this type are symmetrically disposed and occur with equal probability. The strongest spots in Fig.14 are indeed seen to correspond to reciprocal-lattice points forming two centred-$\sqrt{2}$-rectangle arrays, in the $\{110\}^*$ planes (that is,

$\{110\}$ planes in the reciprocal lattice) of these two orientations, as is shown in Fig.16. These $\{110\}^*$ planes are parallel to the plane of the rolled strip. The simultaneous presence of all these diffractions indicates a range of rotation of the order of $\pm$ 10° about the rolling direction.

The additional less strong diffractions in Fig.14 lie on intermediate horizontal layer lines and indicate a similar range of about $\pm$ 10 - 15° of lattice rotation about the rolling direction, away from the mean. They correspond to reciprocal-lattice points lying on the intermediate planes of $\{1\bar{1}2\}^*$ type which are normal to the rolling direction, and these are indicated in Fig.16 in the positions where they would cross the above $\{110\}^*$ plane.

The reflection patterns in Figs.10 and 11 show an azimuthal spread of more than $\pm$ 35° away from the mean orientation, and this is evidently because the X-ray beam impinges (at $\simeq$10° grazing incidence) on a much larger area of specimen than in the transmission case, and because the direction of plastic flow varies appreciably in different regions. Although twinning of the main $\{110\}\langle 1\bar{1}2\rangle$ orientation on $\{111\}$ planes normal to the rolling plane would introduce other azimuthal orientations, this would not affect the above conclusion of about $\pm$ 35° azimuthal spread being

present. If such twinning on these particular {111} planes were present, however, it would lead to 200 diffractions at the same level as the 111 diffractions in Figs.10 and 11; but absence of 200 arcs in these positions indicates little such twinning. The {111} twinning is thus mainly on the {111} planes which are inclined to the rolling plane and rolling direction at only a relatively small angle, i.e. 35^{o} 16' to the rolling plane.

3.1.2. The orientation of AgCl and AgBr compressed between lubricated flats.

Figs. 17 to 19 are typical of the X-ray diffraction patterns obtained from the surfaces of the specimens compressed between oil-lubricated polished steel flats in a vice. They are clearly similar to Fig.10, showing the orientation to be of the same type, with a ⟨110⟩ direction parallel to the compression axis, i.e. normal to the surface. This ⟨110⟩ compression texture was observed after compression (see section 2.1.) of specimens initially resolidifed from the melt, and of specimens initially prepared by compacting the granular material in a die.

As in Figs.10 and 11, Figs. 17 to 19 contain arcs which show the presence of extensive {111} twinning of the main ⟨110⟩ orientation. The presence of considerable intensity of the 200 arc in Fig.17, at the same horizontal

Figs. 17 to 19. X-ray diffraction patterns from AgCl and AgBr compressed between lubricated flats.

Fig.17.
AgCl.

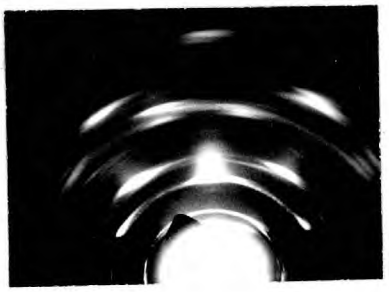


Fig.18.
AgCl.



Fig.19.
AgBr.



level as the 111 arcs, is noticeable as compared with the absence of such 200 diffractions in Figs.10 and 11. The occurrence of these and other arcs on the layer lines shows complete azimuthal randomness of the lattice orientation, which is indeed to be expected in the present case. The radial outward flow of material past the compressing surfaces during compression is evidently closely similar in type to that occurring in the rolling direction when the material is rolled. Compression under these conditions allowing extensive lateral flow is thus effectively equivalent to rolling simultaneously in all directions radially.

3.1.3. The orientation of granular AgCl and AgBr compressed in a die.

Figs. 20 and 21 from the AgCl and AgBr, respectively, are typical of the electron-diffraction patterns obtained from the surfaces exposed by etching the ½ inch diameter compressed specimens (compressed in the die at 32 tons/in^2) to about 1 μ depth. These are closely similar in type to the X-ray patterns such as Figs.22 and 23, which are from etched surfaces of AgCl and AgBr, respectively; and the X-ray patterns from unetched specimens were similar to Figs.22 and 23 except that the arcs were of slightly weaker intensity.

Comparison of Figs.20 and 21 with Fig. 24 shows

Figs.20 to 24. Electron diffraction and X-ray diffraction patterns from granular AgCl and AgBr compressed in a die.

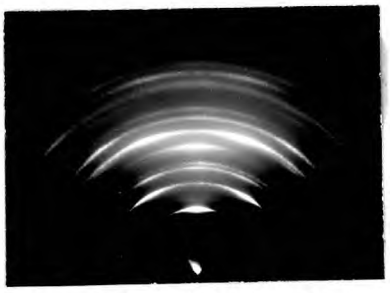


Fig.20.AgCl (E.D.)

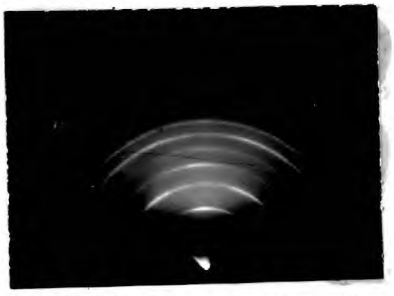


Fig.21.AgBr (E.D.)



Fig.22.AgCl (X-ray)



Fig.23.AgBr (X-ray)

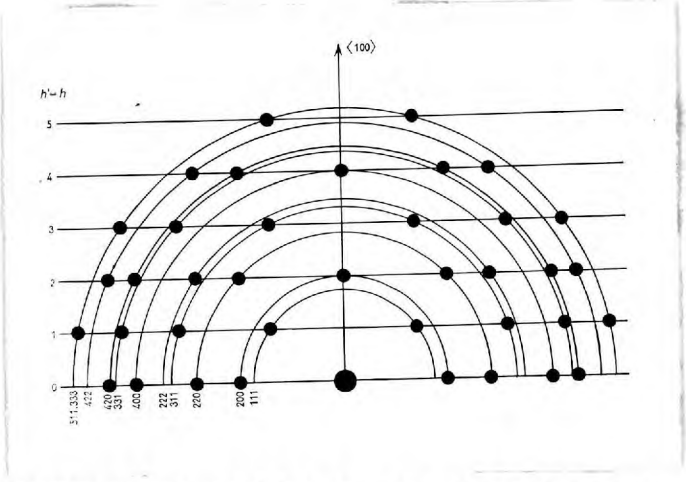


Fig.24. Theoretical diffraction positions in electron diffraction reflection pattern from a one-degree ⟨100⟩ - oriented f.c. cubic structure.

that most of the strong arcs correspond to a well-developed one-degree orientation with the ⟨100⟩ axis normal to the surface, i.e. along the compression axis. This ⟨100⟩ texture was also observed from alkali halides of the NaCl structure type, compacted similarly (Dobson and Wilman, 1961).

In Figs. 20 and 21, and all the similar photographs obtained, there is however a 222 diffraction arc slightly displaced away from the plane of incidence, and strong 220 arcs at a level much higher than the 220 arcs associated with the ⟨100⟩ orientation, cf. Fig.24. At first sight these diffractions suggest the presence of a moderate proportion of the halide oriented with a ⟨111⟩ axis along this slightly oblique radius of the 222 diffraction arc. This would lead to an angle of $70\frac{1}{2}^{o}$ between the radii to the centres of these 220 arcs, however, whereas in all the patterns (e.g. Figs.20 and 21) this angle is estimated to be nearer to 60^{o} than 70^{o}. This observation, together with the noticeable displacement of the 222 arc away from the plane of incidence, and the strong similarity of the positions of these arcs to those in Fig.13, indicate that the best interpretation is that they are due to a ⟨110⟩ orientation with the ⟨110⟩ axis inclined away from the specimen normal by about 30^{o} as in Fig.13. Such an orientation seems quite likely to be developed in part, in the present case, due to considerable lateral flow of the

granules past the compressing end of the die, into the neighbouring voids between the granules.

To test whether this auxiliary texture was also developed when finer particles were used in the die, a specimen was prepared from AgBr of mean particle diameter 0.3 mm., and a practically identical pattern was obtained.

3.2. Discussion of the Rolling and Compression Textures of AgCl and AgBr.

The results described in section 3.1. show that AgCl and AgBr develop preferred orientations when rolled or compressed, analogous to the well-known deformation textures observed in metals (see Table 1, for such textures).

The $\{110\}$ rolling texture is often very strongly defined in its azimuthal orientation, and this is clearly determined, particularly from the transmission X-ray patterns, as having a $\langle 1\bar{1}2 \rangle$ lattice direction aligned along the rolling direction. This texture is the same as the principal texture of cold-rolled face-centred cubic metals (see, for example, Barrett, 1952; Hu and Cline, 1961). In these metals the normal slip system is of $\{111\}\langle 1\bar{1}0 \rangle$ type and in AgCl it is along $\langle 1\bar{1}0 \rangle$ but of 'pencil glide' type (Nye, 1949). The observed twinning on the $\{111\}$ planes which are not steeply inclined to the rolling plane seems to correspond to the greater resolved shear component of the stress on these planes than on the other two octahedral planes.

During the rolling process there is interfacial slip between the rolled strip and the metal rollers because of the acceleration of the strip as it passes between the rollers, and there are frictional forces on the strip, at its interface with the rollers (see van Rooyen and Backofen, 1957; Capus and Cockcroft, 1962). Surface irregularities on the rollers

will therefore plough through the strip as it is rolled. This action is very similar to the ploughing of abrasive emery particles through the specimen surface during the abrasion of the material on emery papers (see below).

Furthermore, in the present results, the variation in the angle of tilt of the $\langle 110 \rangle$ orientation axis away from the rolling-plane normal (from 0°, Figs.10 and 11, to $\simeq 30^{\circ}$, Fig.13) may be compared with the tilt ($\simeq 20^{\circ}$) observed in AgCl and AgBr abraded unidirectionally on 4/0 emery paper. This emphasises the similarity between the abrasion and rolling processes.

In the abrasion of AgCl and AgBr (King and Wilman, 1961) the $\{110\}$ orientation developed has a mean preferred azimuthal orientation with a $\langle 1\bar{1}2 \rangle$ direction, or a direction close to this, along the abrasion direction; thus the 'abrasion texture' is closely similar to the rolling texture and indicates a similar nature and direction of the plastic flow. The $\langle 110 \rangle$ axis of the abrasion texture is also in general inclined away from the specimen normal, back towards the direction from which the abrasive particles came. This tilt can be correlated approximately with the direction of the resultant compressive stress (normal load + tangential force overcoming friction) exerted by the indenting particles (King, 1960; King and Wilman, 1961).

The correspondence in type between the $\{110\}$ rolling texture and the $\{110\}$ compression texture, observed when extensive lateral flow is permitted, is understandable, since the compression causes a radial flow of material similar to that which would be obtained if the material were rolled simultaneously radially in all directions. Previous determinations of compression textures of metals have evidently been made using compression in this way between lubricated parallel plates; but the present results show that a different texture is in general expected when lateral flow is severely limited as in compacting materials in powder form in a die. Such compression of the AgCl and AgBr led to a strong $\{100\}$ orientation like that found (Dobson and Wilman, 1961) in similarly compacted alkali halides of NaCl structure type, which normally slip on $\{110\}$ planes along $\langle 1\bar{1}0\rangle$ directions. Similarly, these alkali halides behaved like the AgCl and AgBr in developing the same azimuthally limited $\langle 110\rangle$ texture when abraded.

3.3. Unidirectional Abrasion of a Cleavage Face of a Calcite Single Crystal.

(a) The crystallographic structure of calcite.

The cleavage faces of calcite ($CaCO_3$) may be described as $\{10\bar{1}4\}$ type planes in the hexagonal lattice to which is referred the true rhombohedral unit cell; as $\{10\bar{1}1\}$ type planes using a unit cell with its c-axis one fourth the true structural length (this cell is generally used for morphological purposes, see Palache, Berman and Frondel, 1951); or as $\{100\}$ type planes in the pseudo face-centred cubic structure ($\alpha = 101^{\circ}\ 55'$) with respect to the cleavage pseudo rhombohedron. For convenience the latter pseudo face-centred cubic system is used here to specify the abrasion directions on the cleavage face of the crystal.

Before dealing with the abrasion results it is necessary to consider more fully the crystallographic structure of calcite, and the ways in which this structure may be represented.

Fig.25 (Wyckoff, 1948) shows the relation between the correct unit rhombohedron (primitive cell) of the $CaCO_3$ structure, and its cleavage rhombohedron. The rhombohedral primitive cell is the vertically elongated cell having $a_{rh} = 6.36$ kX and $\alpha = 46^{\circ}\ 06'$ and it contains two molecules of $CaCO_3$. The obtuse rhombohedron also shown in Fig.25 has the

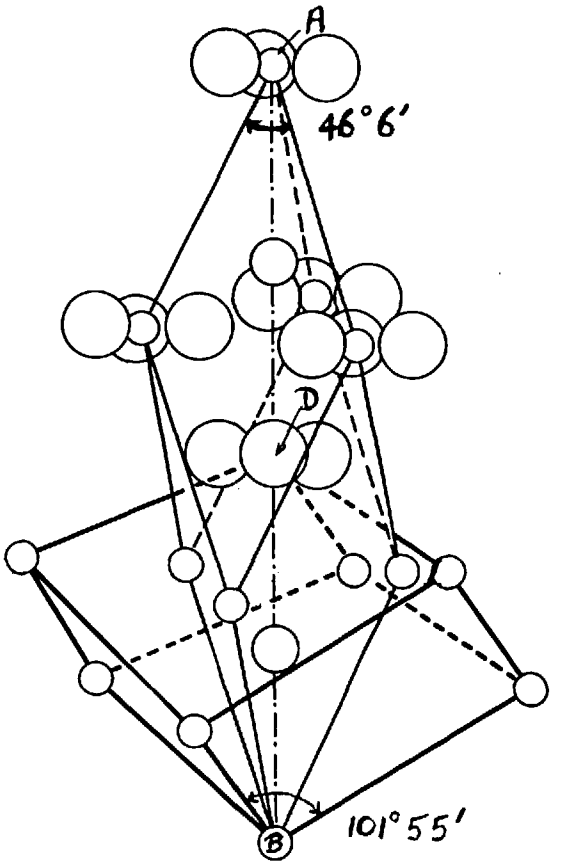


Fig.25. A drawing to show the relation between the correct unit rhombohedron of the calcite (calcium carbonate) arrangement and its cleavage rhombohedron. The true bimolecular unit is the elongated cell, the cleavage pseudo-cell is that outlined by the thicker lines. The smallest circles represent carbon atoms, the medium-sized circles calcium atoms and the largest circles oxygen atoms. (Wyckoff, 1948).

same shape and orientation as the cleavage rhombohedron, and has a diagonal length (DB) half the diagonal length of the true rhombohedron (AB). Furthermore, it should be noted that the orientation of the CO_3 group at D is 180^o rotated about the trigonal axis away from the orientation of the CO_3 groups at A and B, so that the cleavage rhombohedron shown is a pseudo-cell and not a true unit cell.

In the rhombohedral lattice, either rhombohedral axes (a_r, b_r and c_r) or hexagonal axes (a, b and c) may be used (see Fig. 84 , Appendix A). The relation between the rhombohedral and hexagonal indices is given in Appendix A. However, it must be remembered that calcite has trigonal and not hexagonal symmetry. There is, nevertheless, a close connection between the trigonal and hexagonal systems and some crystallographers group all the classes of these two systems together in sub-divisions of one large hexagonal system.

Thus, there is a hexagonal cell corresponding to the true rhombohedral unit cell. In fact the morphological hexagonal unit cell generally used is that of long-standing convention and has a c lattice dimension one quarter of the true structural unit (Palache, Berman and Frondel,1951). Hence to express a plane described in this system, in terms of the true hexagonal structure, the l index must be quadruplicated, and to express it in terms of the hexagonal cell corresponding

to the cleavage pseudo-cell the l index must be doubled.

However, account must also be taken of the fact that the rhombohedral system has only threefold symmetry about the trigonal axis and not sixfold symmetry as for the hexagonal system. The rhombohedral axes of the half-height cell are rotated by 60° (or 180°, or 300°) about the trigonal axis with respect to the axes of the quarter-height cell, and the axes of the true rhombohedral cell are rotated by a further 60° (or 180°, or 300°). In fact it is most convenient to consider the rotation to be 180° in each case (see Fig.86), and then the corresponding sets of hexagonal axes are also each rotated by 180°. Then the $\{10\bar{1}1\}$ cleavage face in the quarter-height hexagonal system is the $\{10\bar{1}4\}$ plane in the true hexagonal system and the $\{\bar{1}012\}$ plane in the half-height hexagonal system.

However, a crystal structure having a 60° rhombohedral cell may be expressed in terms of a face-centred cubic lattice and, if the rhombohedral cell has an angle not widely different from 60°, the structure may be similarly expressed in terms of a pseudo face-centred cubic lattice having axes a_{fr}, b_{fr} and c_{fr}. See Fig.85 and Appendix A for the transformation equations. Fig.86 shows the relative orientations of the axes of the cleavage rhombohedron and the axes of the corresponding hexagonal and pseudo-cubic lattices. The axes of the cleavage

rhombohedron are rotated by 180° about the c axis of the corresponding hexagonal lattice (the trigonal axis of the rhombohedral cells) from the positions of the axes of the true rhombohedral lattice.

It is the pseudo face-centred cubic(face-centred rhombohedral) representation of the cleavage rhombohedron, which is used here to describe the crystallographic structure of calcite, because the cleavage faces of the calcite cleavage cell are $\{100\}$ type faces and the cell edges are $\langle 100 \rangle$ type directions in this pseudo face-centred cubic structure.

(b) The abrasion experiments.

Fig. 26 shows the $\langle 100 \rangle$ and $\langle 110 \rangle$ directions on the (001) cleavage face of calcite along which abrasion experiments were performed. The diagram shows the abraded (001) face uppermost and the crystal extending down beneath the plane of the paper. The abrasion directions indicated are the directions of motion of the abrading emery particles over the calcite cleavage face. The axes are described by the usual right hand convention and hence the c axis is upwardly inclined out of the plane of the paper.

Fig. 26 also shows the variation of the "relative hardness", as determined by Tertsch (1949) in terms of the reciprocal of the wear rate, with azimuth on a cleavage face. The Vickers diamond-indentation hardness, H_D, of the

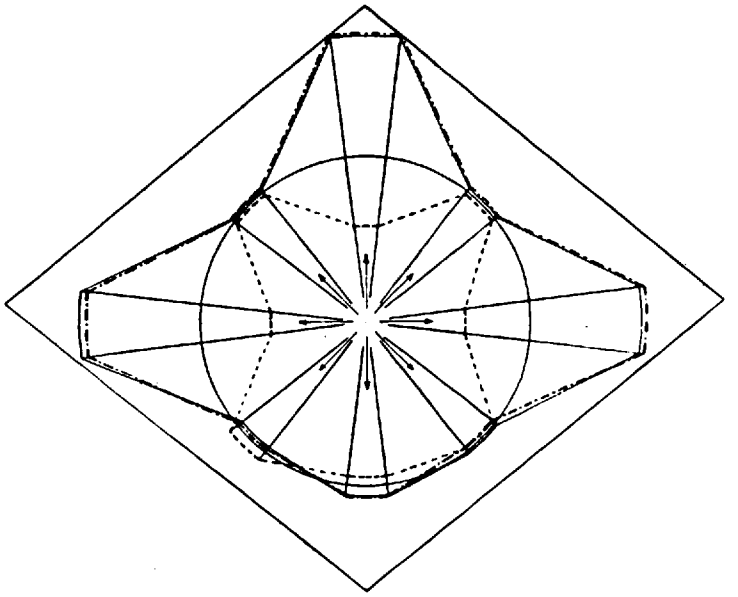


FIG.26A VARIATION OF RESISTANCE TO ABRASION OF A CALCITE CLEAVAGE FACE. (TERTSCH, 1949)

------ CURVE OF 'REDUCED WEIGHT LOSS' WEIGHT LOSS DIVIDED BY BEARING SURFACE AREA.

—— CURVE OF 'RELATIVE HARDNESS'.

-·-·-·- CURVE OF MEAN VALUES OF 'RELATIVE HARDNESS' OBTAINED BY CONSIDERING THE CRYSTAL SYMMETRY.

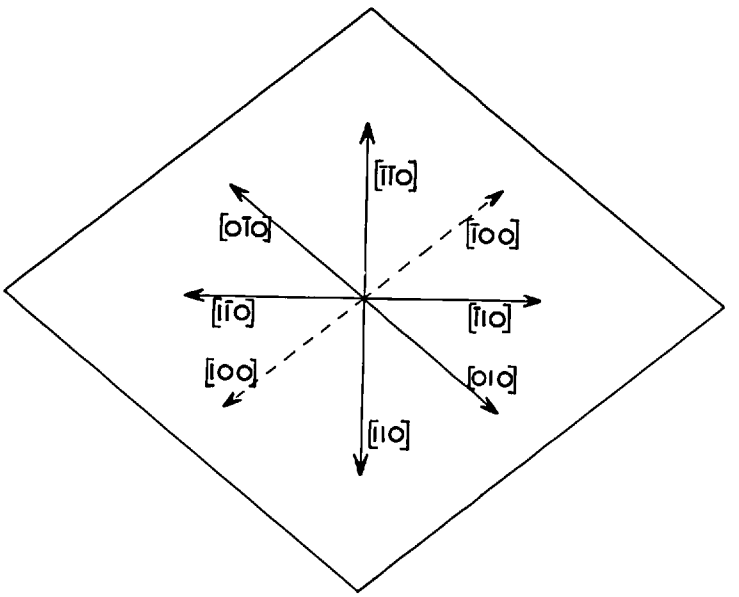


FIG.26B DIRECTIONS OF ABRASION ON A CALCITE CLEAVAGE FACE (PSEUDO F.C. CUBIC INDICES).

cleavage face of the specimen studied here abraded on dry 3/0 emery paper, was 140 kg/mm^2.

The pseudo-cube edges of the abraded cleavage face were 2.5 cm long and the crystal was approximately 1.0 cm high. The side faces of the specimen were ground flat, perpendicular to the (001) cleavage face and parallel to [100] and [010] directions (pseudo-cube edges) on that face. A smaller specimen abraded face 1.2x 0.8 cm and height 0.3 cm, was used for the electron diffraction examinations (section 3.3.3).

The friction and wear results described in section 3.3.1 were obtained by abrading the cleavage face of the larger single crystal in different directions, on various grades of emery paper and with a known load (see sections 2.3 and 2.4). Optical examination of grooves formed by abrasion on grade 3 emery paper is discussed in section 3.3.2.

3.3.1. Friction and wear of a calcite single crystal during unidirectional abrasion.

The values of the coefficient of friction, μ, and the wear rate, M (mass loss per unit distance of sliding), were determined for the abrasion of the (001) pseudo-cube-face cleavage of the calcite single crystal, along different directions, on the whole range of dry emery papers (particle diameter D 5 to 150 microns, see table 2, section 2.1), under a load of 1018 to 1010 g. The results have been scaled down to correspond to a load of exactly 1 kg, for easier comparison with other results and are given in full in Appendix B. No significant error is introduced by this step.

The specimen was always "run-in" on the grade of emery paper under consideration, at the same load, the emery paper being flooded with propyl alcohol to eliminate the pick-up of any emery particles by the specimen. This abrasion was continued until the specimen surface attained a roughness characteristic of the emery grade concerned. Determinations of μ and M were then made on dry emery paper of the same grade, each abrasion stroke being always on fresh emery paper.

On the coarser grades of emery paper ($D > 70$ microns) μ is practically constant, but as D decreases there is a rapid decrease in μ. Fig.27 shows this variation of μ with D for abrasion in $[\bar{1}10]$ and $[1\bar{1}0]$ directions, and similar loci were

obtained for the other directions.

This form of the μ,D curve was first observed, for graphite and also for lead, by Porgess and Wilman (1960) in this laboratory; and it was also found for all the metals and non-metals subsequently investigated (Goddard, Harker and Wilman, 1959; Avient, Goddard and Wilman, 1960; King and Wilman, 1961, 1962b). The lowering of μ at small emery-particle size results from the load being supported only partly on emery-calcite contacts (or emery-metal contacts, in abrasion of metals) and partly on calcite-calcite contacts where calcite has been worn off from the front region of the specimen's bearing surface and partially clogs the abrading emery surface. The proportion of calcite-calcite contacts increases as the emery particle diameter D decreases.

The wear rate, M, was determined at the same time as μ over the whole range of emery particle sizes, and it was found that M varied with D in a similar manner to μ except that, on the coarser grades (D $>$ 70 microns), M continued to increase slightly with D, Fig. 28 shows the variation of M with D for abrasion along $[1\bar{1}0]$ and $[\bar{1}10]$ directions.

Figs. 29 and 30 show the variation of M with μ for abrasion along all the directions studied. The variation is approximately linear for abrasion on emery grades with D greater than about 30 microns, but for the finer grades the

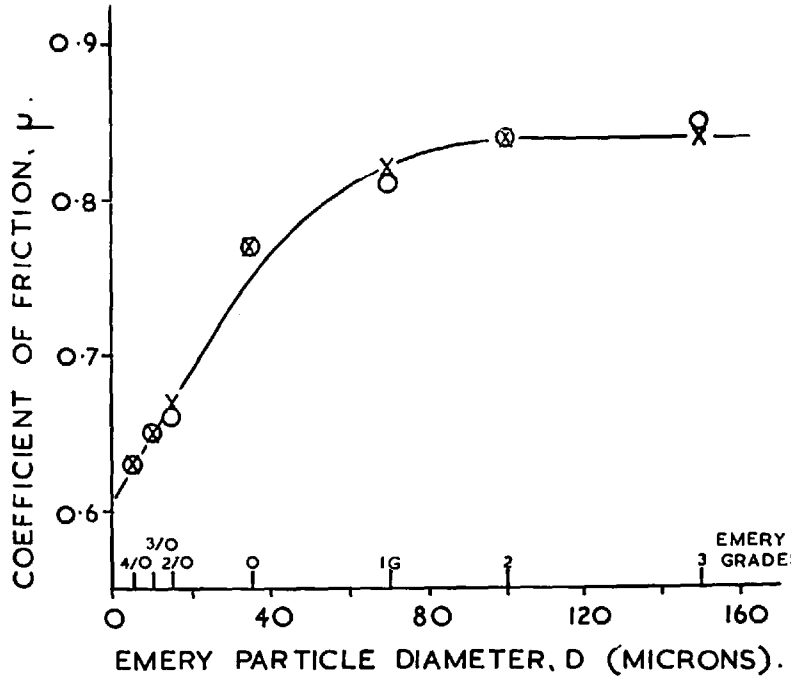


FIG.27

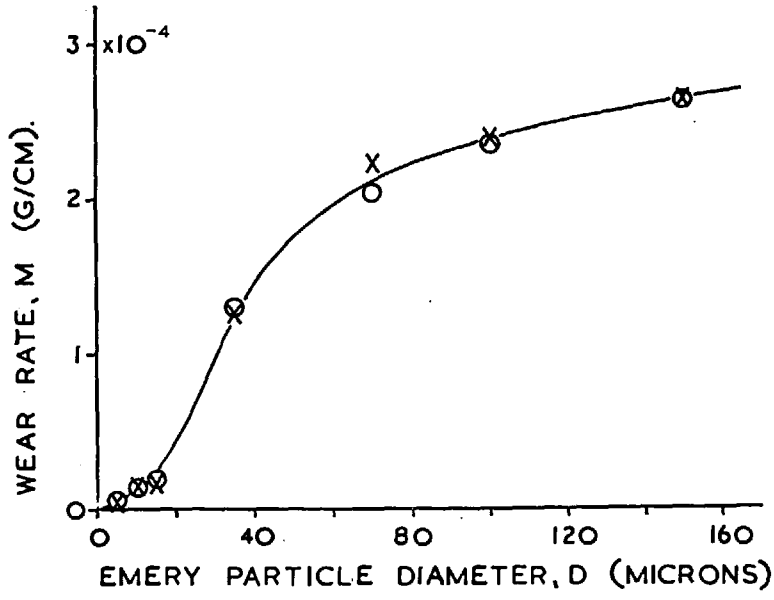


FIG.28

FIGS. 27 & 28 VARIATION OF COEFFICIENT OF FRICTION μ (FIG. 27) AND WEAR RATE M (FIG. 28) WITH EMERY PARTICLE DIAMETER D, FOR CALCITE ABRADED ALONG DIRECTIONS $[\bar{1}10]$ (o) AND $[1\bar{1}0]$ (X) AT 1 KG LOAD.

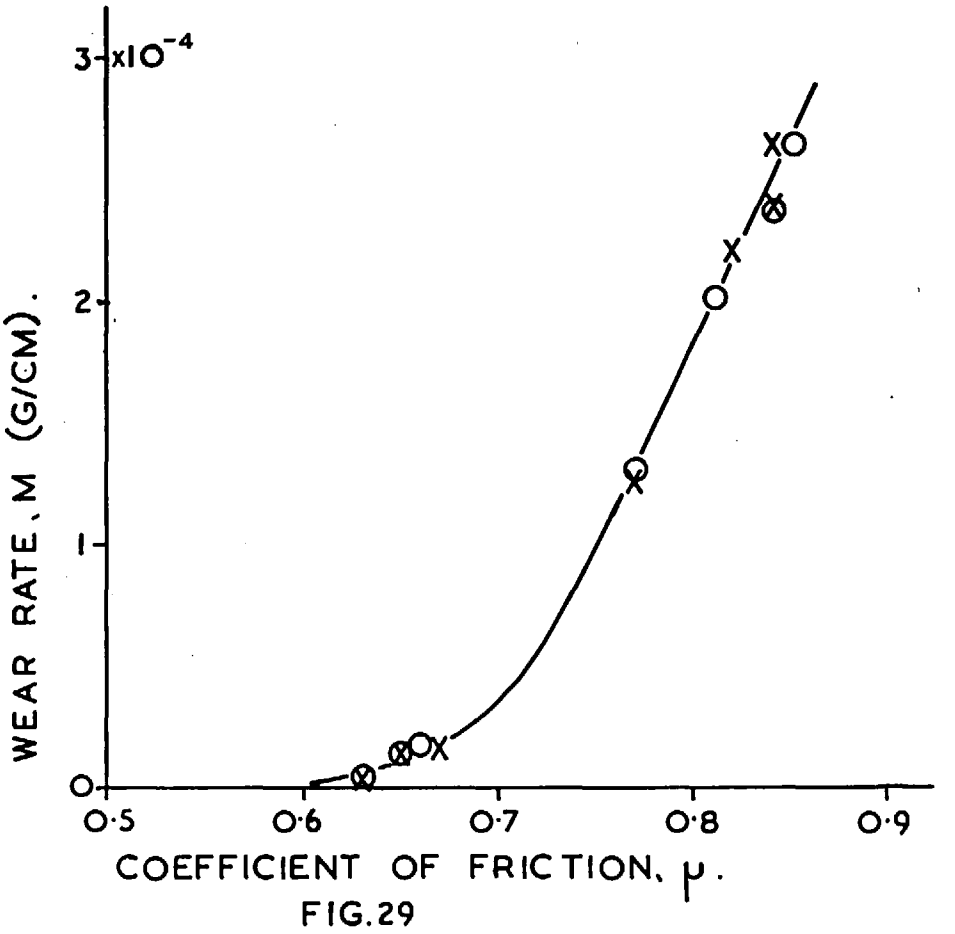


FIG.29

FIG.29 VARIATION OF WEAR RATE M WITH COEFFICIENT OF FRICTION μ, FOR CALCITE ABRADED ALONG DIRECTIONS $[\bar{1}10]$ (O) AND $[1\bar{1}0]$(X) AT 1 KG LOAD.

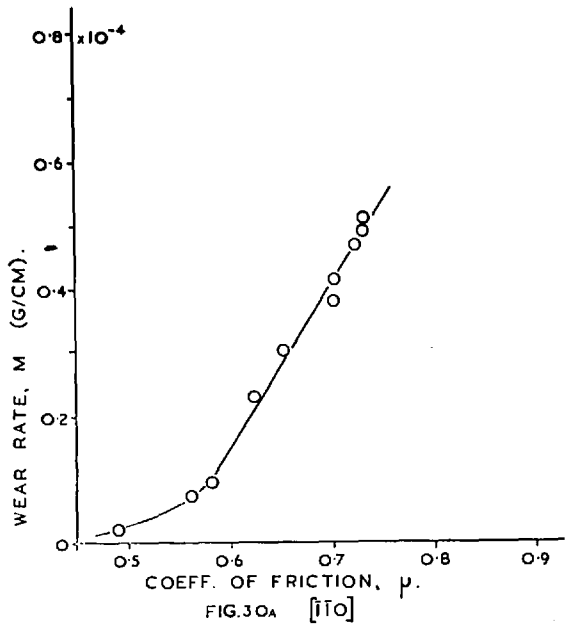


FIG.30A [1$\bar{1}$0]

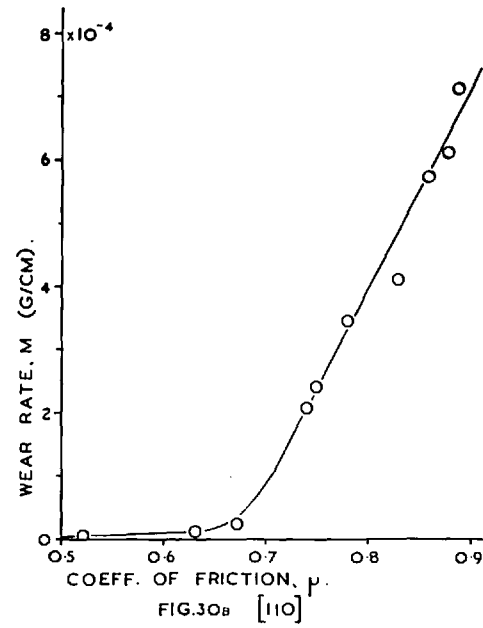


FIG.30B [110]

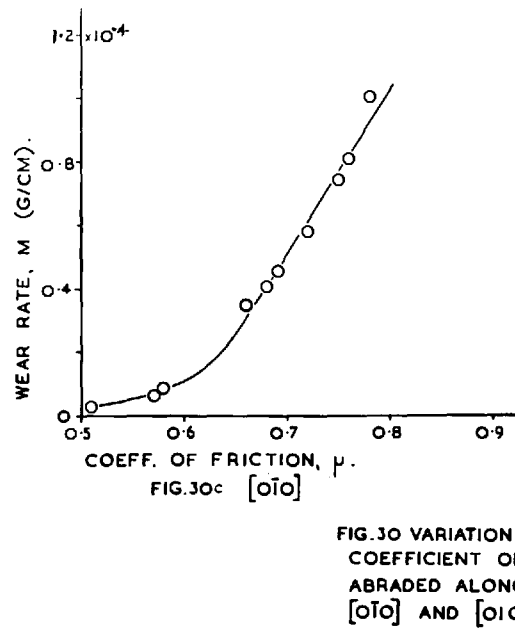


FIG.30C [0$\bar{1}$0]

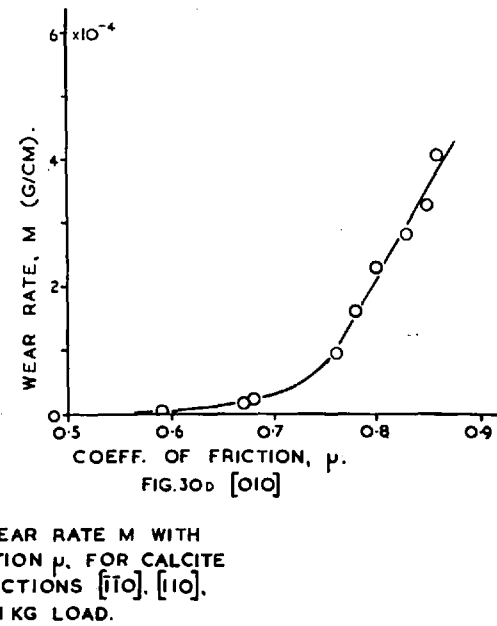


FIG.30D [010]

FIG.30 VARIATION OF WEAR RATE M WITH COEFFICIENT OF FRICTION μ, FOR CALCITE ABRADED ALONG DIRECTIONS [1$\bar{1}$0], [110], [0$\bar{1}$0] AND [010], AT 1 KG LOAD.

loci curve round towards the M axis. The coefficient of friction of calcite sliding on calcite was estimated to be 0.2 to 0.3.

For abrasion along both a $[1\bar{1}0]$ and a $[\bar{1}\bar{1}0]$ direction the inclination of the cleavage planes to the abrasion direction is the same. In both cases one cleavage plane is inclined forwards and the other plane is inclined backwards by the same angle. Hence the values of μ and M would be expected to be the same for abrasion along $[1\bar{1}0]$ and $[\bar{1}10]$ on any particular grade of abrasive. This is in fact observed, as is clearly seen in Figs. 27 and 28, (the variation of μ and M with emery particles diameter D) and Fig. 29 (the variation of M with μ).

Abrasion along $[\bar{1}\bar{1}0]$ and $[\bar{1}10]$ directions gave rise to the greatest variation in the values of μ and M. On dry grade 3 emery paper and for a load of 1 kg μ was 0.73 and 0.89 and M was 4.9×10^{-5} and 7.1×10^{-4} g/cm in directions $[\bar{1}\bar{1}0]$ and $[\underline{1}10]$ respectively, see Fig. 30a and Fig. 30b. This very large difference results from the fact that, when the abrasion is along $[\bar{1}\bar{1}0]$ (i.e. the abrasive particles are moving along a $[\bar{1}\bar{1}0]$ direction with respect to the abraded cleavage face), the other two cleavage faces are inclined back into the crystal towards the direction from which the abrasive particles came. As a result, fracture along these planes does not give rise

to the considerable wear which occurs on abrasion along a $[\bar{1}10]$ direction. When the abrasion is along $[1\bar{1}0]$ these two cleavage planes are inclined forwards into the crystal in the direction of motion of the abrading particle, and hence considerable fracture occurs, often ahead of the indenting abrasive particle, and a much higher wear rate is observed, in fact fifteen times that measured along $[\bar{1}\bar{1}0]$.

For abrasion along $[0\bar{1}0]$ and $[010]$ a smaller change in μ and M was observed, as can be seen from Figs. 30c and 30d, although there was still a difference by a factor of four in the two wear rates (1.0 and 4.0 X 10^{-4} g/cm). In both cases one cleavage plane is parallel to the abrasion direction. The other cleavage plane is backwardly inclined into the crystal when the abrasion is along a $[0\bar{1}0]$ direction, and forwardly inclined when the abrasion is along a $[010]$ direction. Hence fracture on these cleavage planes leads to greater wear in the latter case than in the former. Micrographs of individual grooves in section 3.3.2 further illustrate these differences in abrasion with azimuth.

3.3.2. Optical examination of abrasion grooves on a calcite single crystal.

Short abrasion strokes of about 2 mm length were made, using dry grade 3 emery paper and a load of 1 kg, on the (001) pseudo-cubic cleavage free of the calcite along the same directions as those considered in the friction and wear experiments of section 3.3.1. The cleavage face was smoothed on emery papers down to 4/0 grade and then lightly etched in $\frac{N}{5}$ HCl solution before making the short abrasion stroke. Such short strokes were used so that individual grooves could be examined, and Figs. 31 to 42 are typical photomicrographs thus obtained using the transmission method with the crystal abraded face downwards on the microscope stage, i.e. the light passes through the crystal onto the abraded face. The magnification was x 300 and the direction of motion of the abrasive particles over the calcite face was from left to right in all cases. In these photographs extensive fracture is clearly seen to occur outside the well-defined groove formed by the abrasive particle.

When the abrasion was parallel to a $[\bar{1}\bar{1}0]$ direction cracks were observed on both sides of some of the grooves, these cracksbeing inclined by about 50° to the abrasion direction, i.e. parallel to the cleavage planes of the crystal (see Fig. 31). However, these cracks were absent from many

Figs.31 to 42. Short abrasion strokes on a cleavage face of calcite under 1 kg load and using grade 3 emery paper. (Abrasion direction, left to right).

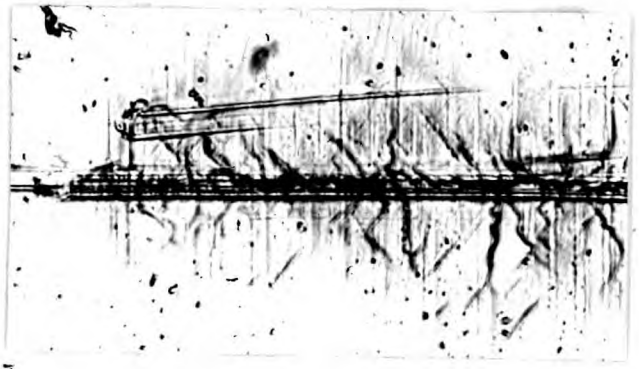


Fig. 31. x 300

Figs.31 and 32.
Abrasion direction $[\bar{1}\bar{1}0]$



Fig. 32. x 300

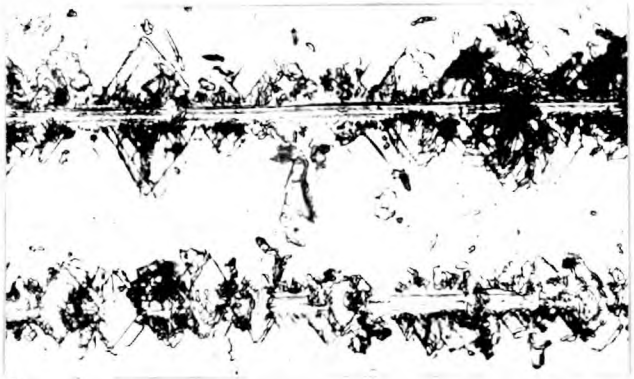


Fig. 33. x 300

Figs.33 and 34.
Abrasion direction, $[\bar{1}10]$



Fig. 34. x 300

Fig. 35. x 300

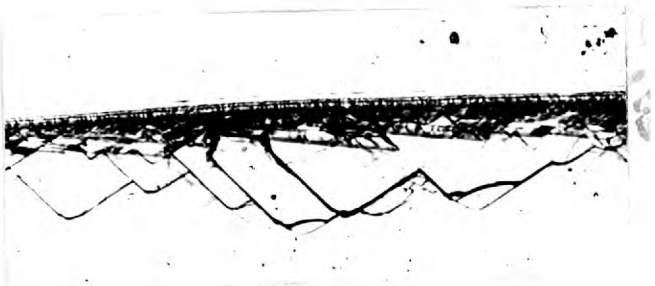


Figs.35 and 36.
Abrasion direction, $[\bar{1}10]$

Fig. 36. x 300



Fig. 37. x 300



Figs.37 and 38.
Abrasion direction, $[1\bar{1}0]$

Fig. 38. x 300



Fig. 39. x 300



Figs.39 and 40.
Abrasion direction, [0$\bar{1}$0]

Fig. 40. x 300

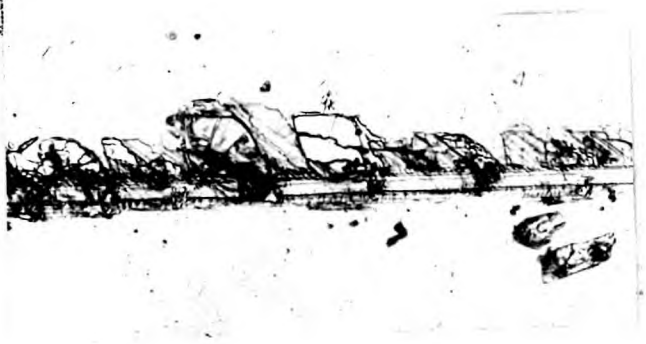


Fig. 41. x 300



Figs.41 and 42.
Abrasion direction, [010]

Fig. 42. x 300



Figs.43 and 44. Calcite wear particles from the emery paper, after abrasion on dry grade 3 emery paper at 1 kg load.

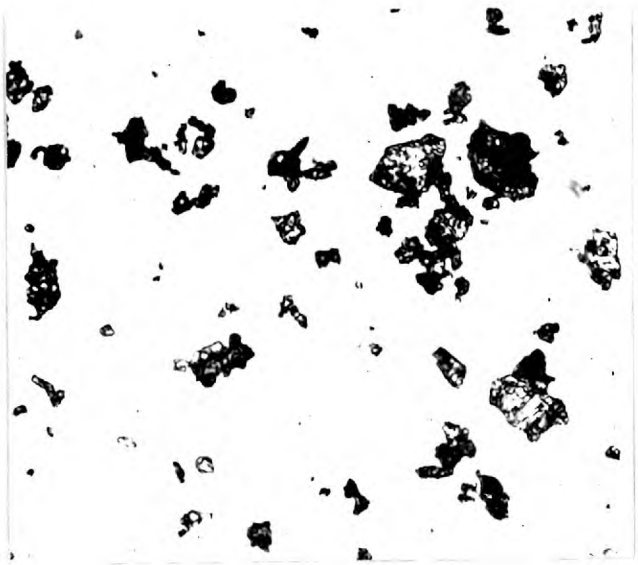


Fig. 43. x 300
Abrasion direction, $[\bar{1}10]$

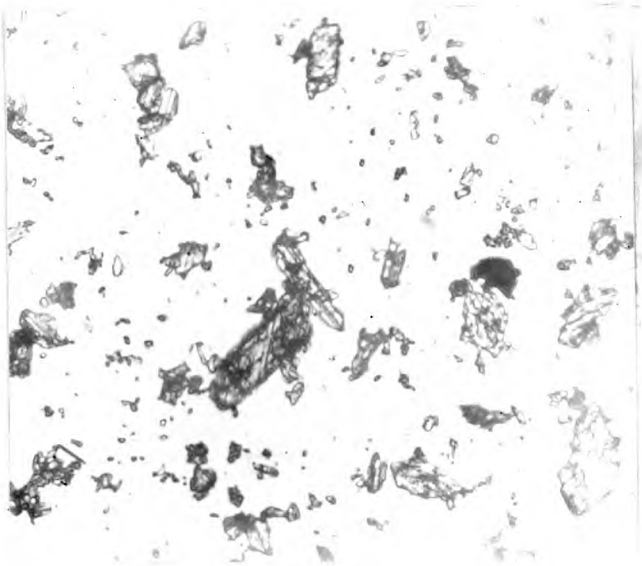


Fig. 44. x 300
Abrasion direction, $[\bar{1}10]$

of the grooves (Fig.32).

There were also some lines normal to the abrasion direction. There is little evidence of large fragments of the crystal being removed as wear outside the individual grooves, nor is there any cracking ahead of the indenting particle. However, subsequent abrasion over such a cracked surface may well lead to the removal of calcite in the form of large cleaved fragments.

The grooves formed by abrasion along a $[1\bar{1}0]$ direction (Figs. 33 and 34) show a marked difference from the grooves described above. Cracks, outside the main groove, at 50^{o} to the abrasion direction are always observed. They are much more abundant and also extend ahead of the ploughing particle and the end of the groove (Fig. 34).

Several fragments of calcite many times larger than the groove cross-section are removed as wear particles from the vicinity of the main groove (see Figs. 43 and 44). It was also observed that there were about three times as many abrasion grooves (and hence emery-calcite contacts) formed for a 2 mm abrasion stroke along $[1\bar{1}0]$, which was the direction with the highest wear rate, as along $[\bar{1}\bar{1}0]$.

Photographs of abrasion grooves along the opposite diagonal of the pseudo-cube-face cleavage in a $[\bar{1}10]$ direction, Figs. 35 and 36, and a $[\bar{1}\bar{1}0]$ direction, Figs. 37 and 38, showed

that very similar grooves are obtained along both these directions, with cracks forming outside the grooves, making an angle of about 40° to the abrasion direction. These cracks are thus parallel to the calcite cleavage faces which intersect the abraded face. This similarity results from these cleavage planes being identically inclined to the abrasion direction for abrasion along $[\bar{1}10]$ and along $[1\bar{1}0]$. This similarity is emphasised by the values of the friction coefficient and the wear rate which were both equal in these two directions (section 3.3.1).

Figs. 39 to 42 are microphotographs of typical grooves formed by abrasion of the cleavage face in a direction parallel to one of the inclined cleavage faces, i.e.,along a pseudo-cube face edge. Figs. 39 and 40 show grooves for abrasion parallel to $[0\bar{1}0]$, and cracks are again formed outside the main groove, these cracks being parallel to the edges of the pseudo-cube face cleavage, and the intersections of the inclined cleavage faces with the abraded cleavage face. Thus in the present case one such direction is parallel to the abrasion direction whilst the other is inclined at 78° to the abrasion direction. Figs. 41 and 42 show grooves caused by abrasion parallel to $[0\bar{1}0]$,and are very similar to Figs. 39 and 40 except that greater wear results when the abrasion direction is $[010]$.

Typical calcite wear particles resulting from abrasion on grade 3 emery paper (dry) at 1 kg load are shown in Figs. 43 and 44. These are similar conditions to those used in the short-stroke abrasion experiments. It is readily seen that very many such particles have a diameter of about 30 microns,whilst the abrasion groove photographs show a groove width of less than 10 microns.

All these results show conclusively that considerable cleavage and fracture occurs outside the region of the main groove during abrasion by these coarse grade emery particles, with resultant very high wear rates.

3.3.3. Electron diffraction examination of a unidirectionally abraded cleavage face of calcite.

(a) Abrasion of calcite along a ⟨100⟩ direction.

Figs. 45 to 51 are photographs of the diffraction patterns obtained from a calcite cleavage face abraded on 3/0 emery paper wet with propyl alcohol at 1 kg load, along a ⟨100⟩ direction (i.e. parallel to a pseudo-cube edge), and etched to various depths. The direction of motion of the abrasive particles over the calcite surface is indicated by an arrow on photographs obtained with the electron beam perpendicular to the abrasion direction (subsequently referred to as the perpendicular setting). The specimen was also examined with the electron beam parallel to the abrasion direction (subsequently referred to as the parallel setting).

Figs. 45a and 45b were obtained from the surface without etching and at the perpendicular and parallel settings respectively. Both patterns consist of rings of uniform intensity, indicating that the abraded surface region is composed of randomly oriented crystallites (cf. Fig. 59).

Figs. 46a and 46b were obtained after etching for 2 seconds in a solution of N/100 HCl (the etchant used throughout, in these electron diffraction studies) which etches the crystal at a rate of ~ 2 μ/min. These patterns are similar to those obtained from the unetched surface except

Figs.45 to 51. Unidirectional abrasion of a calcite cleavage face along a ⟨100⟩ direction, on 3/0 emery paper wet with propyl alcohol and at 1 kg load. (a) and (b) are at the perpendicular and parallel settings respectively.

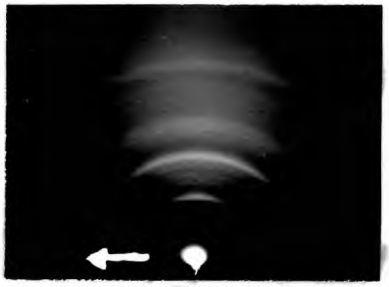


Fig. 45a. ⊥

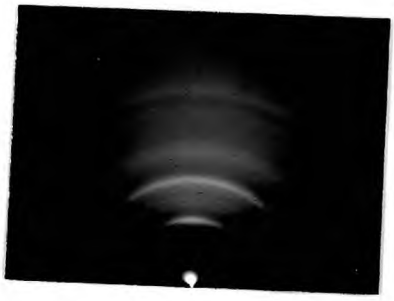


Fig. 45b. ∥

Fig. 45. Abraded surface unetched.

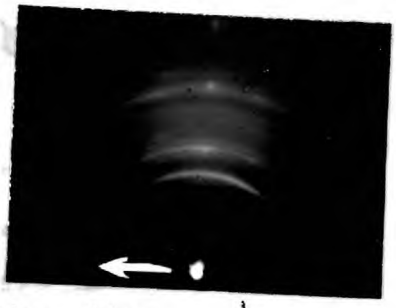


Fig. 46a. ⊥

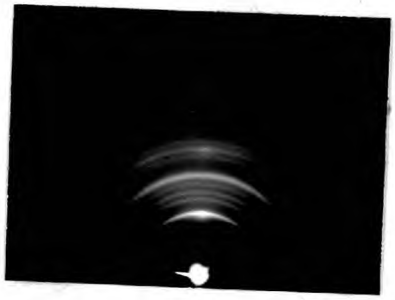


Fig. 46b. ∥

Fig. 46. Etched 2 sec. in N/100 HCl.



Fig. 47a. ⊥

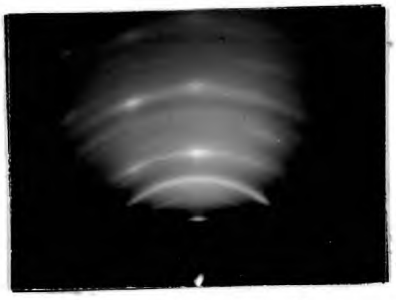


Fig. 47b. ∥

Fig. 47. Etched 5 sec.

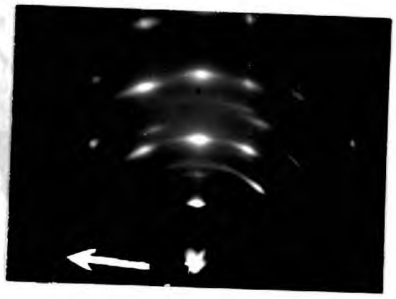


Fig. 48a. ⊥

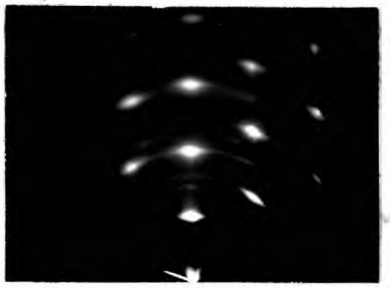


Fig. 48b. ||

Fig.48. Etched 15 sec.

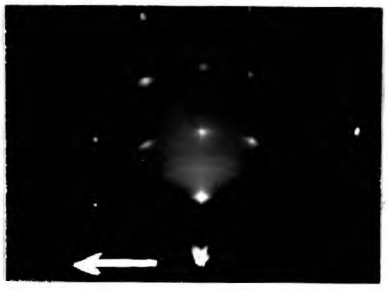


Fig. 49a. ⊥

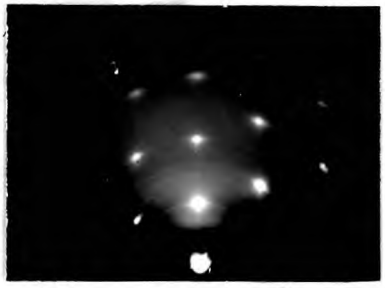


Fig. 49b. ||

Fig.49. Etched 40 sec.

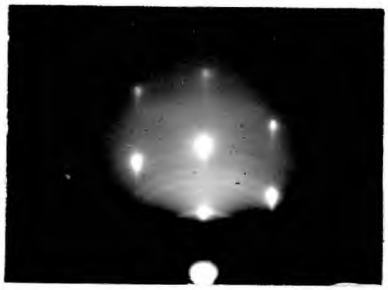


Fig. 50.

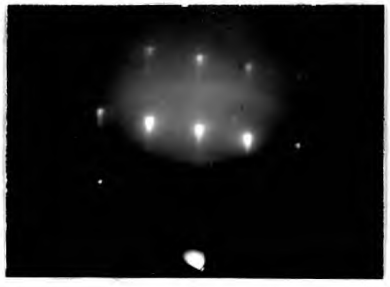


Fig. 51.

Figs.50 and 51. Etched 2 min. Abrasion direction 78° (Fig.50) and 98° (Fig.51) to electron beam, showing the two components of the patterns obtained at the perpendicular setting.

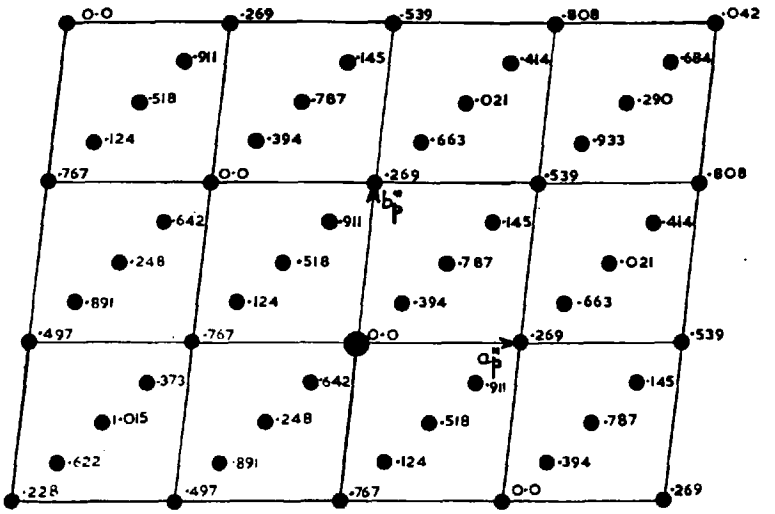


Fig.52. Projection of the pseudo-cubic (face-centred rhombohedral) reciprocal lattice of calcite onto a cleavage plane of the crystal. The c* axis is vertical and the a* and b* axes are inclined upwards out of the plane of the paper by 15° 5', their projections onto this plane, a_p^* and b_p^*, being 0.159 kX^{-1}. The heights of other diffractions above this plane are given as multiples of a_p^* (i.e. a_p^* is taken as unit length).

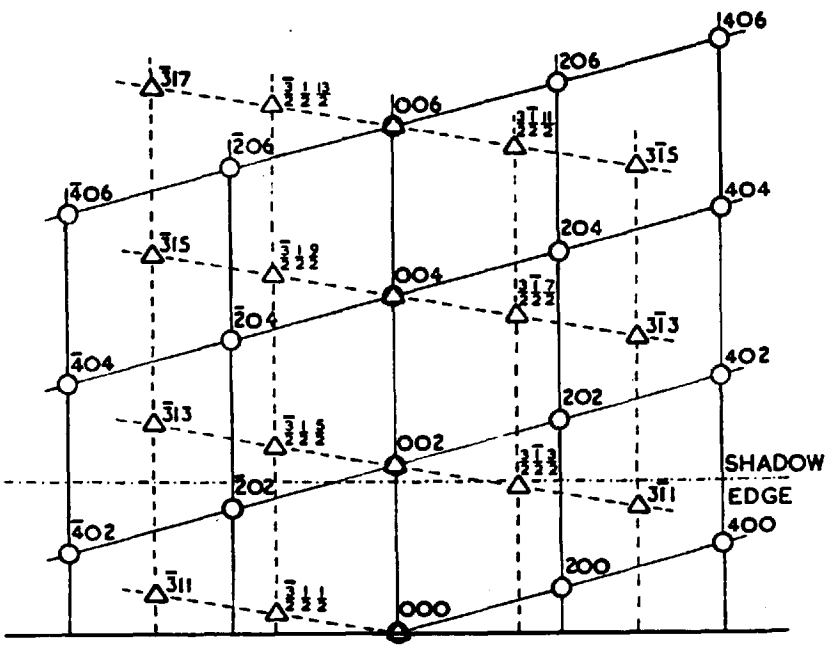


Fig.53. Positions of diffractions from {010}* and {130}* reciprocal-lattice planes (denoted by 0 and △ respectively) of the pseudo-cubic reciprocal lattice when these planes lie in the Ewald plane and normal to the electron beam.

that the rings are intensified in the regions corresponding to diffractions from the single crystal. Further etching (Figs.47 and 48) shows these diffractions more strongly intensified. It is also noted that, in the perpendicular setting, these short arcs are elongated around the ring positions in the direction of motion of the abrasive particles over the abraded calcite surface. This corresponds to a rotation of the single crystal pattern about an axis lying approximately in the surface and normal to the abrasion direction, (cf.Figs.50 and 51 and also Figs.52 and 53). Fig.49, obtained after 40 seconds etching, shows predominently the single crystal pattern, corresponding to undeformed regions of the crystal, although faint rings are still visible.

When the electron beam is parallel to a pseudo-cube edge (i.e. in this case parallel to the abrasion direction) a cube face in the reciprocal lattice, $\{010\}^*$, is perpendicular to the beam and the resultant single-crystal pattern is a pseudo-square pattern as seen in Fig.49b. However, when the electron beam is perpendicular to a pseudo-cube edge a $\{100\}^*$ plane is not exactly perpendicular to the electron beam but rather at 78° to it. Furthermore, a $\{310\}^*$ plane at 98° to the electron beam. Hence, a rotation of about 10° would bring either of these planes normal to the electron beam. In fact the patterns corresponding to both these planes are observed

at this perpendicular azimuth even after 40 seconds etching (Fig.49a). Thus arcs related to diffractions from $\{100\}^*$ and $\{310\}^*$ planes are seen on patterns obtained after a few seconds etching.

The positions of these single crystal diffractions may be more clearly seen from Figs. 52 and 53. Fig. 52 is a projection of the pseudo-cubic reciprocal lattice onto the cleavage plane of the crystal. The c* axis rises vertically out of the plane of the paper and a* and b* are upwardly inclined by 15^o 5' from the plane of the paper, whilst their projection onto the cleavage plane (i.e. the plane of the paper) are a_p^* and b_p^*.

Since a* and b* are 0.165 kX^{-1} (calculation given in Appendix A), a_p^* and b_p^* are 0.165 x cos.15^o 5' = 0.1593 kX^{-1}. Thus 0.1593 kX^{-1} is taken as the unit length of the projection (Fig.52) and the heights of the other diffractions above the cleavage plane are given in the figure as multiples of this unit length. All the diffractions have a vertical repeat height of c* (0.165 kX^{-1} = 1.036 units). The positions of diffractions from reciprocal-lattice planes perpendicular to this cleavage plane may thus be obtained from Fig.52 by considering planes normal to the projection plane. Fig. 53 shows such diffractions for $\{010\}^*$ and $\{130\}^*$ planes parallel to the Ewald plane.

From consideration of the pseudo-cubic reciprocal lattice there is no direct indication that diffractions would occur at distances of a quarter and three quarters of the diagonal of this reciprocal-lattice unit cell (i.e. along the trigonal axis). However, as has previously been mentioned, this is only a pseudo-cell and does not take account of the different orientations of the CO_3 groups. If the reciprocal lattice of the true rhombohedral cell is determined (see Appendix A for the calculations), then it is seen that diffractions corresponding to these reciprocal-lattice points along the trigonal axis do occur.

(b) Abrasion of calcite perpendicular to a ⟨100⟩ direction.

The crystal cleavage face was also abraded perpendicular to a ⟨100⟩ direction so that a ⟨100⟩ direction was parallel to the electron beam in the perpendicular setting and a $\{100\}^*$ plane was normal to the beam. The abrasion was again on 3/0 emery paper wet with propyl alcohol at 1 kg load.

The patterns obtained (see Figs. 54 to 58) showed a variation in the deformation texture with depth similar to those described above. The patterns obtained with the beam at 45° to the abrasion direction (Figs. 55b and 56b) showed little forward rotation of the arcs and thus confirmed that the rotation observed in the perpendicular setting corresponds to a forward rotation about an axis lying in or near the abraded

Figs. 54 to 58. Unidirectional abrasion of a calcite cleavage face perpendicular to a ⟨100⟩ direction, on 3/0 emery paper wet with propyl alcohol, 1 kg load.

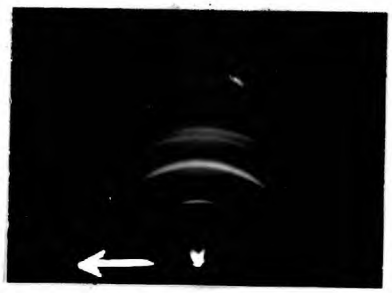


Fig. 54a. ⊥

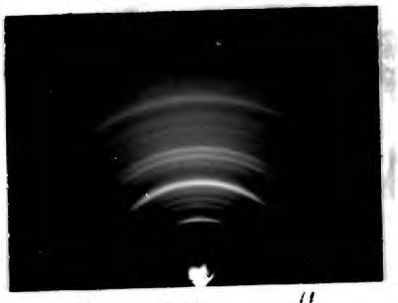


Fig. 54b. //

Fig.54. Abraded surface unetched.

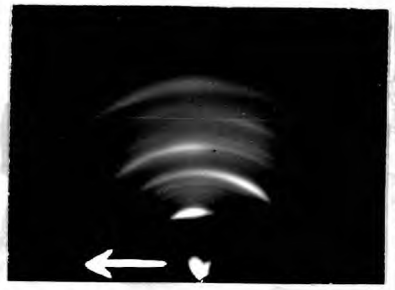


Fig. 55a. ⊥



Fig. 55b. 45°.



Fig. 55c. //

Fig.55. Etched 5 sec.

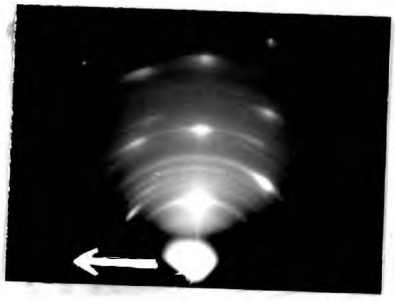


Fig. 56a. ⊥



Fig. 56b. 45°.

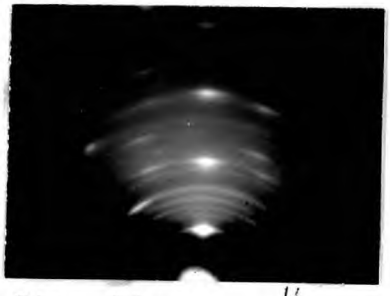


Fig. 56c. //

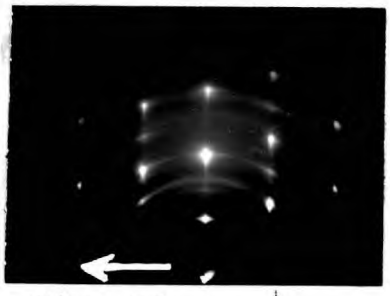


Fig. 57. ⊥
Etched 40 sec.



Fig. 58. ⊥
Etched 90 sec.

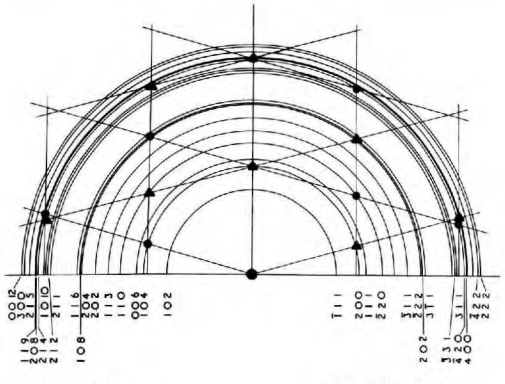


FIG.59 THEORETICAL RING DIFFRACTION PATTERN FOR CALCITE SHOWING DIFFRACTION POSITIONS FROM (100) PLANES. ▲(SEE FIG.50) AND ●(SEE FIG.56c).

surface and approximately perpendicular to the abrasion direction. This rotation axis is therefore apparently a $\langle 100 \rangle$ lattice row or a direction near to a $\langle 100 \rangle$ lattice row.

On one photograph of the diffraction pattern in the perpendicular setting from the unetched, abraded surface (Fig.54a, see also Fig.59) the intensity of the 422 ring is strengthened over an arc of about 40°, having its mean backwardly inclined by about 10° to the normal to the surface in the direction of motion of the abrasive particles over the specimen (right to left). The 400 and 420 rings are also strengthened at positions corresponding to the single crystal diffraction positions. However, there is not enough preferred orientation of the pattern for this orientation to be reliably identified.

The occurrence of additional diffraction spots, particularly prominent in Fig.57, may be accounted for by twinning on the (001) cleavage face. The additional diffractions form a pattern which is mirror symmetrical, about the plane of incidence, to the main spot pattern and may be obtained by a 180° rotation of the single crystal reciprocal lattice about the $\langle 001 \rangle^*$ direction, i.e. the normal to the abraded (001) surface. This is equivalent to twinning on this (001) plane.

Calcite is known to twin on $\{0\bar{1}12\}$, $\{0001\}$, $\{10\bar{1}1\}$

and $\{02\bar{2}1\}$ planes with respect to the hexagonal quarter cell mentioned in section 3.3 (Palache, Berman and Frondel,1951) these planes being $\{110\}$, $\{111\}$, $\{100\}$ and $\{\bar{1}11\}$ type planes respectively in terms of the pseudo-cubic axes. Although twinning on a pseudo-cube face is not the most common twin system in the mineral growth forms, it is observed here when the abrasion is along such a twin plane.

Calcite surfaces abraded under the same conditions on dry 3/0 emery paper yielded patterns similar to those described above, both for the unetched surface and after etching. There were no extra diffraction rings, as have been observed previously for metals, and also AgCl, AgBr and silicon, when abraded on dry emery papers of these fine grades. These extra diffractions are shown to correspond to diaspore (see section 3.5.3), α-AlOOH, a known component of emery, and under these conditions it is concluded that the abraded surfaces pick up emery particles from the emery paper on which it slides. In the absence of observation of any such pattern from diaspore, it is concluded that calcite does not pick-up emery particles when abraded dry on emery papers.

3.4. Discussion of Results for the Abrasion of Single-crystal Calcite.

The wear measurements for the abrasion of calcite (section 3.3.1) show that the wear rate varies considerably with azimuth; far more so than indicated by Tertsch's results (see Fig.26a). However, the conditions for Tertsch's experiments were considerably different. He determined the wear by abrading a clamped calcite crystal of approximately 4 cm^2 abrading surface area on a rotating disc using wet abrasive powder. The specimen was 7.5 cm from the centre of the disc and hence the abrasion grooves so formed on the crystal were curved, the total curvature being about 15^o over the length of the specimen. Therefore, the abrasion was not strictly parallel to a particular crystallographic direction but over a range of directions within this 15^o spread. This reduced the sensitivity of the measurement of the variation of the wear rate with azimuth, as compared with the present results. Also, since the crystal was continuously passing over the same circular path on the disc, there may have been appreciable clogging of this abrading region by the worn-off calcite.

In the present experiments the crystal was always abraded over a fresh emery surface, and this minimized the effect of clogging of the abrasive by the calcite wear fragments.

As a result of abrading the whole of the crystal

bearing surface parallel to a particular azimuth, and the continual use of a fresh abrading surface, the wear rate is seen to vary considerably with abrasion direction. The coefficient of friction also varies with abrasion direction.

From the results described in section 3.3 it is clear that there is considerable cleavage and fracture of calcite when abraded by hard particles such as emery. Even though well defined grooves are formed on the abraded calcite face by the ploughing particles the cracking that occurs during the abrasion extends far beyond these grooves and wear particles many times the diameter of the indenting emery tips are formed.

These observations are confirmed by the electron diffraction study of the abraded calcite surface. The transition from the surface, consisting of randomly oriented crystal fragments with little or no preferred orientation, to the underlying single crystal shows that there is a forward rotation of the crystals about an axis approximately normal to the abrasion direction and lying in the surface plane, this rotation extending through an angle of up to about 20°, near the surface (i.e. as revealed after etching for 5 seconds, corresponding to a depth of about 2,000Å assuming uniform removal of the calcite during etching). After etching the specimen for 90 seconds the electron diffraction pattern is almost entirely an undisturbed single-crystal pattern. Thus

the depth of the deformed region formed on abrasion on fine emery paper of grade 3/0 is about 3 microns.

Similar lattice reorientations have been observed after unidirectional abrasion on Cu and Fe (Evans, Layton and Wilman, 1951; Agarwala and Wilman, 1955) and on Cu, Ni and Au (Goddard, 1959). There are two possible explanations of such lattice rotations in terms of the rotational slip process, as Scott and Wilman (1958) pointed out. The process of pure rotational slip (Wilman 1950, 1951) would produce a coherent fragmentation of the lattice in the form of lamellae normal to the observed rotation axis, which is usually normal to the abrasion direction and in the specimen surface. However, in many cases this would involve the rotational slip being on planes other than the usual slip planes.

Alternatively, the observed rotation axis could correspond to the axis of flexure, in flexural rotational slip (Whapham and Wilman, 1956) where, in this case, there is small rotation but large flexure with the axis of flexure being parallel to the slip lamellae. Scott and Wilman (1958) concluded that the evidence pointed to such flexural rotational slip as the operative process, in the case of abraded Be.

Extensive plastic deformation by slip processes has been observed to occur in the abrasion process for the abrasion of rocksalt (Raether, 1947; Dobson and Wilman, 1962b),

and calcite (Gay, Hirsch and Kellar, 1952). King and Tabor (1954) concluded that, in the sliding of rocksalt on rocksalt (cleavage surfaces) and of smooth steel balls on rocksalt cleavage surfaces, the frictional behaviour is primarily due to the local plastic flow and strong interfacial adhesion at the regions of real contact, as for the friction of metals. The results of Dobson and Wilman (1963) indicate that, even for the abrasion of rocksalt on emery papers when the sliding conditions are very abrasive, causing much widespread fracture, the friction coefficient is determined mainly by the plastic flow properties of the rocksalt, and scarcely at all by the occurrence of the fractures.

The present results for the abrasion of calcite show that there is a considerable variation of the wear rate, and to a lesser extent the coefficient of friction, with the direction of abrasion. The direction of highest wear rate, $[1\bar{1}0]$, is also the direction of highest friction. For abrasion along such a direction the cleavage planes are so oriented relative to the abrasion direction that large fragments of the single crystal readily cleave off the main crystal as the ploughing emery particles progress through the surface. It is interesting to note that for the abrasion of a cube face of a single crystal of rocksalt, which corresponds to the pseudo-cube cleavage face of calcite, there was only a 3% variation of the wear-rate with azimuth, along the $\langle 100 \rangle$ and $\langle 110 \rangle$ type directions (Dobson and Wilman, 1963).

3.5. Unidirectional Abrasion of Silicon Single Crystals.

3.5.1. Friction and wear of silicon single crystals during unidirectional abrasion.

Unidirectional abrasion experiments were made along different azimuths on (111), (110) and (001) faces of silicon single crystals, using various grades of emery paper, both dry and wet with propyl alcohol, at approximately 1.04 kg load. The wear rates were scaled down to correspond to a load of exactly 1 kg, for comparison with results for the abrasion of other materials, and the full wear and friction results are given in Appendix C.

When silicon is abraded on dry emery papers there is pick-up of the abrading emery particles which become embedded in the abraded surface (see section 3.5.3 for electron diffraction patterns from such dry abraded surfaces showing rings due to diaspore, a known component of emery). Hence, during these abrasion experiments the crystal was etched in a mixture of 40% HF and concentrated HNO_3 in the proportions 1 : 5 by volume, before abrasion on a different grade of emery paper, to remove any picked-up emery particles. This etchant removed the abraded surface at a rate of approximately 20 microns/minute.

When the abrasion was on emery papers wet with propyl alcohol there was little or no pick-up of emery (as confirmed

by the absence of rings due to diaspore in the electron diffraction patterns from such wet abraded silicon surfaces, section 3.5.3). The specimen was desiccated before the mass loss was determined by weighing. In all these wet or dry experiments the specimen was "run-in" on emery paper of the grade concerned before wear and friction measurements were taken using that grade.

(a) Abrasion of a (111) face of silicon.

Figs. 60 and 61 show the variation of the coefficient of friction μ and the wear rate M respectively with emery particle diameter D for abrasion of a (111) face of a silicon single crystal along a $[\bar{1}10]$ direction, both dry and wet with propyl alcohol at 1 kg load.

The coefficient of friction is seen to be constant on emery papers having D greater than about 30 microns and equal to 0.50 for dry abrasion and 0.43 for abrasion under propyl alcohol. On the finer grades the value of μ falls to 0.36 (on 4/0 emery) when abraded wet. This lowering of μ is in agreement with previous results for the abrasion of metals and non-metals (see section 3.2.1) and is a consequence of the partial clogging of these fine-grade emery papers by wear debris. However, on dry emery papers μ increases as D decreases to a value of 0.60 (4/0 emery paper), a result not previously reported. This is attributed to the appreciable pick-up of

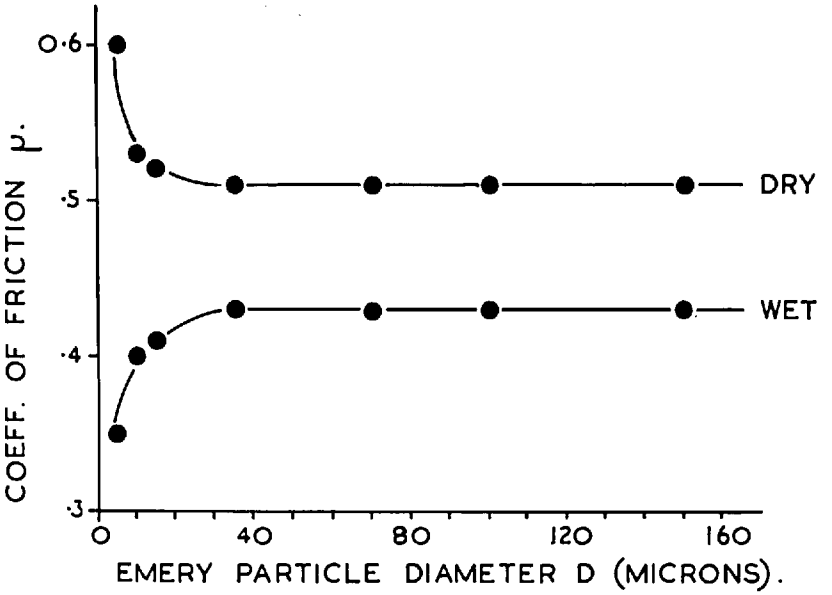


FIG.60

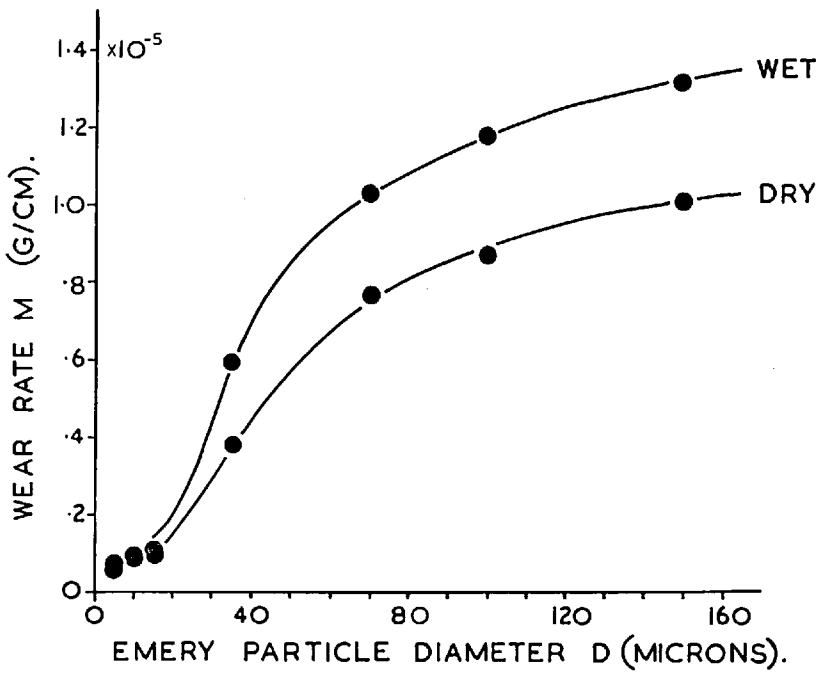


FIG.61

FIGS.60 & 61 VARIATION OF COEFFICIENT OF FRICTION (FIG.60) AND WEAR RATE (FIG.61) WITH EMERY PARTICLE DIAMETER, FOR ABRASION OF A (111) FACE OF A SILICON SINGLE CRYSTAL ALONG [$\bar{1}$10] AT 1 KG LOAD, ON EMERY PAPERS DRY AND WET WITH PROPYL ALCOHOL.

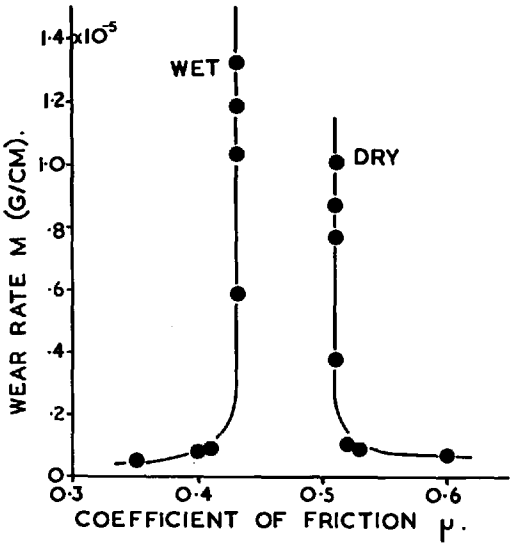


FIG.62 VARIATION OF WEAR RATE WITH COEFFICIENT OF FRICTION, FOR ABRASION OF A (111) FACE OF A SILICON SINGLE CRYSTAL ALONG [$\bar{1}$10] AT 1 KG LOAD, ON EMERY PAPERS DRY AND WET WITH PROPYL ALCOHOL.

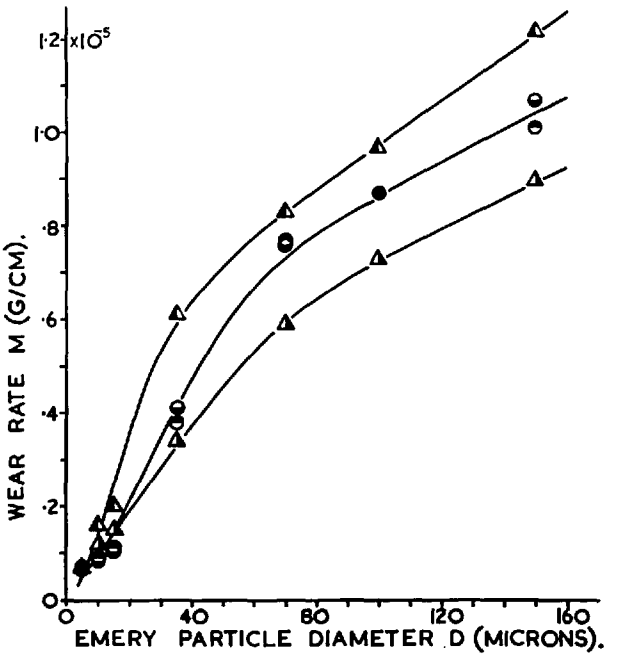


FIG.63 VARIATION OF WEAR RATE WITH EMERY PARTICLE DIAMETER FOR DRY ABRASION OF A (111) FACE OF A Si SINGLE CRYSTAL ALONG DIRECTIONS [$\bar{1}$10] (⊖), [1$\bar{1}$0] (⊖), [$\bar{1}$2$\bar{1}$] (△) AND [12$\bar{1}$] (△) AT 1 KG LOAD.

emery when the crystal is abraded dry on these fine-grade emery papers. Part of the load is then supported on emery-emery contacts for which the coefficient of friction is high ($\sim$1.0, see Goddard and Wilman, 1962).

Fig. 62 shows the variation of M with μ for abrasion along $[\bar{1}10]$ under both wet and dry conditions. It shows clearly that, on abrasives of particle diameter D greater than about 30 microns, the wear rate increases with D whilst the friction remains constant. Also, on all grades of abrasive (D from 5 to 150 microns), the use of a low viscosity lubricant (propyl alcohol) results in a higher wear rate and a lower friction coefficient than for abrasion on dry emery of the same grade, the slope of the (M,μ) locus for D greater than 30 microns being unaltered.

It appears, therefore, at the slow sliding speeds used here ($\sim$5 cm/sec), that the main effect of such a lubricant is to greatly reduce the rate and amount of pick-up of abrasive particles by the silicon. Thus, more of the load is supported on emery-silicon contacts and is effective in causing wear, and the friction is less raised by the high-friction emery-emery component. In fact the amount of pick-up is extremely small, as is shown by the electron diffraction patterns from the surface, which show an absence of rings due to diaspore. However, a small amount of pick-up may occur since the (M,μ)

locus for wet abrasion curves towards the M axis at its lower end (Fig. 62), and a linear (M,μ) locus is to be expected theoretically when pick-up is absent (Avient, Goddard and Wilman, 1960).

Although part of the load might be supported hydrodynamically on the liquid film, this is probably negligible at such slow sliding speeds and with a low-viscosity liquid, since such an effect would also reduce the wear, which is not observed.

Fig. 63 shows the variation of the (M,D) locus with azimuth, for dry abrasion parallel to $[\bar{1}10]$, $[1\bar{1}0]$, $[\bar{1}2\bar{1}]$ and $[1\bar{2}1]$ directions, and it is seen that the wear rate varies with azimuth, being least for abrasion along a $[1\bar{2}1]$ direction and greatest along a $[\bar{1}2\bar{1}]$ direction whilst the wear rates along $[\bar{1}10]$ and $[1\bar{1}0]$ directions are approximately equal. However, the magnitude of the variation in M with azimuth is small.

The Vickers indentation hardness H_D (see sections 1.8 and 2.5) of (111), (110) and (001) faces of silicon crystals on 3/0 emery paper wet with propyl was determined and found to be between 1040 and 1060 kg/mm^2 on all faces. A value of 1050 kg/cm^2 was taken as the mean hardness of such abraded faces, and this is in good agreement with values obtained by Wang and Alexander (1955) and by Mil'vidskii and Lainer (1961).

(b) Abrasion of a (110) face and a (001) face of silicon.

Single crystals of silicon were abraded wet (using propyl alcohol as lubricant) on grades 3 and 0 emery paper, parallel to $\langle 110 \rangle$, $\langle 112 \rangle$ and $\langle 100 \rangle$ directions on a (110) face and parallel to $\langle 110 \rangle$ and $\langle 100 \rangle$ directions on a (001) face. The values of the coefficient of friction and the wear rate for abrasion along these directions, and also along $[\bar{1}10]$ and $[\bar{1}2\bar{1}]$ directions on a (111) face, are given in Table 3.

There is hardly any variation of the coefficient of friction with azimuth, within the experimental error. However, the wear rate does vary with azimuth, the greatest difference being between the $\langle 112 \rangle$ and $\langle 110 \rangle$ azimuths on a (110) face, the wear rates on grade 3 emery paper being approximately 19×10^{-6} and 13×10^{-6} g/cm respectively. Little variation of the wear rate with azimuth is observed for abrasion of the (001) cube face.

The unidirectional abrasion of silicon does not appear to have been studied previously. However, silicon and germanium have the same crystallographic structure as diamond, and the dependence of the wear rate of diamond on abrasion direction during polishing has been extensively studied (Tolkowsky, 1920; Slawson and Kohn,1950; Wilks, 1952;

Table 3. Wear rate M and coefficient of friction μ for unidirectional abrasion of (111), (110) and (001) faces of silicon on 3 and 0 grade emery papers wet with propyl alcohol at 1 kg load.

		Emery paper grades.			
	Abrasion Direction	3 grade $M(10^{-6}g/cm)$	μ	0 grade $M(10^{-6}g/cm)$	μ
(111) face	$\bar{1}10$	13.2	0.44	5.9	0.44
	$\bar{1}2\bar{1}$	16.4	.44	7.2	.43
(110) face	$\bar{1}10$	13.6	.45	5.3	.45
	$1\bar{1}0$	12.6	.45	5.4	.44
	100	16.8	.44	7.9	.44
	$\bar{1}00$	16.8	.45	7.9	.44
	$1\bar{1}\bar{2}$	18.0	.44	6.5	.43
	$\bar{1}12$	20.2	.45	7.7	.43
(001) face	$\bar{1}10$	17.5	.44	6.7	.42
	$1\bar{1}0$	18.0	.44	6.8	.43
	100	16.6	.44	6.2	.43
	$\bar{1}00$	17.0	.44	6.4	.42

Denning, 1953, 1955; Wilks and Wilks 1954; Hukao, 1955; Seal, 1957; Bowden and Scott, 1958). The results of all these workers are in substantial agreement and show that the wear rate depends very markedly on the direction of abrasion.

A diamond may readily be abraded on a (100) face if the direction of abrasion is $[010]$ or $[001]$ but not if the direction of abrasion is $[011]$ or $[0\bar{1}1]$. On (110) faces the $[001]$ directions are those of high wear rate and the $[\bar{1}10]$ directions are those of low wear rate. All directions on (111) faces are of low wear rate but there are conflicting reports of the variation of the relative resistance to abrasion with azimuth. Wentorf (1959) states that the $\langle 112 \rangle$ directions are the directions of least wear on an octahedral face.

The overall variation in wear rate between the most and least wear resistant directions is by a factor of between 100 and 500. This is in direct contrast to the present results for silicon where the overall variation is by less than a factor of 2. However, diamond is the hardest known natural substance. Ordinarily, the abrasion or polishing process is thought of as the ploughing of the harder abrading particles through the abraded surface. For the abrasion of diamond the abrasive particles cannot be appreciably harder than diamond and such an abrasion process is unlikely. Wentorf (1959) suggested that a scratched diamond surface fails in tension behind the

scratching particle, and that the octahedral cleavage planes are most easily pulled apart and give rise to the strong dependence of wear on crystal orientation. For the abrasion of silicon ($H_D \sim 1050$ kg/mm^2) it is likely that the usual ploughing process occurs.

3.5.2. Optical examination of abrasion grooves on silicon single crystals.

In order to study the shape and nature of individual abrasion grooves short abrasion stokes ($\sim$2mm) were made on the specimen using dry grade 3 emery paper.

Figs. 64 to 67 are photographs of such grooves for a (111) face obtained using the Vickers projection microscope at a magnification of 300 times. Similar grooves were observed on the (110) and (001) faces of silicon crystals. Although the grooves have a reasonably well-defined shape there is appreciable cracking and conchoidal fracture. Fig. 64 shows the end of an abrasion groove parallel to $[\bar{1}1\bar{1}]$ direction.

The amount of fracture which occurs does not vary appreciably with direction of abrasion, as is seen from Fig.67, which shows a groove along the $[\bar{1}10]$ direction crossing a groove along the $[\bar{1}2\bar{1}]$ direction. It is probable that this conchoidal fracture is responsible for most of the wear which occurs during abrasion, although there is some plastic deformation, as indicated by the electron diffraction study of the abraded silicon surface (see section 3.5.3).

Figs. 64 to 67. Individual abrasion grooves on a (111) silicon face abraded parallel to $[\bar{1}10]$ and $[\bar{1}2\bar{1}]$ directions on dry grade 3 emery paper at 1 kg load (abrasion direction left to right).



Fig. 64. x 300
Abrasion along $[\bar{1}2\bar{1}]$

Fig. 65. x 300
Abrasion along $[\bar{1}2\bar{1}]$



Fig. 66. x 300
Abrasion along $[\bar{1}10]$



Fig. 67. x 300
Abrasion along $[\bar{1}10]$ and $[\bar{1}2\bar{1}]$

3.5.3. Electron diffraction examination of a unidirectionally abraded single crystal of silicon.

An octahedral face of a silicon single crystal was unidirectionally abraded parallel to $[\bar{1}10]$ and $[\bar{1}2\bar{1}]$ directions on grade 3/0 emery paper, both dry and wet with propyl alcohol, at 1 kg load. Electron diffraction patterns were obtained from the freshly abraded surface and also from the surface as revealed by etching in a 1 : 200 solution and a 1 : 50 solution of 40% HF and concentrated HNO_3 by volume. These solutions removed the abraded surface at a rate of approximately 2 and 0.5 microns/minute respectively as determined by weighing.

The specimen was usually examined with the electron beam perpendicular, at 45^{o} and parallel to the abrasion direction, these settings being referred to below as the perpendicular, 45^{o} and parallel settings. The arrow on photographs attained at the perpendicular setting indicates the direction of motion of the abrasive particles over the specimen surface.

(a) Abrasion of silicon along (111) $[\bar{1}10]$ on 3/0 emery paper flooded with propyl alcohol, at 1 kg load.

The use of propyl alcohol as a lubricant during the unidirectional abrasion virtually eliminates the pick-up of abrasive emery by the silicon and diffraction patterns due to silicon alone were obtained, Figs. 68 to 72.

Figs. 68a and 68b were obtained from the abraded surface before etching, at the perpendicular and parallel settings respectively. A pattern consisting of rings of uniform intensity was obtained at both settings, indicating that the abraded surface region is composed of randomly oriented crystallites (cf. Fig.73). Silicon has a diamond-type crystallographic structure and therefore yields a ring or spot pattern corresponding to the face-centred cubic crystals except that rings or spots with indices for which $(h + k + l)/2 = 2m + 1$ where m is an integer, are forbidden by the structure factor. The probable reason for their appearance is double scattering.

In Fig. 68a faint diffractions from the undisturbed single crystal lattice are seen. These diffractions from the single crystal result from part of the electron beam striking a portion of the underlying single crystal which has been exposed, assumedly as a result of fracture during the abrasion process.

Patterns obtained after etching the specimen in 1 : 200, HF : HNO_3 for four seconds (Fig.69) show that the single crystal spot pattern is now very prominent, although there is still some polycrystalline silicon giving rise to the rings of uniform intensity. The positions of the diffractions from the single crystal at the perpendicular and parallel settings are indiced in Fig. 73. In the perpendicular setting (Fig.69a) these diffraction spots are elongated round the ring

Figs.68 to 72. Unidirectional abrasion of a silicon single crystal along (111) $[\bar{1}10]$ on 3/0 emery paper wet with propyl alcohol, at 1 kg load (Etch 1 : 200, HF : HNO_3).

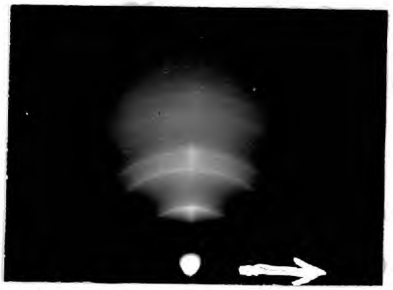


Fig.68a. ⊥

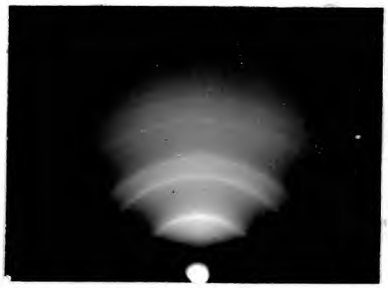


Fig.68b //

Fig.68. Unetched surface.

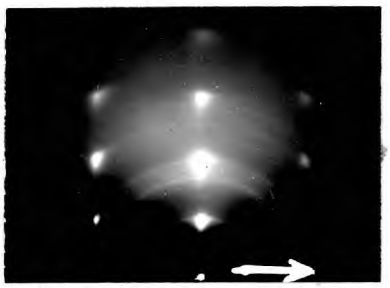


Fig.69a. ⊥



Fig.69b. 45°

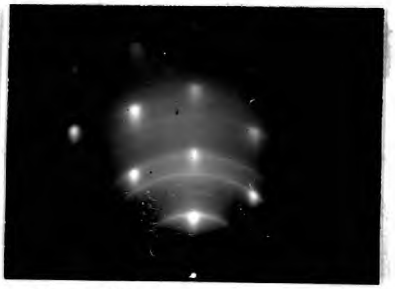


Fig.69c. //

Fig.69. Etched 4 sec.

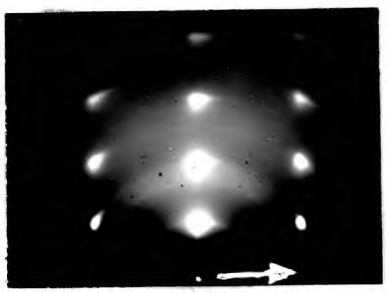


Fig.70a. ⊥

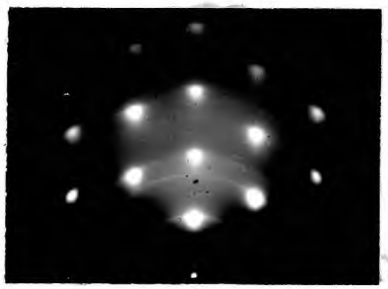


Fig.70b //

Fig.70. Etched 8 sec.

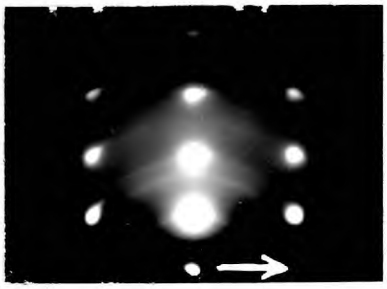


Fig.71. ⊥
Etched 16 sec.

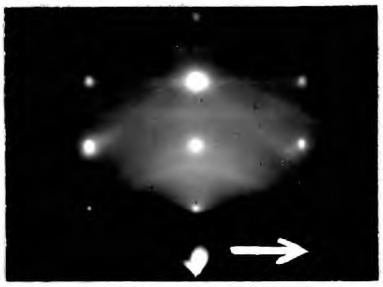


Fig.72. ⊥
Etched 2 min.

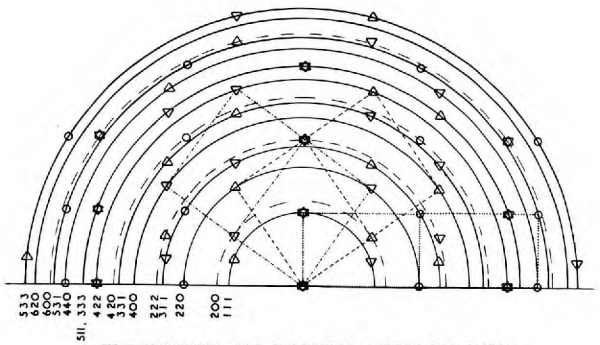


FIG.73 THEORETICAL RING DIFFRACTION PATTERN FOR SILICON. FORBIDDEN RINGS, FOR WHICH (H+K+L)/2 IS AN ODD INTEGER, ARE SHOWN THUS — — — . DIFFRACTIONS, FROM A 111 FACE OF THE CRYSTAL, DENOTED BY THE SAME SYMBOL APPEAR PRACTICALLY TOGETHER AT THE FOLLOWING TYPES OF AZIMUTHAL DIRECTION OF THE ELECTRON BEAM :-
△ [$\bar{1}$10]; ▽ [1$\bar{1}$0]; o [$\bar{1}$2$\bar{1}$].

positions in the direction of motion of the abrasive particles over the abraded silicon surface, in a similar manner to that observed for the abrasion of calcite (section 3.3.3). In the patterns obtained at the 45° and parallel settings these diffractions are not elongated in this manner (Figs.69b and 69c). This corresponds to a rotation of the single crystal pattern about an axis normal to the abrasion direction and lying approximately in the surface.

Patterns obtained after further etching of the specimen (Figs. 70 to 71) show stronger diffractions from the single crystal. After 2 minutes etching patterns were obtained with strong Kikuchi lines present (Fig.72) but further etching (a total of 6 minutes) was necessary to obtain patterns free of any random orientation. This corresponds to a depth of about 3 microns, as determined from the mean etch rate.

(b) Abrasion of silicon along (111) $[\bar{1}2\bar{1}]$ on 3/0 emery paper flooded with propyl alcohol, at 1 kg load.

The abrasion of the octahedral face of a silicon single crystal along a $[\bar{1}2\bar{1}]$ direction on 3/0 emery paper with propyl alcohol, resulted in a similar change of the electron diffraction pattern of the surface, as revealed by gradually etching down to the underlying single crystal (Figs.74 to 77), as observed for abrasion along a $[\bar{1}10]$ direction.

A forward rotation of the single crystal spot pattern was again observed and diffraction patterns solely from the

Figs.74 to 77. Unidirectional abrasion of a silicon single crystal along (111) [$\bar{1}$21] on 3/0 emery paper wet with propyl alcohol, at 1 kg load (Etch 1 : 50, HF : HNO_3).

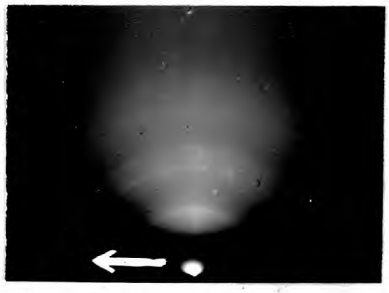


Fig.74a. ⊥



Fig.74b. //

Fig.74. Unetched surface.

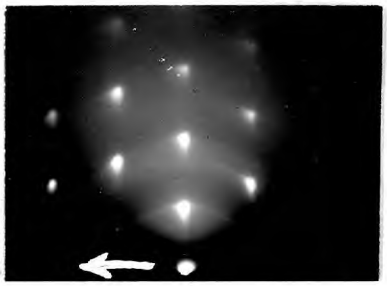


Fig. 75. ⊥
Etched 2 sec.

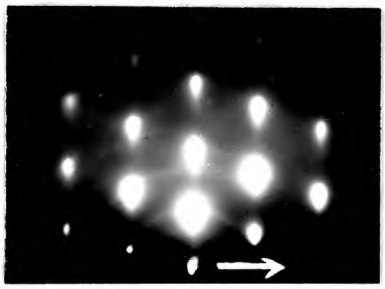


Fig.76a. ⊥

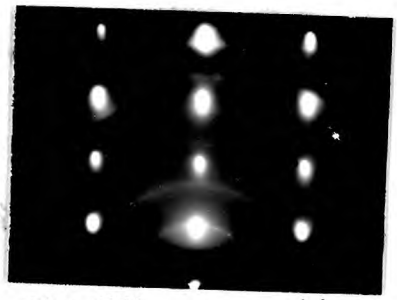


Fig.76b. //

Fig.76. Etched 4 sec.

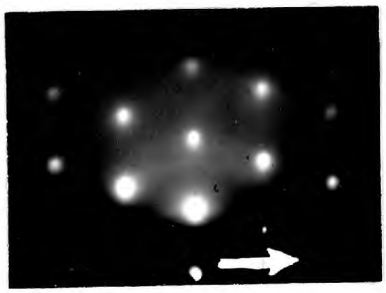


Fig.77. ⊥
Etched 40 sec.

undisturbed single crystal region were obtained after etching for one minute in 1 : 50, HF : HNO_3 solution. Figs.74 to 77 show this gradual transition from the randomly oriented polycrystalline abraded surface to the almost perfect single crystal.

(c) Abrasion of silicon along (111) $[\bar{1}10]$ on dry 3/0 emery paper, at 1 kg load.

Figs. 78 to 81 are photographs of electron diffraction patterns obtained from a (111) face of the silicon single crystal after dry abrasion parallel to a $[\bar{1}10]$ direction.

Figs. 78a and 78b were obtained from the freshly abraded, unetched surface in the perpendicular and parallel settings respectively. The pattern is seen to consist of rings from randomly oriented crystallites of silicon (see Fig.68) with many extra rings superimposed on it. These extra rings were identified from the A.S.T.M. file of X-ray powder pattern data (1955) as due to diaspore, α-AlOOH, which is found to be always a component of emery. Hence it is evident that silicon picks up emery particles from the fine-grade abrasive emery sheet during dry abrasion.

Examination of the specimen after four seconds etch in 1 : 50, HF : HNO_3 yielded a strong single crystal spot pattern, with a similar rotation to that observed as a result of abrasion on wet 3/0 emery paper. This pattern is superimposed on the ring pattern. Further etching (9 seconds)

Figs.78 to 81. Unidirectional abrasion of a silicon single crystal along (111) $[\bar{1}10]$ on dry 3/0 emery paper, at 1 kg load (Etch 1 : 50, HF : HNO_3).

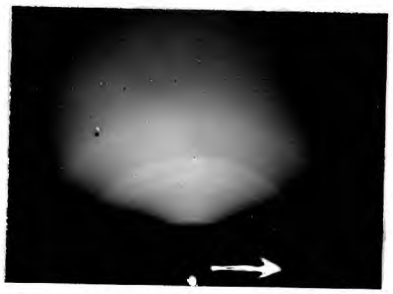


Fig.78a. ⊥

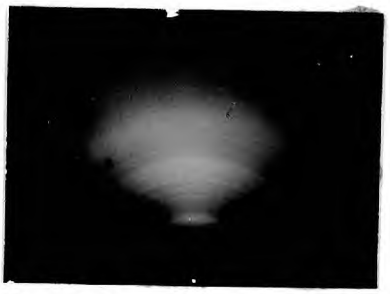


Fig.78b. //

Fig.78. Unetched specimen.

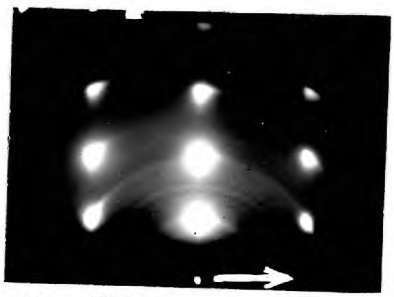


Fig.79a. ⊥

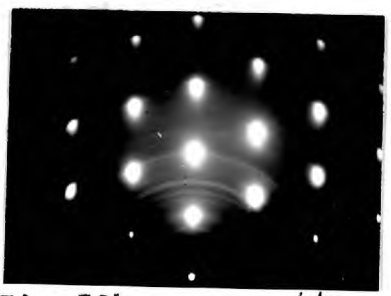


Fig.79b. //

Fig.79. Etched 4 sec.

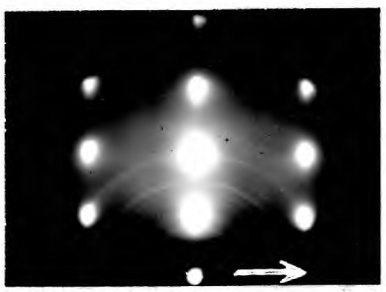


Fig.80. Etched 9 sec ⊥

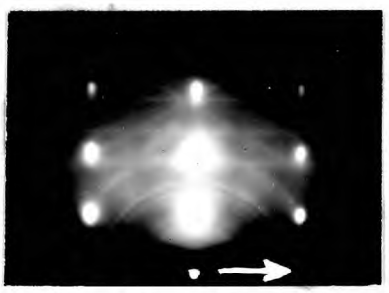


Fig.81. Etched 19 sec. ⊥

yields a similar pattern without the rotation and strong Kikuchi lines are visible after 19 seconds etch. Still further etching is required to remove all traces of the diaspore ring pattern.

Fig. 82 was obtained from a (110) face of a silicon single crystal which had been polished and etched at the Standard Telecommunication Laboratories, Harlow. Other silicon specimens from this laboratory yielded single crystal diffraction patterns but a strong one-degree orientated ring pattern was obtained from this specimen.

Using graphite (d_{100} = 1.230 Å) to calibrate the ring pattern, the equivalent net-plane spacings were compared with those given on the A.S.T.M. index cards. It was evident that these spacings corresponded to α- Al_2O_3, corundum, which was obviously embedded in the silicon surface. Such pick-up and embedment of the corundum must have occurred during the polishing process, probably because the specimen was not kept wet enough during this process, and the subsequent etching had not been sufficient to remove this worked layer. The corundum is partially oriented with (0001) planes parallel to the surface (see theoretical pattern, Fig. 83). The corundum probably becomes oriented either by suffering cleavage on certain planes after embedment, or by becoming fragmented, the fragments becoming partly embedded and attaining the orientation

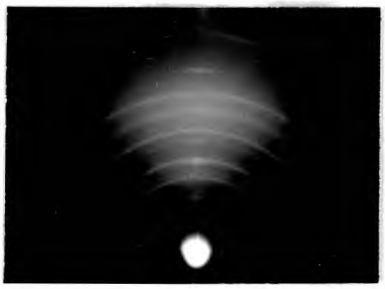


Fig. 82. Silicon (110) face polished using corundum, α-Al_2O_3. Pattern shows embedded corundum oriented with (0001) planes parallel to the specimen surface.

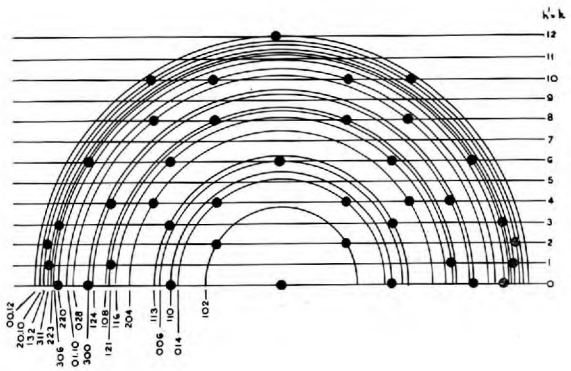


Fig. 83. Theoretical pattern from α-Al_2O_3 (corundum) in one-degree orientation (hexagonal cell).

by progressive impacts. Similar patterns due to (0001) one-degree oriented corundum were obtained by Harvey (1959, see also Harvey and Wilman 1960) from a niobium specimen after polishing it with levigated alumina (α-Al_2O_3) on a 'Selvyt' cloth lubricated with benzene, attached to a polishing wheel.

These results show clearly that silicon readily picks up abrasive particles when it is abraded, unless strong precautions are taken to keep the abraded surface well lubricated.

3.6. Discussion of Results for the Abrasion of Single-Crystal Silicon.

Although cutting and abrasion processes are often used in the manufacture of semiconductor devices, the present results form the first known investigation of the friction and wear of silicon and its dependence on the direction of abrasion. They show that, within experimental error, the coefficient of friction does not vary with direction or plane of abrasion, and the wear rate on grade 3 emery paper wet with propyl alcohol varies by less than a factor of two. This is in marked contrast to the variation of the wear rate of diamond, which has the same crystallographic structure as silicon. The overall variation of the wear rate with azimuth during the polishing of diamond is by a factor of 100 to 500 (see section 3.5.2).

The optical examination of individual abrasion grooves and the electron diffraction study of the fully abraded surface lead to the conclusion that much of the damage caused by abrasion (surface scratches) is produced by conchoidal fracture and cracking of the surface regions by the abrading emery particles. Buck (1960) examined scratches made on an etched germanium surface (orientation unspecified) by a few SiC particles (600 mesh, nominal particle size 25μ) in water on a glass plate. The scratches so formed were similar to those observed on silicon crystals in the present results for short

abrasion strokes on emery paper (section 3.5.2).

The preparation of semiconductor devices often involves cutting specimens from large single crystals followed by abrading, lapping or polishing. The damage caused by these operations often has drastic effects on the electrical properties of the semiconductor and it is necessary to remove the damaged layer by etching. It is therefore important to know the depth of the surface damage.

The damage to silicon or germanium surfaces resulting from such treatment causes changes in surface recombination velocity, field effect mobility, conductivity, etching rate, X-ray rocking curves and other properties. These effects provide methods of estimating the depth of the damaged layer. Buck (1960, see also Buck and McKim, 1956) has shown that reasonable agreement is found amongst the various estimates of the depth of surface damage resulting from a particular surface preparation treatment, as determined by measuring changes in one of these properties.

Depths of damage of 3 and 7 to 10 microns were estimated for silicon crystals lapped with 3200 and 600 mesh abrasives respectively (particles sizes 5 and 25 microns) used in a water slurry on glass (see Buck, 1960). The depth of damage on a germanium crystal is approximately twice that on silicon for the same abrasive treatment. Camp (1955) reported

depths of damage of 3, 4 and 5 microns on {110}, {111} and {100} faces respectively of germanium lapped a 3200 mesh abrasive (5 microns).

Pugh and Samuels (1961, 1962), using a metallographic taper-sectioning technique, have studied the structure of the damaged layer produced on {111} surfaces of germanium by abrasion. They concluded that the abrasion process involves both cleavage and non-crystallographic fracture and that the surface layer contains many cracks initiated by these fracture processes. They also conclude, from depth of deformation measurements, that the cracked layer is the classical damaged layer as determined by established methods (e.g. Buck,1960). Examination of the taper sections indicates extremely fine cracks extending for considerable depths below the surface irregularities, and that the grooves produced by abrasion on 220 grade SiC papers (particle size 70 μ) contain many cleavage facets. The results of Pugh and Samuels (1961, 1962) also indicate that the cracked layer (damaged layer) extends to a depth about four times the depth of the surface irregularities. Wolff, Wilbur and Clark (1957) showed by optical means that a large proportion of {111} cleavage facets are developed in lapped germanium surfaces.

The nature of the damage caused by these cutting and abrading processes is not yet fully understood. The present

electron diffraction results show that the outer region of the damaged layer is composed of randomly oriented crystallites. Silicon and germanium are known to deform plastically at temperatures above 900°C and 500°C respectively and slip occurs on $\{111\}$ planes along $\langle 1\bar{1}0\rangle$ directions (Gallagher, 1952; Treuting, 1952, 1955). Pearson, Read and Feldmann (1957) observed plastic deformation in very small silicon crystals at temperatures as low as 600°C. Although very high local temperatures are obtained between sliding surfaces (Bowden and Tabor, 1950), there cannot be enough plastic flow in the present case to give an oriented surface layer.

However, the sub-surface regions yield single crystal electron diffraction patterns with asymmetric arcing, indicating some plastic deformation by lattice rotations. Avient (1962) observed two sets of additional diffractions on an abraded silicon single crystal, which could correspond to flexural rotational slip involving flexure of the $(1\bar{1}1)$ and $(\bar{1}11)$ slip planes about their respective axes, $\langle\bar{1}12\rangle$ and $\langle 1\bar{1}2\rangle$, both of which are perpendicular to the slip direction $\langle 110\rangle$. Previous observations of similar lattice rotations in metals have been referred to previously (section 3.5) in the discussion of the deformation of calcite single crystals during abrasion.

It appears most likely that the two regions of deformation observed in the present investigation, the outer-

most polycrystalline region and the oriented sub-surface region, correspond approximately to the outermost region of surface irregularities and the cracked layer containing deep, fine cracks, observed in germanium by Pugh and Samuels (1961).

However, a complete description of the nature of the abrasion damage has to explain the effects on various phenomena such as X-ray rocking curves, etching rates and the lifetime of minority carriers. The measurable effects on these phenomena are all felt to about the same depth (Buck, 1960), which is approximately the depth of the cracked layer.

A mechanically damaged semiconductor surface etches more rapidly than a thoroughly etched surface. However, the damaged surface contains many cracks so that its true surface area is much larger than its apparent surface area. Thus, the etchant attacking a larger specimen area and, if the etch rate is determined from the mass loss and the apparent surface area, the measured etch rate will be larger than that for a relatively flat, thoroughly etched surface.

The presence of high dislocation densities in damaged semiconductor surfaces has been suggested (Hopkins, 1955; Dash, 1958), but no direct evidence of such high densities have been reported at room temperature. Johnston, Stokes and Li (1958) were able to generate dislocations in germanium by fracturing a crystal at room temperature under an etching

solution. In this situation the fracture stress is much higher than it is in air.

Dash (1959) has shown that a scratch made on silicon at room temperature serves as a source of dislocation loops which move into the bulk of the crystal on subsequent heating. He does not interpret this as proving necessarily that dislocations were near the surface at room temperature; they may well be there, but if so they are evidently too dense to be resolved by conventional techniques. Dash (1959) also observed slip bands, in the neighbourhood of an indentation ($\sim$100 μ diameter) made with a 10^{-3} inch radius diamond point, after heating the specimen to 1000^{o}C for a few minutes. Thus some of the elastic energy in the indentation was released at an elevated temperature, causing plastic flow. Allen (1959) proposed "dislocation cracks" to explain phenomena produced by local impact on InSb. The particular configuration of dislocations produced was called a "dislocation crack" because of its close resemblance in macroscopic features to an ordinary crack. The stress required to produce a "dislocation crack" was shown to be of the same order as the fracture stress. Cottrell (1958, see also Mott, 1956b) proposed theoretical mechanisms by which a crack might be formed as a result of accumulations of dislocations at a suitable barrier. It is evident, however, that the true nature and mechanism of the surface damage in semiconductors on abrasion is as yet not fully understood.

CONCLUSION.

4. CONCLUSION.

The present experiments have been carried out in an attempt to understand more fully the nature of the abrasive wear process.

A detailed study of the textures developed on the compression and rolling of readily plastically deformable non-metals (AgCl and AgBr) shows that the surface re-orientation developed in these materials on unidirectional abrasion on emery papers is closely related to the rolling texture and the compression texture observed when extensive lateral flow is permitted. This close correspondence to the rolling texture seems to be due to the indenting emery particles being mostly very obtuse tipped, so that in the abrasion the plastic flow under the emery particles is indeed not very different in type and direction to the plastic flow under the roller in rolling.

It has been shown that, in the unidirectional abrasion of single crystals of silicon, under dry conditions and also in the presence of a low-viscosity lubricant, the wear occurs chiefly by cracking and conchoidal fracture of the abraded surface in the region of the grooves formed by the indenting hard abrasive particles of emery. The nature of this fragmentation is shown clearly for the abrasion of calcite, which, like silicon, is very brittle. However, the abrasion of both these materials also results in considerable plastic flow

taking place, causing lattice rotations, about a direction approximately normal to the abrasion direction and lying in the mean plane of the surface.

Previous workers, studying the abraded surfaces of silicon or germanium single crystals (eg. Pugh and Samuels, 1961, 1962), have made no mention of any such plastic flow, but the present results show clearly that such plastic deformation does occur, even at room temperature, in conjunction with the brittle fracture.

The results also show that there is considerable pick-up of emery particles by the silicon surface when the crystal is abraded on dry emery papers. This pick-up may be virtually eliminated by the use of a lubricant (in the present case, propyl alcohol).

ACKNOWLEDGMENTS.

ACKNOWLEDGMENTS.

The author wishes to express his sincere thanks to Dr. H. Wilman, for his constant interest in the work, and also for many helpful suggestions and discussions.

He also wishes to thank The Standard Telecommunication Laboratories, Harlow, for the bursary which made this research possible.

APPENDICES.

APPENDIX A.

Inter-relationship between the axes and net-plane indices in the rhombohedral, hexagonal and cubic axes of reference for calcite.

In the study of crystals it is often necessary to change the axes of reference and the corresponding net-plane indices to another set; this can be done by fairly simple algebraic operations. A rhombohedral lattice may be described in terms of rhombohedral or hexagonal axes. Fig.84 shows the relation between two such sets of axes. A translation of distance a_r along the rhombohedral axis $\underline{a}_r$ corresponds to a translation $\left[1/3,\ 2/3,\ 1/3\right]$ in the hexagonal system, in the relative setting chosen here, i.e.

$$a_r = \left[1/3,\ 2/3,\ 1/3\right]_h$$

Similarly $b_r = \left[\bar{2}/3,\ \bar{1}/3,\ 1/3\right]_h$ and $c_r = \left[1/3,\ \bar{1}/3,\ 1/3\right]_h$ ...1

If the Miller indices of a net plane (or the Laue indices of a diffracted beam) are (p q r) relative to the rhombohedral axes, then correspondingly the indices are (h k l) relative to these hexagonal axes, where:-

$$\left.\begin{array}{l} p = (h + 2k + 1)/3 \\ q = (-2h - k + 1)/3 \\ r = (h - k + 1)/3 \end{array}\right\} \ldots 2 \quad \text{and} \quad \left.\begin{array}{l} h = -q + r \\ k = p - r \\ l = p + q + r \end{array}\right\} \ldots 3$$

The c/a hexagonal ratio in terms of the rhombohedral angle α is given by:-

$$c/a = 3/2\sqrt{(\cot^2 \alpha/2 - 1/3)}. \qquad \ldots 4$$

The rhombohedral angle α' of the half-height rhombohedron, where α is the angle of the full-sized rhombohedron, is given by :-

$$\tan \frac{\alpha'}{2} = 2 \sin \frac{\alpha}{2}. \qquad \ldots 5$$

A 60° rhombohedral lattice can also be represented as a face-centred cubic lattice, and if the rhombohedral angle is not exactly 60° the lattice can be represented as a face-centred rhombohedral lattice (pseudo face-centred cubic lattice). Fig. 85 shows the relation between the two sets of axes. A translation a_r along the rhombohedral axis $\underline{a}_r$ corresponds to a translation $\left[0, \frac{1}{2}, \frac{1}{2}\right]$ in the face-centred lattice, in the relative setting chosen here, i.e.

$$a_r = \left[0, \tfrac{1}{2}, \tfrac{1}{2}\right]_{fr}$$

Similarly $b_r = \left[\tfrac{1}{2}, 0, \tfrac{1}{2}\right]_{fr}$ and $c_r = \left[\tfrac{1}{2}, \tfrac{1}{2}, 0\right]_{fr}$ ...6

In general, if a net plane has Miller indices (p q r) relative to the rhombohedral axes, then its indices relative to the face-centred rhombohedral axes will be (P Q R), where:-

$$\left.\begin{aligned} p &= (Q + R)/2 \\ q &= (R + P)/2 \\ r &= (P + Q)/2 \end{aligned}\right\} \ldots 7 \text{ and } \left.\begin{aligned} P &= -p + q + r \\ Q &= p - q + r \\ R &= p + q + r \end{aligned}\right\} \ldots 8$$

The relation between the rhombohedral angle α and the face-centred rhombohedral angle α_{fr} is given by:-

$$\tan \frac{\alpha_{fr}}{2} = 2 \sin \frac{\alpha}{2}. \qquad \ldots 9$$

From equations (2) and (8) a direct relation may be obtained between the Miller indices (h k l) and (P Q R) of a net-plane(or the Laue indices of a diffracted beam) relative to the hexagonal and the face-centred rhombohedral (pseudo face-centred cubic) axes of the lattice, i.e.

$$\left.\begin{aligned} P &= (-2h - 4k + 1)/3 \\ Q &= (4h + 2k + 1)/3 \\ R &= (-2h + 2k + 1)/3 \end{aligned}\right\} \quad \ldots 10 \quad \text{and} \quad \left.\begin{aligned} h &= (Q - R)/2 \\ k &= (-P + R)/2 \\ l &= P + Q + R \end{aligned}\right\} \quad \ldots 11$$

Relation between the crystal lattices and the reciprocal lattices of the true rhombohedral cell and the pseudo face-centred cubic (face-centred rhombohedral) cell, for calcite.

For a rhombohedral lattice having axial length a and angle α, the corresponding reciprocal-lattice cell axial length a* and angle α^* are given by

$$a^* = \frac{\sin\alpha}{a\sqrt{1 - 3\cos^2\alpha + 2\cos^3\alpha}}$$

$$\cos\alpha^* = \frac{-\cos\alpha}{1 + \cos\alpha}$$

From the lattice dimensions of the true rhombohedral cell (a_{rt} = 6.36 kX, α_{rt} = 46° 6') the reciprocal lattice dimensions are calculated to be

a^*_{rt} = 0.239 kX^{-1} and α^*_{rt} = 114° 10'.

The lattice dimensions of the corresponding hexagonal lattice are a_h = 4.98 kX and c_h = 17.02 kX. Thus in Figs.84 and 86 the half-height rhombohedron (which has its trigonal axis half the length of the trigonal axis of the true cell) has a lattice dimension a_r given by

$a_r^2 = (c_h/6)^2 + (a_h/\sqrt{3})^2$, and hence

a_r = 4.04 kX.

The face-centred rhombohedral cell (i.e. the pseudo-cubic cell) has an angle α_{fr} = 101° 55', and its lattice dimension a_{fr} can be calculated from Fig. 85,

$a_{fr} = a_r \sec(\alpha_{fr}/2)$,

= 6.41 kX, and thus

a^*_{fr} + 0.165 kX^{-1} and α^*_{fr} = 74° 55'

The face-centred rhombohedral, pseudo-cubic cell.

If one considers the reciprocal lattice of the pseudo-cubic cell with c^*_{fr} vertical and a^*_{fr} and b^*_{fr} slightly upwardly inclined to the horizontal plane (the angles between these reciprocal axes being $74^\circ\ 55'$, as determined above) then this horizontal plane corresponds to a pseudo-cube face in the crystal lattice and hence a cleavage face (001). The (100)* and (010)* planes are therefore vertical and the angle between the projections of a* and b* onto the cleavage plane equals $\alpha^*_{fr.p}$ and is given by:-

$$\cos \alpha^*_{fr.p} = \frac{\cos \alpha^*_{fr}}{1 + \cos \alpha^*_{fr}}$$

and $$\alpha^*_{fr.p} = 78^\circ\ 5'.$$

APPENDIX B.

Values of the wear rate, M, and the friction coefficient, μ, for unidirectional abrasion of a (001) calcite cleavage face on dry emery papers at 1 kg load along different directions.

Emery	Direction of Abrasion							
	$[\bar{1}\bar{1}0]$		$[110]$		$[1\bar{1}0]$		$[\bar{1}10]$	
Grade	M(g/cm)	μ	M(g/cm)	μ	M(g/cm)	μ	M(g/cm)	μ
4/0	2.3×10^{-6}	0.49	5.0×10^{-6}	0.52	3.0×10^{-6}	0.63	4.0×10^{-6}	0.63
3/0	7.3×10^{-6}	.56	9.8×10^{-6}	.63	1.5×10^{-5}	.65	1.5×10^{-5}	.65
2/0	9.5×10^{-6}	.58	2.7×10^{-5}	.67	1.6×10^{-5}	.67	1.8×10^{-5}	.66
0	3.8×10^{-5}	.70	3.4×10^{-4}	.78	1.3×10^{-4}	.77	1.3×10^{-4}	.77
1	4.1×10^{-5}	.70	4.1×10^{-4}	.83	-	-	-	-
1G	4.7×10^{-5}	.72	5.7×10^{-4}	.86	2.2×10^{-4}	.82	2.0×10^{-4}	.81
2	5.1×10^{-5}	.73	6.1×10^{-4}	.88	2.4×10^{-4}	.84	2.3×10^{-4}	.84
3	4.9×10^{-5}	.73	7.1×10^{-4}	.89	2.6×10^{-4}	.84	2.6×10^{-4}	.85
$3/0_H$	3.0×10^{-5}	.65	2.6×10^{-4}	.75	-	-	-	-
0_H	2.3×10^{-5}	.62	2.1×10^{-4}	.74	-	-	-	-

Values of M and μ for dry abrasion of calcite cleavage face, 1 kg load (continued).

Emery Grade	Direction of Abrasion [0$\bar{1}$0] M(g/cm)	μ	[010] M(g/cm)	μ
4/0	3.0×10^{-6}	0.51	3.6×10^{-6}	0.59
3/0	6.4×10^{-6}	.57	1.6×10^{-5}	.67
2/0	8.6×10^{-6}	.58	2.3×10^{-5}	.68
0	4.5×10^{-5}	.69	1.6×10^{-4}	.78
1	5.8×10^{-5}	.72	2.3×10^{-4}	.80
1G	7.4×10^{-5}	.75	2.8×10^{-4}	.83
2	8.0×10^{-5}	.76	3.3×10^{-4}	.85
3	1.00×10^{-4}	.78	4.0×10^{-4}	.86
$3/0_H$	4.1×10^{-5}	.68	9.5×10^{-5}	.76
0_H	3.5×10^{-5}	.66	-	-

APPENDIX C.

Values of the wear rate, M, and the friction coefficient, μ, for unidirectional abrasion of a (111) surface of a silicon single crystal on emery papers at 1 kg load along different directions.

(a) Dry Abrasion.

Emery	Direction of Abrasion							
	$[\bar{1}10]$		$[1\bar{1}0]$		$[\bar{1}2\bar{1}]$		$[1\bar{2}1]$	
Grade	M(g/cm)	μ	M(g/cm)	μ	M(g/cm)	μ	M(g/cm	μ
4/0	7×10^{-7}	0.60	6×10^{-7}	0.60	7×10^{-7}	0.60	7×10^{-7}	0.60
3/0	9×10^{-7}	.53	8×10^{-7}	.54	1.6×10^{-6}	.56	1.2×10^{-6}	.55
2/0	1.1×10^{-6}	.52	1.0×10^{-6}	.53	2.0×10^{-6}	.54	1.5×10^{-6}	.54
0	3.8×10^{-6}	.51	4.1×10^{-6}	.51	6.1×10^{-6}	.51	3.4×10^{-6}	.51
1G	7.7×10^{-6}	.51	7.6×10^{-6}	.51	8.3×10^{-6}	.51	5.9×10^{-6}	.51
2	8.7×10^{-6}	.51	8.7×10^{-6}	.51	9.7×10^{-6}	.51	7.3×10^{-6}	.51
3	1.01×10^{-5}	.51	1.07×10^{-5}	.51	1.22×10^{-5}	.51	9.0×10^{-6}	.51

(b) Wet abrasion, using propyl alcohol.

Emery Grade	Direction of Abrasion $[\bar{1}10]$ M(g/cm)	μ	$[\bar{1}2\bar{1}]$ M(g/cm)	μ
4/0	5×10^{-7}	0.35	6×10^{-7}	0.35
3/0	8×10^{-7}	.40	9×10^{-7}	.40
2/0	9×10^{-7}	.41	9×10^{-7}	.41
0	5.9×10^{-6}	.43	7.2×10^{-6}	.43
1G	1.03×10^{-5}	.43	1.19×10^{-5}	.44
2	1.18×10^{-5}	.43	1.37×10^{-5}	.44
3	1.32×10^{-5}	.43	1.64×10^{-5}	.44

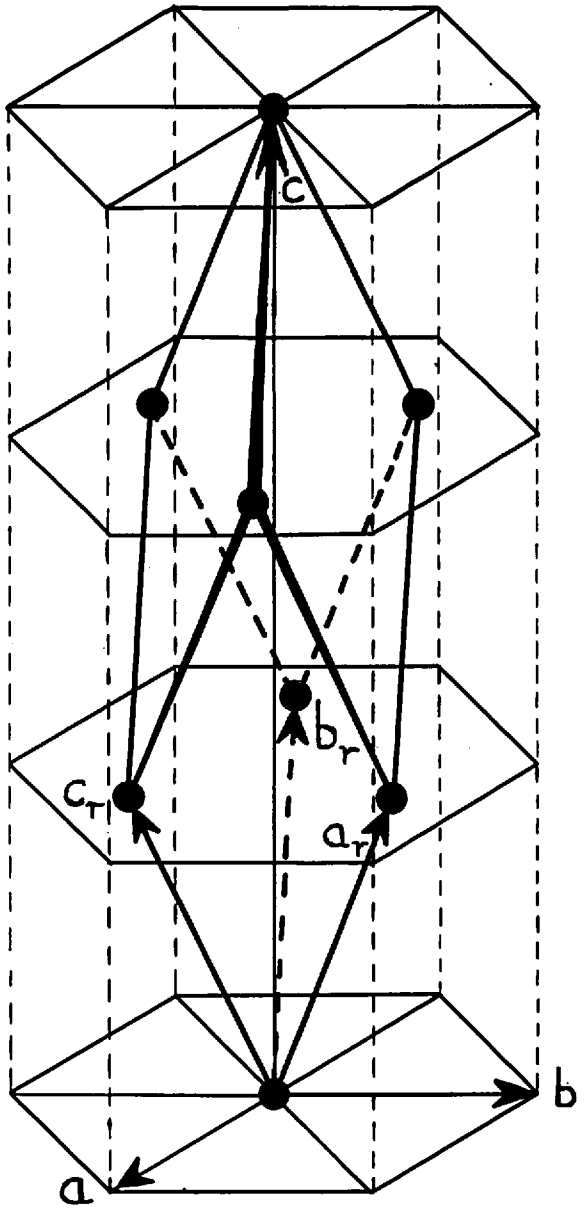


Fig. 84. Diagram showing the relation between a rhombohedral set of axes (a_r, b_r, c_r) and a hexagonal set of axes (a, b, c), which may be used to describe a rhombohedral lattice.

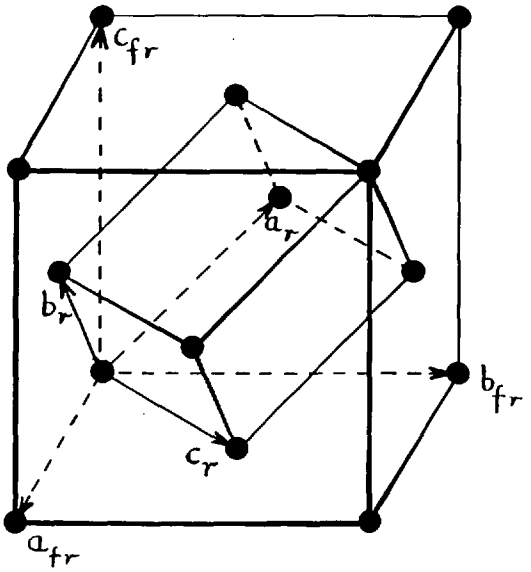


Fig. 85. Diagram showing the representation of a 60° rhombohedral lattice (axes a_r, b_r, c_r) by a face-centred cubic lattice (axes a_{fr}, b_{fr}, c_{fr}). If the rhombohedral angle is not exactly 60°, the lattice can be represented as a pseudo-face-centred cubic (face-centred rhombohedral) lattice.

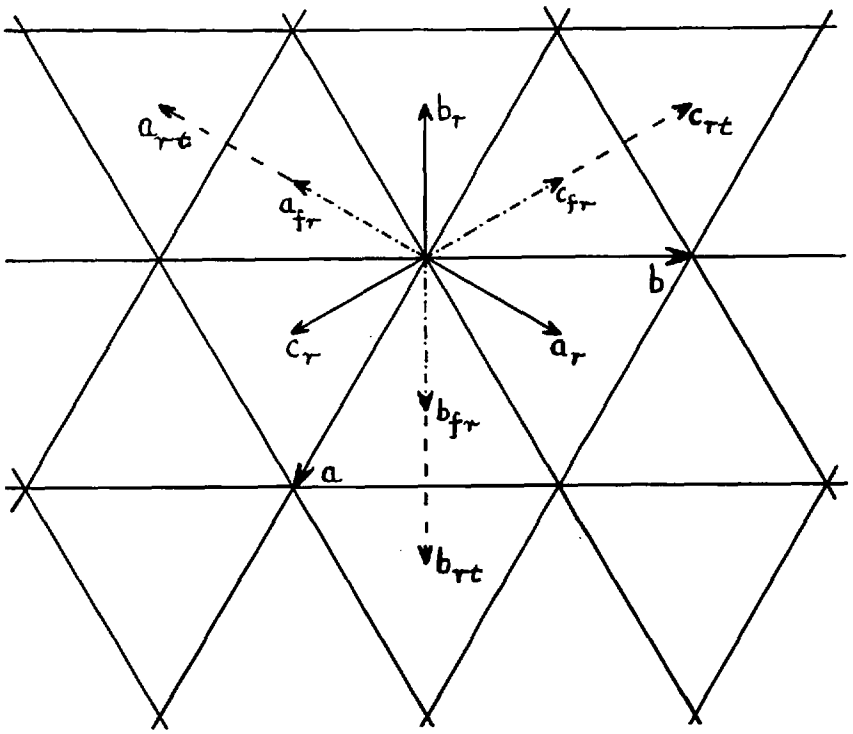


Fig. 86. Projection on to the hexagonal basal plane of the axes of the calcite half-height rhombohedron (a_r, b_r, c_r), the corresponding hexagonal axes (a, b, c, with c vertically out of the plane of the paper) and pseudo face-centred cubic axes (a_{fr}, b_{fr}, c_{fr}). The rhombohedral and pseudo-cubic axes rise from the basal plane to a height one third of the hexagonal c spacing. Also shown are the axes (a_{rt}, b_{rt}, c_{rt}) of the true rhombohedron of calcite. These axes rise from the basal plane to a height twice that of the other axes.

REFERENCES.

REFERENCES.

Agarwala, R.P. and Wilman, H. (1953) Proc.Phys.Soc., B66, 717.
(1954) Proc.Roy.Soc., A223, 167.
(1955) J.Iron and Steel Inst.,179, 124.

Allen, J.W. (1959) Phil.Mag., 4, 1046.

Amontons, G. (1699) Histoire de l'Académie Royale des Sciences avec les Mémoires de Mathématique et de Physique, p.206.

Archard, J.F. (1953) J. Applied Phys.,24, 981.
(1957a) Proc.Roy.Soc., A243, 190.
(1957b) Conf.Lub.& Wear (Inst.of Mech. Eng.), Discussion.
(1959) Wear, 2, 413.
(1961) J. Applied Phys., 32, 1420.

Archard, J.F. and Hirst, W. (1957) Proc.Roy.Soc., A238, 515.

Averbach, B.L. Felbeck, D.K., Hahn, G.T., and Thomas, D.A. (1959) "Fracture", Proceedings of a conference on the atomic mechanisms of fracture, Swampscott, Mass., 1959, Wiley, N.Y., Chapman & Hall, London.

Avient, B.W.E. (1962) Ph.D. Thesis, Univ. of London.

Avient, B.W.E., Goddard, J. and Wilman, H. (1960) Proc.Roy.Soc., A258, 159.

Barrett, C.S. (1939) Trans. AIME, 135, 296.
(1952) "Structure of Metals", 2nd Edn., McGraw-Hill, London.

Barwell, F.T. (1957a) J. Inst.Metals, 86, 257.
(1957b) Conf.Lub. & Wear (Inst.of Mech. Eng.), "A Review of Wear".

Becker, R. (1925) Physik Z., 26, 919.

Becker, R. and Boas, W. (1929) Metallwirtsch., 8, 317.

Bénard, J. and Lacombe, P. (1946) Metaux et Corrosion, 21, 30.

Beeching, R. (1936) "Electron Diffraction", Methuen, London.

Biggs, W.D. (1960) "The Brittle Fracture of Steel", Macdonald & Evans, London.

Boas, W. and Schmid, E. (1931) Z. tech.Physik, 12, 71.

Bowden, F.P. and Leben, L. (1939) Proc.Roy.Soc., A169, 391 & 413.

Bowden, F.P., Moore, A.J. and Tabor, D. (1943) J. Applied Phys., 14, 80.

Bowden, F.P. and Scott, H.G. (1958) Proc.Roy.Soc., A248, 368.

Bowden, F.P. and Tabor, D. (1950) "The Friction and Lubrication of Solids", Clarendon Press, Oxford. 2nd Edn. 1955.

Bowden, F.P. and Young, J.E. (1951a) Proc.Roy.Soc., A208, 311.
(1951b) Proc.Roy.Soc., A208, 444.

Bowden, F.P., Young, J.E. and Rowe, G. (1952) Proc.Roy.Soc., A212, 485.

Brinnell, J.A. (1900) II Congr. Int. Méthodes d'Essai, Paris.

Brown, A.F. and Honeycombe, R.W.K. (1951) Phil. Mag., 42, 1146.

Buck, T.M. (1960) "The Surface Chemistry of Metals and Semiconductors" ed.H.C.Gate p.107, Wiley, N.Y. & London.

Buck, T.M. and McKim, F.S. (1956) J. Electrochem. Soc., 103, 593.

Buerger, M.J. (1930) American Mineralogist, 15, 45.

Burgers, J.M. (1939) Proc. Kon. Ned. Akad. Wet., 42, 293 & 378.
(1940) Proc. Phys. Soc., 52, 23.

Burwell, J.T. and Strang, C.D. (1952) Proc.Roy.Soc., A212, 470.

Cahn, R.W. (1951) J.Inst. Metals, 79, 129.

Camp, P.R. (1955) J. Electrochem,Soc., 102, 586.

Capus, J.M. and Cockcroft, M.G. (1962) J. Inst. Metals, 90, 289.

Clark, W,T., Connolly, A. and Hirst, W. (1963) Brit. J. Applied Phys.,14, 20.

Cottrell, A.L. (1949) Prog.Metal Phys., 1, 77, Butterworths, London.
(1953a) Prog. Metal Phys., 4, 205, Butterworths, London.
(1953b) "Dislocations and Plastic Flow in Crystals", Clarendon Press, Oxford.
(1958) Trans. AIME, 212, 192.

Courtel, R. (1949a) C.R. Acad.Sci., Paris, 228,2031
(1949b) Rev. de Metallurgie, 46, 24.
(1950a) Rev. de Metallurgie, 47, 700.
(1950b) Metaux et Corrosion, 25, 117, 145 & 188.

Courtel, R. and Leger, R. (1948) J. Rech. Centre Nat. Rech. Sci., 7, 161.

Courtel, R. and Loriers, J. (1950) C.R. Acad.Sci., Paris, 230, 735.

Courtney-Pratt, J.S. and Eisner, E. (1957) Proc.Roy.Soc., A238, 529.

Dash, W.C. (1958) J. Applied Phys., 29, 228.
(1959) J. Applied Phys., 30, 459.

Denning, R.M. (1953) American Mineralogist, 38, 108.
(1955) American Mineralogist, 40, 186.

Dobson, P.S. (1961) Ph.D. Thesis, Univ. of London.

Dobson, P.S. and Wilman, H. (1961) Acta Cryst., 14, 1275.
(1962a) Acta Cryst., 15, 556.
(1962b) Acta Cryst., 15, 794.
(1962c) Acta Cryst., 15, 800.
(1963) Brit.J. Applied Phys., 14, 132.

Duwell, E.J. (1962) J. Applied Phys., 33, 2691.

Evans, D.M., Layton, D.N. and Wilman, H. (1951) Proc.Roy.Soc., A205, 17.

Evans, D.M. and Wilman, H. (1950) Proc.Phys.Soc., A63, 298.

Frenkel, J. (1926) Zeits. Phys., 37, 572.

Finch, G.I., Quarrell, A.G. and Wilman, H. (1935) Trans. Faraday Soc., 31, 1051.

Finch, G.I. and Wilman,H. (1937) Ergebn. der exact. Naturwiss., 16, 353.

Forty, A.J. (1957) Proc.Roy.Soc., A242, 392.

Gallagher, C.J. (1952) Phys. Rev., 88, 721.

Gay, P. and Hirsch, P.B, (1953) "Properties of Metallic Surfaces", p 123, Inst. Metals Monograph & Report No.13, London.

Gay, P., Hirsch, P.B. and Kellar, J.N. (1952) Acta Cryst., 5, 7.

Germer, L.H. (1936) Phys. Rev., 50, 659.

Gilman, J.J. (1955) Acta Metallurgica, 3, 277.

Goddard, J. (1959) Ph.D. Thesis, Univ. of London.

Goddard, J., Harker, H.J. and Wilman, H. (1959) Nature, 184, 333.
(1962) Proc. Phys.Soc., 80, 771.

Goddard, J. and Wilman, H. (1962) Wear, 5, 114.

Greenwood, J.A., Minshall, H. and Tabor, D.	(1961) Proc.Roy.Soc., A259, 480.
Greenwood, J.A. and Tabor, D.	(1955) Proc.Phys.Soc., B68, 609. (1957) Conf.Lub. & Wear (Inst. of Mech. Eng.), paper 92. (1958) Proc.Phys.Soc., 71, 989.
Griffith, A.A.	(1924) Proc.1st Int. Congr. Applied Mech. (Delft), p.55.
Hall, E.O.	(1954) "Twinning and Diffusionless Transformations in Metals", Butterworths, London.
Halliday, J.S.	(1955) Proc. Inst. Mech.Eng. London, 169, 777.
Harker, H,J.	(1958) Ph.D. Thesis, Univ. of London.
Harkins, W.D., Juna, G. and Loeser, E.H.	(1946) J. Amer. Chem.Soc., 68, 554.
Harvey, J.	(1959) Ph.D. Thesis, Univ. of London.
Harvey, J. and Wilman, H.	(1960) Acta Cryst., 13, 1063.
Heidenreich, R.D. and Shockley, W.	(1947) J. Applied Phys., 18, 1029.
Hertz, H.	(1886) J. reine angew. Math., 92, 156.
Hess, J.B. and Barrett, C.S.	(1949) Trans. AIME, 185, 599.
Hibbard, W.R. and Ming-Kao Yen	(1948) Trans. AIME, 175, 126.
Hirst, W.	(1957) Conf.Lub. & Wear (Inst. of Mech. Eng.), paper 66.
Holm, R.	(1946) "Electrical Contacts", Uppsala, Almquist & Wiksells.

Honeycombe, R.W.K.	(1951) J. Inst. Metals, 80, 45.
Hopkins, R.L.	(1955) Phys. Rev., 98, 1567.
Hu, H.and Cline, R.S.	(1961) J. Applied Physics, 32, 760.
Hu, H., Sperry, P.R. and Beck, P.A.	(1952) Trans. AIME, 194, 76.
Hughes, G. and Spurr, R.T.	(1955) Proc.Phys.Soc., B68, 106.
Hukao, Y.	(1955) Industr. Diam. Rev., 15, 45 & 107.
Irwin, G.R.	(1948) Trans. Amer. Soc. Metals, 40A, 147.
Jillson, D.C.	(1950) Trans. AIME, 188, 1009.
Joffé, A.F.	(1928) "The Physics of Crystals", p.47 McGraw-Hill, N.Y.
Johnsen, A.	(1914) Jahrb. Radioaktivitat u. Elekronik, 11, 226.
Johnston, T.L., Stokes, R.J. and Li, C.H.	(1958) Acta Metallurgica, 6, 713.
Kenyon, D.M.	(1954) See Seal (1957).
Kerridge, M.	(1955) Proc.Phys.Soc., B68, 400.
Kerridge, M. and Lancaster, J.K.	(1956) Proc. Roy.Soc., A236, 250.
Khruschov, M.M.	(1957) Conf.Lub. & Wear (Inst. of Mech. Eng.), paper 66.
King, R.F. and Tabor, D.	(1954) Proc.Roy.Soc., A223, 225.
King, J.N.	(1960) M.Sc. Thesis, Univ. of London.

King, J.N. and Wilman, H. — (1961) Proc.Phys.Soc., 78, 979. (1962a) Acta Cryst., 15, 551. (1962b) Wear, 5, 213.

Klein, D.L. and D'Stefan, D.J. — (1962) J. Electrochem.Soc., 109, 1.

Lancaster, J.K. — (1957) Proc.Phys.Soc., B70, 112.

Lees, C.S. — (1935) Trans. Faraday Soc., 31, 1102.

Mark, H., Polanyi, M. and Schmid, E. — (1922) Z. Physik., 12, 58.

Martel, R. — (1895) Commission des Méthodes d'Essai des Materiaux de Construction, Paris, 3, 261.

McFarlane, J.S. and Tabor, D. — (1948) Proc. 7th Int. Congr. Applied Mech., London, 4, 31.

Meyer, E. — (1908) Z.ver. Dtsch. Ing., 52, 645 ; 740, 835.

Mil'vidskii, M.G. and Lainer, L.V. — (1961) Fizika. Metallor. i Metallovedenie 11, 923.

Ming-Feng, I. — (1952) J. Applied Phys., 23, 1011.

Mohs, F. — (1822) "Grundriss de Mineralogie". Dresden.

Moore, A.J.W. and Tegart, W.I. McG. — (1952) Proc.Roy.Soc., A212, 452.

Mott, B.W. — (1956a) "Micro-indentation Hardness Testing", Butterworths, London. (1956b) J. Iron & Steel Inst., 183, 233.

Müggе, O. — (1898) Neues Jahrb. Mineral Geolg. Palaont., 1, 71.

Nagata, S., Tomoda, Y. and Ide, H. — (1954) Technol. Rep. Osaka Univ. 4, 94.

Nye, J.F.	(1949) Proc.Roy.Soc., A198, 190.
Ono, A.	(1925) Mem.Coll.Eng. Kyushu Imp. Univ. 3, 207.
Orowan, E.	(1934) Z. Physik, 98, 605, 614 & 634. (1942) Nature, 149, 643.
Palache, C., Berman, H. and Frondel, C.	(1951) "The System of Mineralogy of J.D. Dana and E.S. Dana", 7th Edn., Vol.1, Wiley, N.Y.; Chapman & Hall, London.
Parker, R.C. and Hatch, D.	(1950) Proc.Phys.Soc., B63, 185.
Pearson, G.L., Read, W.T.Jr. and Feldmann, W.L.	(1957) Acta Metallurgica, 5, 181.
Piggott, M.R. and Wilman, H.	(1957) Conf.Lub. & Wear (Inst. of Mech. Eng.), paper 18.
Pinsker, Z.G.	(1949) "Electron Diffraction", English Translation 1953, Butterworths, London.
Polanyi, M.	(1921) Z. Physik, 7, 323. (1934) Z. Physik, 89, 660.
Porgess, P.V.K. and Wilman, H.	(1960) Proc.Phys.Soc., 76, 513.
Pugh, E.N. and Samuels, L.E.	(1961) J.Electrochem.Soc., 108, 1043. (1962) J.Electrochem.Soc., 109, 409.
Raether, H.	(1947) Metaux et Corrosion, 22, 2.
Read, W.T.	(1953) "Dislocations in Crystals", McGraw-Hill, N.Y.
Robertson, T.S.	(1953) J. Iron & Steel Inst., 175, 361.
Sabey, Miss B.E.	(1958) Proc.Phys.Soc., 71, 979.
Savage, R.H.	(1948) J. Applied Phys., 19, 1. (1956) J. Applied Phys., 27, 136. (1959a) Nature, 183, 315 & 454. (1956b) Nature, 184, 45.

Schmid, E. (1924) Proc.1st Intern.Congr. Applied Mech., Delft, 342.

Schmid, E. and Boas, W. (1935) "Kristallplastizitat", Springer, Berlin.

Scott, H. (1957) Conf.Lub. & Wear (Inst. of Mech. Eng.), paper 10.

Scott, V.D. and Wilman, H. (1958) Proc. Roy.Soc., A247, 353.

Seal, M. (1957) Conf.Lub. & Wear (Inst. of Mech. Eng.), paper 12.

Seebeck, A. (1833) Prufungs-Programm des Berliner Realgymnasiums.

Shooter, K.V. (1952) Proc.Roy.Soc., A212, 488.

Shore, A.F. (1918) J. Iron & Steel Inst., 2, 59.

Slawson,C.B. and Koln, J.A. (1950) Industr. Diam. Rev., 10, 168.

Smekal, A. (1933) "Handbusch der Physik", 29, 2, Springer, Berlin.

Spurr, R.T. (1956) Brit. J. Applied Phys., 7, 260.

Spurr, R.T. and Newcomb, T.P. (1957a) Proc.Phys.Soc., B70, 98.
(1957b) Conf.Lub. & Wear (Inst. of Mech.Eng.), paper 28.

Steijn, R.P. (1961) J. Applied Phys., 32, 1951.
(1962) Wear, 5, 308.

Stroh, A.N. (1954) Proc.Roy.Soc., A223, 404.
(1955) Proc.Roy.Soc., A232, 548.

Tabor, D. (1951) "The Hardness of Metals", Clarendon Press, Oxford.
(1955) Proc. Roy. Soc., A229, 198.
(1959) Proc. Roy. Soc., A251, 378.

Takahashi, N. (1951) Metaux et Corrosion, 26, 189.

Taylor, G.I.	(1934) Proc.Roy.Soc., A145, 362. (1938) J. Inst.Metals, 62, 307.
Tertsch, H.	(1949) "Die Festigkeitserscheinungen der Kristalle", Springer-Verlag, Berlin
Thomson,G.P.	(1930) Proc.Roy.Soc., A128, 649.
Thomson, G.P. and Cochrane, W.	(1939) "Theory and Practice of Electron Diffraction", Macmillan, London.
Tipper, C.F.	(1957) J. Iron & Steel Inst., 185, 4.
Tolkowsky, M.	(1920) Dissertation, Univ. of London.
Treuting, R.G.	(1952) J. Metals, 4, 1044. (1955) J. Metals, 7, 1027.
van Rooyen, G.T. and Backofen, W.A.	(1957) J. Iron & Steel Inst., 186, 235.
Wang, C.C. and Alexander, B.H.	(1955) Acta Metallurgica, 3, 515.
Wentorf, R.H.	(1959) J. Applied Phys., 30, 1765.
West, C.D.	(1954) Tech. Report O.N.R. Contract No. N 7, 39102.
Wever, F.	(1931) Trans. AIME, 93, 51.
Whapham, A.D.	(1956) J. Inst. Metals, 84, 109.
Whapham, A.D. and Wilman, H.	(1956) Proc.Roy.Soc., A237, 513.
Wilks, E.M.	(1952) Phil.Mag., 43, 1140.
Wilks, E.M. and Wilks, J.	(1954) Phil. Mag., 45, 844.
Wilman, H.	(1948a) Proc.Phys.Soc., 60, 341. (1948b) Proc.Phys.Soc., 61, 416. (1950) Nature, 165, 321. (1951) Proc. Phys.Soc., A64, 329. (1952) Acta Cryst., 5, 782. (1957) Acta Cryst., 10, 824. (1960) Acta Cryst., 13, 1062.

Wolff, G.A., Wilbur, J.M. Jr. and Clark, J.C. (1957) Z. Elektrocham,, 61, 101.

Wooster, W.A. (1938) "A Textbook on Crystal Physics", C.U.P., Cambridge.

Wyckoff, R.W.G. (1948) "Crystal Structures", Vol.1. Interscience, N.Y. & London.

Zapffe, C.A. (1947) Metals Progress, 51, 428.

Zwicky, F. (1923) Physik Z., 24, 131.